E.O. Paton Electric Welding Institute of the National Academy of Sciences of Ukraine

International Scientific-Technical and Production Journal

The Paton WELDING JOURNAL

October 2016
No. 10

Published since 2000

English translation of the monthly «Avtomaticheskaya Svarka» (Automatic Welding) journal published in Russian since 1948

EDITORIAL BOARD
Editor-in-Chief
B.E. Paton

Scientists of PWI, Kiev
S.I. Kuchuk-Yatsenko (*vice-chief ed.*),
V.N. Lipodaev (*vice-chief ed.*),
Yu.S. Borisov, G.M. Grigorenko,
A.T. Zelnichenko, V.V. Knysh,
I.V. Krivtsun, Yu.N. Lankin,
L.M. Lobanov, V.D. Poznyakov,
I.A. Ryabtsev, K.A. Yushchenko

Scientists of Ukrainian Universities
V.V. Dmitrik, NTU «KhPI», Kharkov
V.V. Kvasnitsky, NTUU «KPI», Kiev
V.D. Kuznetsov, NTUU «KPI», Kiev

Foreign Scientists
N.P. Alyoshin
N.E. Bauman MSTU, Moscow, Russia
Guan Qiao
Beijing Aeronautical Institute, China
A.S. Zubchenko
DB «Gidropress», Podolsk, Russia
M. Zinigrad
Ariel University, Israel
V.I. Lysak
Volgograd STU, Russia
Ya. Pilarczyk
Welding Institute, Gliwice, Poland
U. Reisgen
Welding and Joining Institute, Aachen, Germany
G.A. Turichin
St. Petersburg SPU, Russia

Founders
E.O. Paton Electric Welding Institute, NASU
International Association «Welding»

Publisher
International Association «Welding»

Translators
A.A. Fomin, O.S. Kurochko, I.N. Kutianova
Editor
N.G. Khomenko
Electron galley
D.I. Sereda, T.Yu. Snegiryova

Address
E.O. Paton Electric Welding Institute,
International Association «Welding»
11 Kazimir Malevich Str. (former Bozhenko Str.),
03680, Kiev, Ukraine
Tel.: (38044) 200 60 16, 200 82 77
Fax: (38044) 200 82 77, 200 81 45
E-mail: journal@paton.kiev.ua
www.patonpublishinghouse.com

State Registration Certificate
KV 4790 of 09.01.2001
ISSN 0957-798X

Subscriptions
$348, 12 issues per year,
air postage and packaging included.
Back issues available.

All rights reserved.
This publication and each of the articles contained herein are protected by copyright.
Permission to reproduce material contained in this journal must be obtained in writing from the Publisher.

CONTENTS

© PWI, International Association «Welding», 2016

doi.org/10.15407/tpwj2016.10.01

EFFECT OF ANISOTROPY OF PROPERTIES OF NICKEL ALLOY ON STRESSES AND PLASTIC DEFORMATIONS IN WELD ZONE

K.A. YUSHCHENKO, E.A. VELIKOIVANENKO, N.O. CHERVYAKOV, G.F. ROSYNKA and **N.I. PIVTORAK**
E.O. Paton Electric Welding Institute, NASU
11 Kazimir Malevich Str., 03680, Kiev, Ukraine. E-mail: office@paton.kiev.ua

A calculation method was used for investigation of the kinetics of stress-strain state in welding of nickel alloy single crystal taking into account anisotropy of its thermophysical and mechanical properties. It is shown that anisotropy of the properties of single crystal promotes for growth of a rate of plastic deformations in temperature interval BTI-II in comparison with isotropic alloy of such type (having polycrystalline structure). The rate of growth of longitudinal plastic deformations in the single crystal in BTI-II temperature interval can approximately 2.0–2.5 times exceed that in the polycrystalline variant of alloy. This should be taken into account in development of corresponding structures and technology of their manufacture. 9 Ref., 3 Tables, 7 Figures.

Keywords: *mathematical modelling, stress-strain state, single crystals, nickel alloys, properties anisotropy*

Continuous progress in technology of welding of different materials significantly expands the fields of application of new technologies. Recently, an issue of welding of elements of design from materials with single crystal structure has become relevant. It is known fact that the single crystals are characterized by specific anisotropy of thermophysical as well as mechanical properties [1]. Naturally, that the single crystal being welding can have different reaction of material on heat action of the welding process depending on angles between the welding direction and main crystallographic directions. Thus, various kinetics of temperature fields, stresses and deformations, respectively, can be obtained. Due to known fact that resistance of the single crystals to different fracture types is also determined by level of properties' anisotropy, then development of the effective methods preventing crack formation in single crystal welding requires sufficiently clear ideas on kinetics of the welding stresses and deformations taking into account the anisotropy of thermophysical and mechanical properties. Information from this domain is scarce up to the moment, since corresponding experimental researches require large cost and time expenses. Therefore, it is natural in this connection to use current computer methods realizing corresponding mathematical models [2–4] et al.

In this regard, an aim of this work lied in a calculation investigation of kinetics of stress-strain state in welding of the single crystal of nickel alloy taking into account anisotropy of its thermophysical and mechanical properties.

Unfortunately, using commercial software packages of Ansys or Sysweld type is related with sufficiently serious problem of their reworking for taking into account the anisotropy of properties, and, thus, require engaging corresponding developers of these packages. In order to solve this problem on thermal mechanics of material welding the E.O. Paton Electric Welding Institute many years ago has developed the software package «Weldpredictions», which uses the same mathematical models as in mentioned above commercial packages. Regardless the fact that «Weldpredictions» package has less service programs, its developers currently work at the E.O. Paton Electric Welding Institute, therefore, necessary reworking and specifications of mathematical models, calculation algorithms and computer programs for performance of numerical investigations have been fulfilled by them in sufficiently shot terms.

An essence of the main additions, related with anisotropy of indicated above thermophysical and mechanical properties applicable to nickel alloy single crystal:

heat conductance coefficient λ_n determining the components of a vector of heat flow

$$f_n = \lambda_n \frac{\partial T}{\partial n}, \quad (n = x, y, z) \tag{1}$$

in arbitrary point x, y, z of heat conducting medium, according to [1] is the second-rank tensor, in which only diagonal elements differ from zero

$$\lambda_n = \begin{Vmatrix} \lambda_{xx} & 0 & 0 \\ 0 & \lambda_{yy} & 0 \\ 0 & 0 & \lambda_{zz} \end{Vmatrix} \tag{2}$$

(in accordance with Fourier heat conduction theory).

Sum of such tensor on [1]

$$\lambda_{xx} + \lambda_{yy} + \lambda_{zz} = 3\lambda_{av}, \tag{3}$$

where λ_{av} is the average value of heat conductance coefficient.

For single crystal with typical cubic lattice the typical crystallographic directions (Figure 1) are: [001] — along the boundaries; [011] — along small diagonals and [111] — along large diagonals.

© K.A. YUSHCHENKO, E.A. VELIKOIVANENKO, N.O. CHERVYAKOV, G.F. ROSYNKA and N.I. PIVTORAK, 2016

If x, y, z coordinate system matches with [001] directions, then $\lambda_{xx} = \lambda_{yy} = \lambda_{zz} = \lambda_{av} = \lambda_{001}$.

If axis x with [011] direction forms an angle ω, and axis z matches with direction [001], then $\lambda_{zz} = \lambda_{001}$, and λ_{xx} and λ_{yy} are determined by dependencies

$$\lambda_{xx} = \lambda_{011}\cos^2\omega + \left(2\lambda_{001} - \lambda_{011}\right)\sin^2\omega,$$
$$\lambda_{yy} = 2\lambda_{001} - \lambda_{xx} = 2\lambda_{001}\cos^2\omega - \lambda_{011}\cos 2\omega. \quad (4)$$

If axis x makes an angle ρ with direction [111], and plane xOy comes through two small diagonals and cube edges, then $\lambda_{zz} = 3\lambda_{av} - \lambda_{001} - \lambda_{011} = 2\lambda_{001} - \lambda_{011}$ and respectively

$$\lambda_{xx}(\rho) = \lambda_{111}\cos^2\rho + \left(3\lambda_{001} - 2\lambda_{001} + \lambda_{011} - \lambda_{111}\right)\sin^2\rho = \lambda_{111}\cos^2\rho + \left(\lambda_{001} + \lambda_{011} - \lambda_{111}\right)\sin^2\rho. \quad (5)$$

More general positions of the axis x (axis of movement of welding heat source) relatively to the main crystallographic planes (directions) are also possible. However, we will use variant (4) for simplicity.

Already at this it can be shown that orthotropy of λ value according to (4) can result in noticeable effects in temperature fields. Mentioned above is demonstrated below by the example of welding heating with movable power source (arc in argon medium, I = = 95 A, U = 10.5 V, v_w = 8.5 m/h) of fine plate from the single crystal of nickel alloy. The average thermophysical ($c\gamma$, λ, α) and mechanical (E, σ_y) properties used in calculations, are given in Table 1. Size of plate L_x = 85 mm, L_y = 40 mm, δ = 3 mm.

Figure 2 shows the temperature fields close to weld pool moving along axis x depending on angle ω = = 0–π/2 under condition that $\lambda_{011} = 1.5\lambda_{av}$. Scalar value $c\gamma$ was taken constant and equal $c\gamma_{av}$ (T) on Table 1.

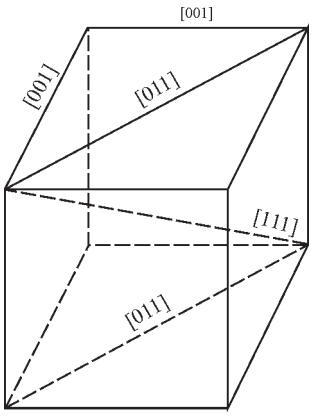

Figure 1. Main crystallographic directions in single crystal with cubic lattice

It can be seen from these data that the temperature fields can significantly vary depending on angles between the welding direction and crystallographic directions of single crystal at value λ indicated anisotropy.

For variant $\omega = \pi/4$, when $\lambda_{xx} = \lambda_{yy} = \lambda_{zz} = \lambda_{av}$ the calculation results agree well with experimental data $\lambda(T)$ and $c\gamma(T)$ according to Table 1 under normal-volumetric distribution of effective power of the source, when coefficient of efficiency η_s = 0.6, and coefficients of concentration of source $K_y = K_x$ = 0.25 mm^{-2}, K_z = 0.8 mm^{-2}.

It is important to carry out comparative evaluation of effect of studied anisotropy of λ on kinetics of deformations and stresses in typical points, critical from point of view of technological strength. From

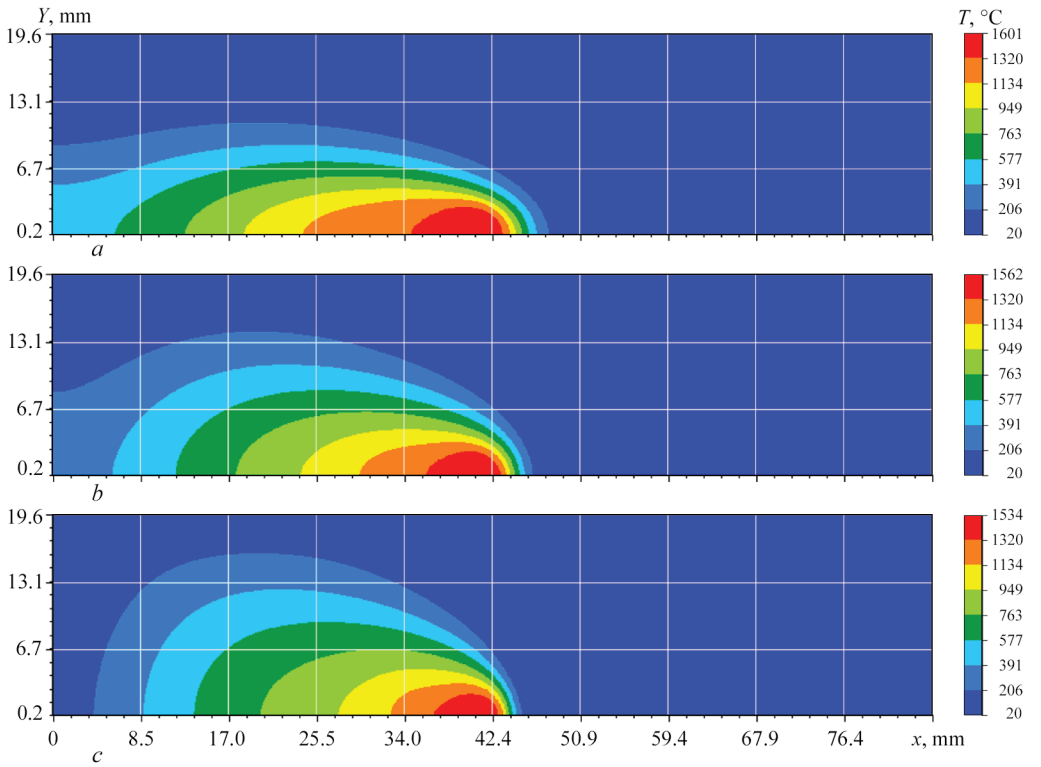

Figure 2. Temperature field close to weld pool: *a* — at ω = 0 (2.85 mm pool width, 9.4 mm length); *b* — $\omega = \pi/4$ (2.55 mm pool width, 7.7 mm length); *c* — $\omega = \pi/2$ (2.35 mm pool width, 6.4 mm length)

Table 1. Average thermophysical and mechanical characteristics of studied alloy

T, °C	$c\gamma$, cal/(mm³·°C)	λ, cal/(mm·s·°C)	$E\cdot10^{-5}$, MPa	σ_y, MPa	$\alpha\cdot10^4$, 1/°C
50	0.0008063	0.0018	1.838	930	0.110
100	0.0007797	0.0019	1.838	930	0.114
200	0.0008506	0.0023	1.838	875	0.122
300	0.0008417	0.0024	1.838	875	0.140
400	0.0008594	0.0027	1.838	825	0.143
500	0.0008683	0.0030	1.838	800	0.150
600	0.0008771	0.0036	1.838	800	0.162
700	0.0008949	0.0036	1.838	800	0.185
800	0.0009746	0.0041	1.838	790	0.240
900	0.0010366	0.0044	1.838	650	0.310
1000	0.0010898	0.0048	1.585	375	0.380
1100	0.0012138	0.0055	0.529	125	0.410
1200	0.0012138	0.0055	0.271	25	0.390

this point of view and applicable to nickel alloys, the points close to the fusion line are critical for risk of formation of transverse hot cracks in corresponding alloy brittleness temperature interval BTI [5]. Evaluation of weldability of this alloy on Varestraint-Test procedure showed that the material has two BTI:

BTI-I ≈ 1350–1250 °C, $\varepsilon_{cr} \approx 0.38$ %;

BTI-II ≈ 1050–800 °C, $\varepsilon_{cr} \approx 0.10$ %.

The positive increments of plastic deformations above ε_{cr} at tensile normal stresses in corresponding direction will promote crack formation.

The calculations, which were carried with the help of «Weldpredictions» package, for points located in the boundary from fusion line $\Delta y = -0.5$ mm (point *1*), $\Delta y = 0.5$ mm (point *2*) and $\Delta y = 1.5$ mm (point *3*) (Figure 3) at different $\omega = 0$–$\pi/2$ showed the level of effect of studied anisotropy of λ on kinetics of changes of corresponding plastic deformations $^{\Delta\varepsilon^p_{xx}}$ and stresses in points *1–3* depending on temperature in these points.

Figures 4 and 5 show such results for point *2*, and Table 2 gives the increments $^{\Delta\varepsilon^p_{xx}}$ and the limits of change of σ_{xx} stresses in the BTI-II for all studied points *1–3*.

It can be seen that anisotropy of λ, corresponding to $\omega = 0$ and $\omega = \pi/2$, in comparison with $\omega = \pi/4$, when anisotropy does not become apparent, results in noticeable change of rate of plastic deformation increments in BTI-II.

Possible anisotropy of a coefficient of relative temperature elongation α in comparisons with α_{av} from Table 1 can also have specific effect on the rate of plastic deformations in the BTI zone.

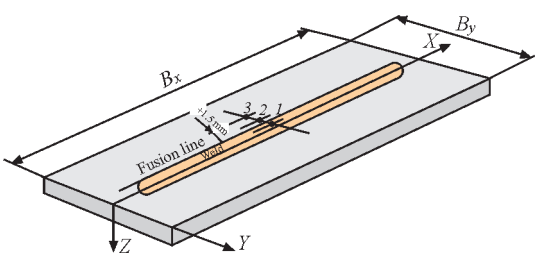

Figure 3. Position of studied points on specimen (B_x — specimen length, B_y — specimen width, *1* — point in weld at –0.5 mm distance from fusion line; *2*, *3* — point in HAZ at 0.5 and 1.5 mm distance from fusion line, respectively)

Since α value determines the components of a vector of normal temperature deformations in a single crystal, then description of its anisotropic changes similar to heat conduction coefficient can be done using dependence (4).

Data given in Table 2 show an effect of ω angle at $\alpha_{011} = 1.5\alpha_{001}$ and $\alpha_{001} = \alpha_{av}$ on Table 1. It can be seen that anisotropy of α similar to anisotropy of λ results qualitatively in similar effect on rate of $^{\Delta\varepsilon^p_{xx}}$ deformations in the BTI-II.

Thus, anisotropy of λ and α in the single crystal depending on angle ω develops some orthotropy in mathematical description of temperature field and temperature deformations with periodicity on angles ω and ρ in π/2. Somewhat another effect can be related with anisotropy of mechanical characteristics (elasticity modulus E and yield strength σ_y).

Tables 3 and Figure 6 give the experimental data relatively to value of elasticity modulus $E(T)$ of the single crystals of nickel alloys on different sources. It can be seen that sufficiently noticeable anisotropy of ω and ρ with π/4 period takes place on this characteristic.

The results of application of these data for the considered calculation model at $\rho = 0$ and different ω are given in Table 2. It follows from them that in comparison with $\omega = \pi/4$ state (isotropy state) reduction of ω results in rise of E and respectively increase of plastic deformations in the BTI-II zone.

Experimental data from work [6] relatively to anisotropy of yield strength $\sigma_{0.2} = \sigma_y(T)$ in Figure 7 for single crystal PWA1480 show that anisotropy is sufficiently large in different deformation planes. However, it is impossible to take it into account based on the Mises yield criterion, since under this condition plastic flow occurs in an elementary volume without specification of flow plane. The Tresca yield criterion is more reasonable for consideration of the plastic flow plane. For it a yield surface can be presented through functional f [3, 7]:

$$f = \tau^2_{\max} - \frac{\sigma^2_y(\Theta, \rho)}{3}, \qquad (6)$$

where $\Theta = \pi/4 - \omega$.

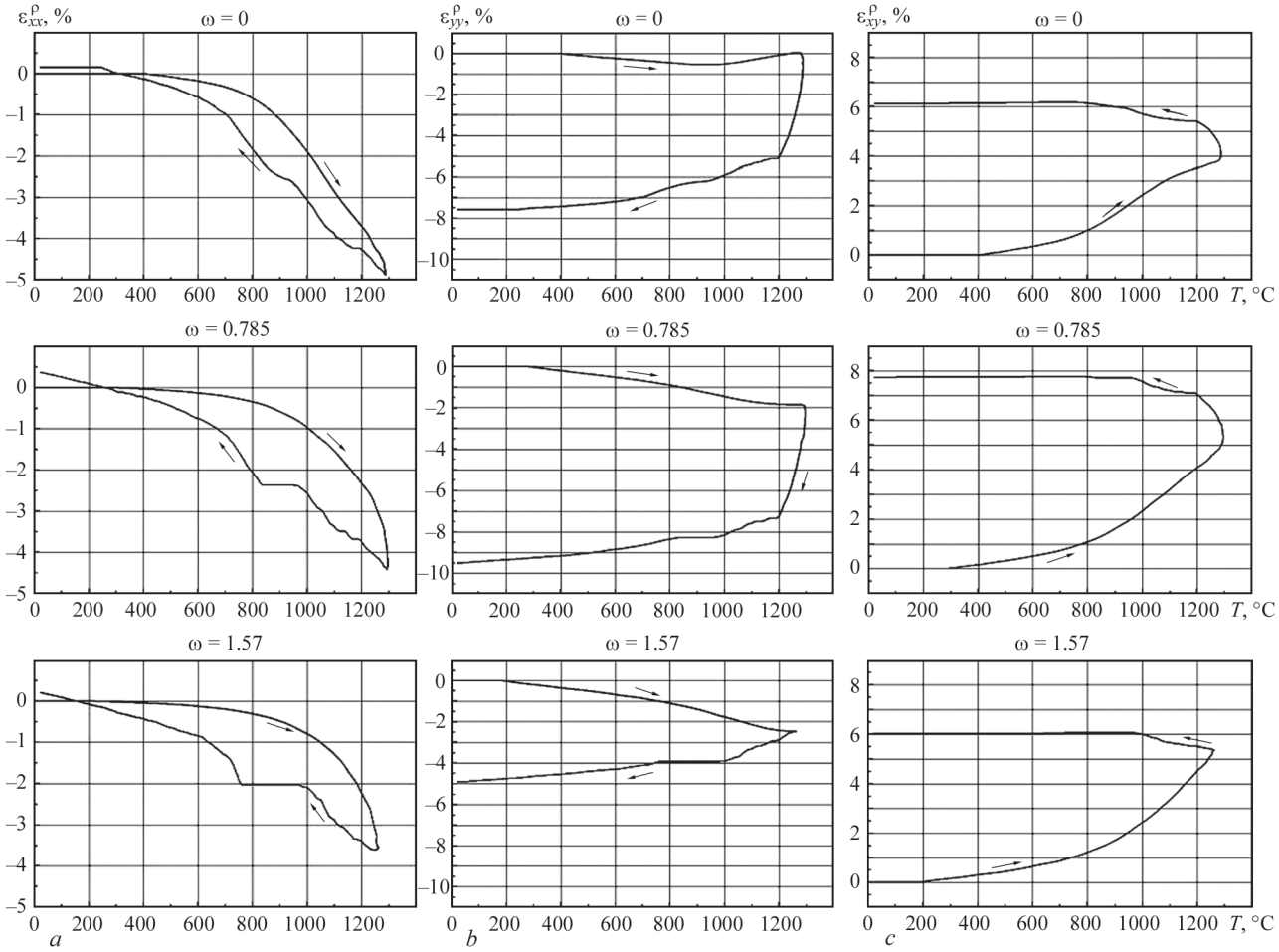

Figure 4. Kinetics of change of plastic deformations: *a* — $\Delta\varepsilon^p_{xx}$, *b* — $\Delta\varepsilon^p_{yy}$, *c* — $\Delta\varepsilon^p_{xy}$ from temperature in point *2* (Δy = 0.5 mm) taking into account anisotropy of λ for different ω

The maximum tangential stresses τ_{max} are determined in form of [8]

$$\tau_{max} = \max\left\{\begin{array}{c}\dfrac{1}{2}\sqrt{\left(\sigma_{xx}-\sigma_{yy}\right)^2+4\sigma^2_{xy}}\\ \dfrac{\sigma_{xx}+\sigma_{yy}}{4}+\dfrac{1}{4}\sqrt{\left(\sigma_{xx}-\sigma_{yy}\right)^2+4\sigma^2_{xy}}\end{array}\right. \quad (7)$$

and act in a slip plane, position of which is determined by condition if:

$$\sigma = \frac{\sigma_{xx}+\sigma_{yy}}{2} > 0$$

then a slip plane is located at π/4 angle to axis *z* and at φ angle to axis *x*, where φ is determined by condition

$$\mathrm{tg}\,2\varphi = \frac{2\sigma_{xy}}{\sigma_{xx}-\sigma_{yy}}. \quad (8)$$

Table 2. Comparison of deformations $\Delta\varepsilon^p_{xx}$ and σ_{xx} stresses in BTI-II (1050–800) °C

Characteristics of variant		Point *1* (Δy = –0.5 mm)		Point *2* (Δy = 0.5 mm)		Point *3* (Δy = 1.5 mm)	
		$\Delta\varepsilon^p_{xx}$, %	σ_{xx}, MPa	$\Delta\varepsilon^p_{xx}$, %	σ_{xx}, MPa	$\Delta\varepsilon^p_{xx}$, %	σ_{xx}, MPa
Main. Complete anisotropy		0.8	100–900	0.9	100–900	1.7	–200–850
Anisotropy of λ	ω = 0	1.7	100–800	1.5	100–900	1.8	–200–800
	ω = π/4	0.8	100–900	0.9	100–900	1.7	–200–850
	ω = π/2	0.4	100–900	0.6	100–900	1.4	–200–800
Anisotropy of α	ω = 0	1.5	180–900	2.0	150–900	2.5	–200–880
	ω = π/4	0.8	180–900	0.9	150–900	1.7	–200–850
	ω = π/2	0.3	180–900	0.3	150–900	1.0	–200–800
Anisotropy of *E*	ω = 0	0.2	100–850	0.4	200–850	1.3	–200–800
	ω = π/8	0.5	180–850	0.7	180–850	1.4	–200–800
	ω = π/4	0.8	180–900	0.9	200–900	1.7	–200–800
Anisotropy of σ_y	ω = 0	1.0	100–1000	1.4	100–1000	1.5	–200–1000
	ω = π/8	0.9	100–1000	1.3	100–1000	1.4	–200–1000
	ω = π/4	0.8	100–1000	0.9	100–1000	1.7	–200–1000
Anisotropy of λ, α, *E*, σ_y	ω = 0	2.0	200–1000	2.5	200–1000	2.5	–200–1000
	ω = π/8	1.6	200–1000	3.5	200–1000	4.0	0–1000
	ω = π/4	0.8	200–1000	0.9	200–1000	1.7	–250–1000

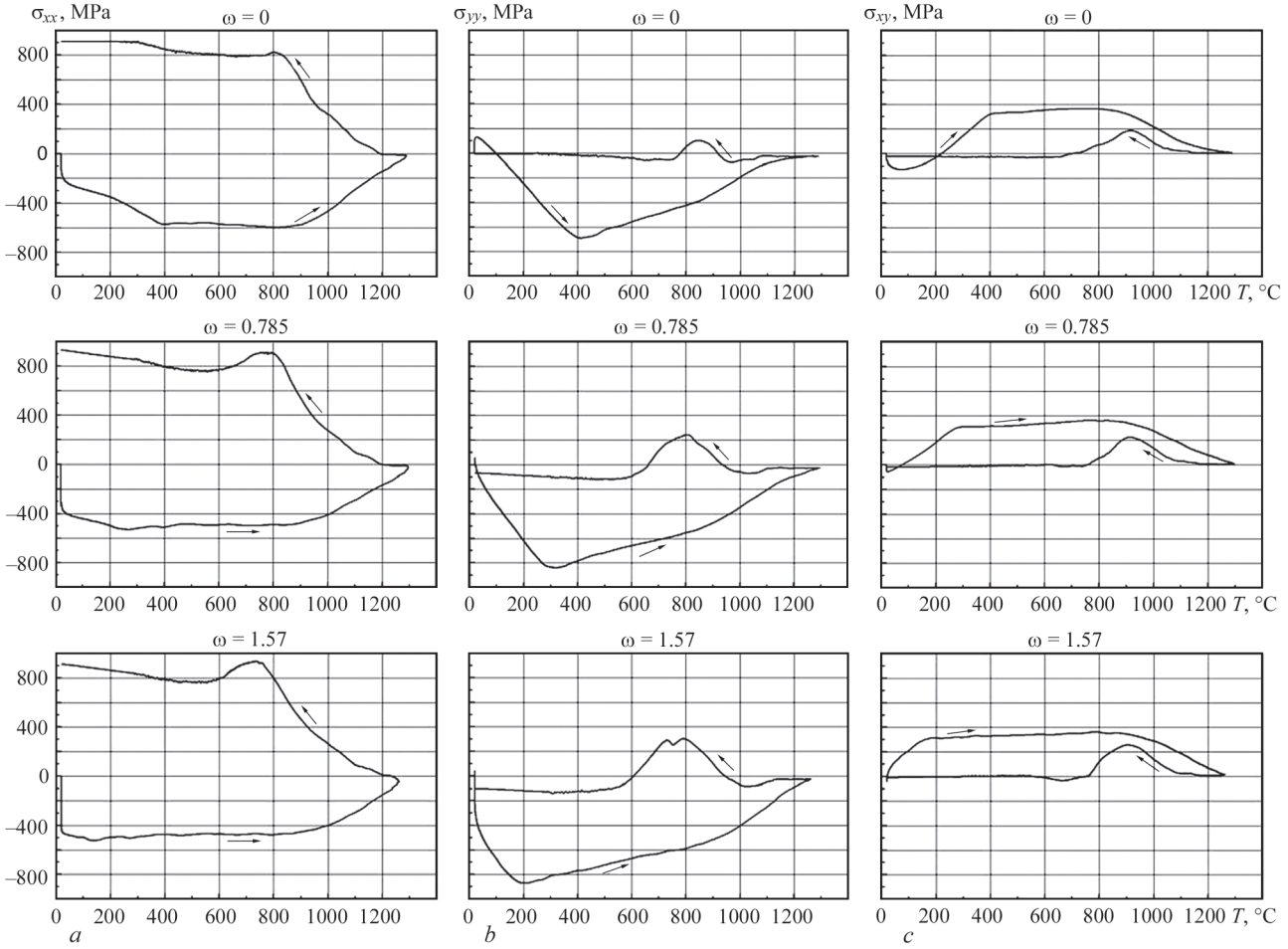

Figure 5. Kinetics of stress change: *a* — σ_{xx}, *b* — σ_{yy}, *c* — σ_{xy} from temperature in point *2* (Δy = 0.5 mm) taking into account anisotropy of λ for different ω

If σ < 0, then the slip plane is parallel to axis *z* and at φ = ±π/4 angle to axis *x*.

Corresponding calculations with initial data in Figure 7 and condition (6)–(8) were made in scope of given work.

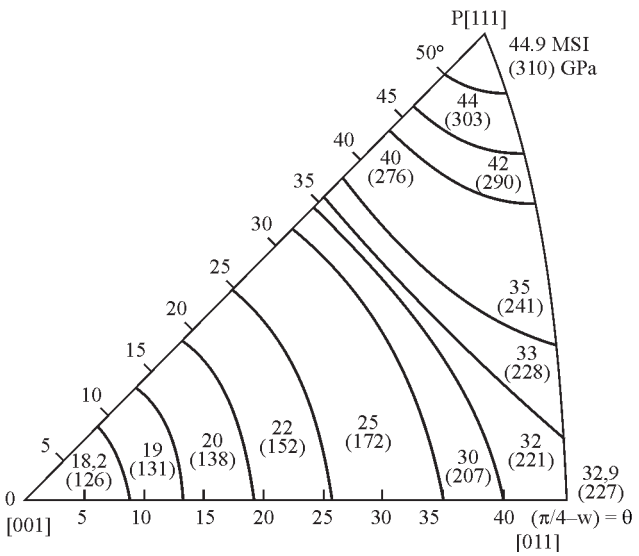

Figure 6. Dependence of elasticity modulus *E* on angles ω and ρ in single crystal of nickel alloy PWA 1480 on data [5] at *T* = 20 °C

Data given in Table 2 demonstrate the level of indicated effect of σ_y anisotropy on the rate of plastic deformations $\Delta\varepsilon^p_{xx}$ in the BTI-II zone.

Thus, effect of anisotropy of each of mentioned parameters λ, α, *E* and σ_y on kinetics of plastic deformations in the BTI-II zone was considered. A variant of simultaneous effect of anisotropy of all these parameters (Table 2) was also studied.

It can be seen that in this case overlaying of effect of separate parameters is also possible, that promotes

Table 3. Value of Young's modulus and characteristics of short-term strength of ZhS-32 alloy [6]

T, K	<hkl>	*E*, GPa	$\sigma_{0.2}$, MPa	σ_t, MPa
293	<001>	112	1005	1315
	<011>	174	820	–
	<111>	272	1330	1650
1073	<001>	97	1045	1310
	<011>	161	815	–
	<111>	247	1145	1295
1173	<001>	82	865	1035
	<011>	144	795	–
	<111>	222	990	1025
1273	<001>	76	620	755
	<011>	121	535	–
	<111>	214	650	735

for significant rise of the rate of plastic deformations in the BTI-II.

Conclusion

One of the significant technological problems in welding heating of the parts (plates) from heat-resistant nickel alloys of ZhS-32 type, having single crystal structure, is prevention of hot crack formation in the brittleness temperature interval.

Available experience of welding of similar details from polycrystalline alloy of close type [9] shows that the main reason of appearance of indicated defects in fusion welding of such alloys is the BTI-II presence in zone of relatively moderate temperatures and related with welding heating thermal-deformation cycles, which develop in the BTI-II sufficiently high rates of plastic deformation development. It is known fact that the single crystals of heat-resistant alloys can be characterized by series of higher properties in comparison with similar alloys of polycrystalline structure.

Research, carried in the present work, shows that anisotropy of the properties of single crystal promotes for rise of plastic deformation rate in the BTI-II temperature interval in comparison with isotropic alloy of such type (having polycrystalline structure).

The rate of growth of longitudinal plastic deformations in single crystal in the BTI-II temperature interval can approximately 2.0–2.5 times exceed that in polycrystalline variant of alloy, that obviously should be taken into account in development of corresponding structures and technology of their manufacture.

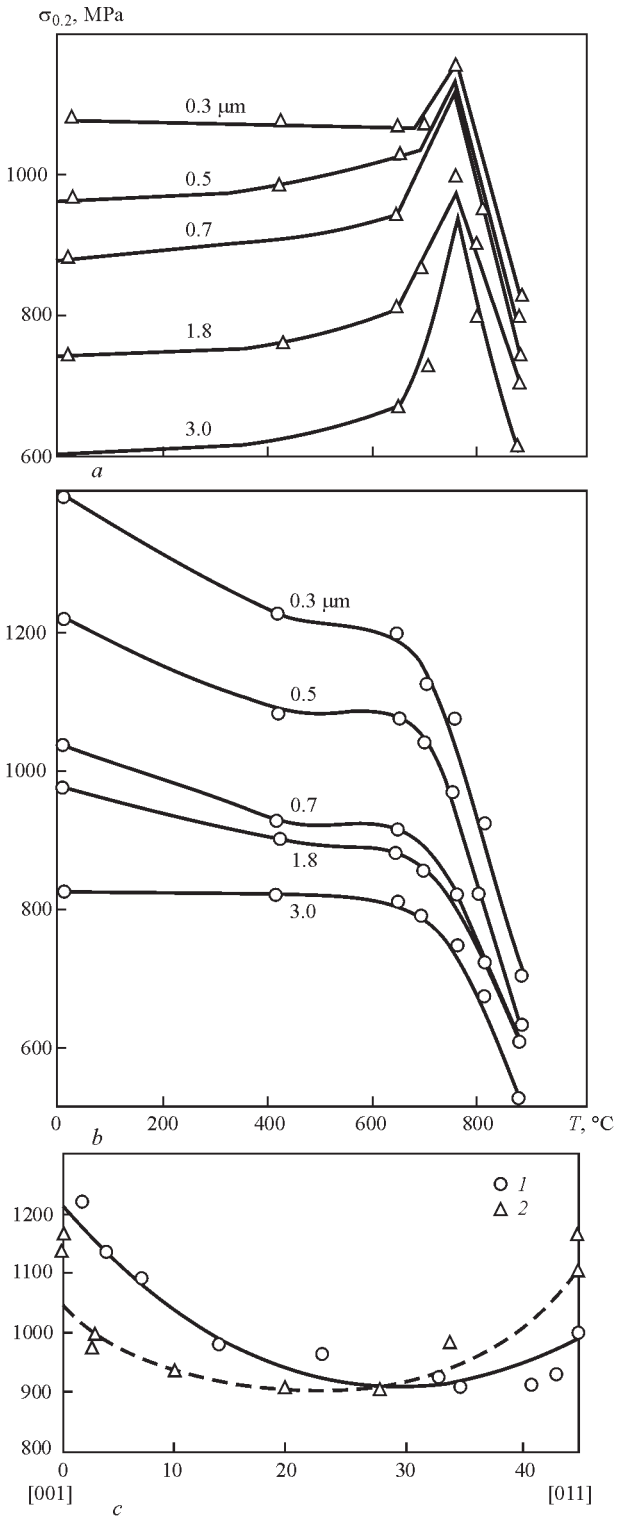

Figure 7. Yield strength of PWA 1480 alloy in sections [001] (*a*) and [111] (*b*) at different size of γ′-phase depending on temperature (*a*, *b*) and tensile and compression yield strength for 593 °C depending on angle $\Theta = (\pi/4) - \omega$ at $\rho = 0$ (*c*) [5] (*1* — tensile load; *2* — compression load)

1. Ashkenazi, E.K., Ganov, E.V. (1972) *Anisotropy of structural materials*: Refer. Book. Leningrad: Mashinostroenie.
2. Ueda, J., Murakawa, H., Nakacho, K. et al. (1995) Establishment of computation welding mechanics. *Transact. of JWRI*, 24(**2**), 73–86.
3. Makhnenko, V.I. (1976) *Computational methods for investigation of welding stress and strain kinetics*. Kiev: Naukova Dumka.
4. Makhnenko, V.I., Velikoivanenko, E.A., Pochinok, V.E. (1999) Numerical methods of the predictions of welding stresses and distortions. *Welding and Surfacing Reviews*, **13**, Pt 1, 147.
5. Goldschmidt, D. (1994) Einkristalline Gasturbinenschaufeln aus Nickelbasis-Legierungen. *Materialwissenschaft und Werkstofftechnik*, **25**, 373–382.
6. Golubovsky, E.R., Svetlov, I.L. (2005) Static and cyclic strength of single crystals of heat-resistant nickel alloys. In: *Abstr. of Pap. of Int. Sci.-Techn. Conf. on Dynamics, Strength and Life of Machines and Constructions* (Ukraine, Kyiv, 1–4 Nov. 2005). Kyiv: IPS, Vol. 1, 96–97.
7. Rabotnov, Yu.N. (1963) *Resistance of materials*. Moscow: Fizmatgiz.
8. Birger, I.A., Mavlyutov, R.R. (1986) *Resistance of materials*: Manual. Moscow: Nauka.
9. Makhnenko, V.I., Savchenko, V.S., Yushchenko, K.A. et al. (1993) Influence of physical characteristics of cast nickel alloys on development of thermodeformation processes in fusion welding. *Avtomatich. Svarka*, **11**, 6–9.

Received 23.05.2016

doi.org/10.15407/tpwj2016.10.02

COMPARISON OF INFLUENCE OF PULSED EFFECTS OF MAGNETIC AND ELECTRIC FIELDS ON STRESSED STATE OF WELDED JOINTS OF ALUMINIUM ALLOY AMG6

L.M. LOBANOV[1], **I.P. KONDRATENKO**[2], **N.A. PASHCHIN**[1], **O.L. MIKHODUJ**[1] and **A.V. CHERKASHIN**[1]
[1]E.O. Paton Electric Welding Institute, NASU
11 Kazimir Malevich Str., 03680, Kiev, Ukraine. E-mail: office@paton.kiev.ua
[2]Institute of Electrodynamics, NASU
56 Pobedy Ave., 03680, Kiev, Ukraine

The residual welding stresses negatively affect the fatigue limit of welded joint, being the main cause for brittle fracture of metal, i.e. corrosion cracking. Therefore, the development of effective methods for control of welding stresses, characterized by low energy consumption and relatively simple realization, is traditionally an urgent problem for modern production. At the present time the methods for reducing welding stresses became widespread, based on the influence of pulses of electric current and magnetic field. Moreover, each of the methods has its advantages and disadvantages, and evaluation of their efficiency in the control of residual welding stresses represents an urgent problem. In the work the comparative evaluation of efficiency of control of residual stresses of AMg6 alloy of welded plates was carried out at treatments by pulsed electromagnetic field (TPEMF) and pulsed current (EDT), applying planar inductors. Using the method of electron speckle interferometry it was revealed that TPEMF and EDT reduce the initial level of welding stresses in the zone of pulsed effects to 100 %. 16 Ref., 1 Table, 4 Figures.

Keywords: *electrodynamic and magnetic pulse treatment, aluminium alloy, welded joint, electron speckle interferometry, efficiency of treatment, residual stresses, electroplastic effect, current density, planar inductor*

The investigations of influence of residual welding stresses on strength of welded joints, especially at cyclic loading are traditionally relevant in engineering practice of service of metallic structures. It is connected with the fact that welding stresses negatively affect the fatigue limit of welded joint, increasing the rates of fatigue crack propagation [1, 2]. In this case the tensile welding stresses at their interaction with corrosive-active environment are the main cause for brittle fracture of metal, i.e. corrosion cracking [3].

Traditionally, technological operations on reduction of welding stresses are sufficiently labor-intensive and are restricted by thermal or mechanical effect on the metal of welded joint. The development of efficient methods for control of welded stresses, characterized by low power consumption and relatively simple realization, is urgent for modern production.

In scientific and technical publications the results of investigations of influence of pulses of electric current (PEC) and magnetic field (PEMF) on relaxation of technological stresses [4–6], including residual welding stresses, are presented [7, 8]. Each of the effects mentioned above, has its advantages and disadvantages and the evaluation of efficiency of control of residual stresses is a relevant problem.

The aim of the present work was the comparative evaluation of parameters of treatment using pulsed electromagnetic field (TPEMF) and pulsed current (EDT) on reduction of residual stresses in welded joints of aluminium alloy.

Methods of investigations. To carry out investigations the specimens of welded joint and base metal of annealed aluminium alloy AMg6 were used. The mode of preliminary annealing of billets (heating to 320 °C during 1.5 h and furnace cooling) guaranteed the absence of technological stresses in metal.

The specimens of welded joint with the weld of 250 mm length were produced of two sheet billets of 360×250×4 mm size in a single pass using automatic TIG welding (Ar) in the installation ASTV-2M. The welding mode at the arc voltage U_a = 18 V, current I_a = 200 A and speed v_w = 3.1 mm/s provided the guaranteed penetration along the whole length of the joint. The schemes of performance of TPEMF and EDT of welded joint are presented in Figure 1.

TPEMF of weld was performed according to the scheme presented in Figure 1, *a*. The inductor *L*, designed as a single-turn plane circuit, was moved along the longitudinal axis of the weld at a pitch of 15 mm after each discharge cycle [8]. The outer diameter of the inductor D_{out} = 45 mm, the inner d_{inn} = 15 mm. The inductor was rigidly fixed on the surface of welded plate, which excluded its movement during the discharge cycle. The magnetic field of the inductor was

© L.M. LOBANOV, I.P. KONDRATENKO, N.A. PASHCHIN, O.L. MIKHODUJ and A.V. CHERKASHIN, 2016

excited by a current pulse generated during discharge of the capacitor on the electric circuit composed of the circuit inductivity and active resistance of conductors. The charge of the capacitor C with electric capacity of 600 μF was carried out from the source of a constant voltage of 3 kV. The commutation of electric circuit was performed by the control key *K*. During passing of electric current through the planar inductor, the magnetic field was excited, which, interacting with electric conductive plate, excited eddy currents. The interaction of magnetic field and the eddy currents induced by it led to generation of electrodynamic force, which being applied to the surface, generated the so-called magnetic pressure. The maximum amplitude of discharge current I_d^{PEMF} and the duration of its effect t_d^{PEMF}, recorded using the Rogowski coil [8], were, respectively, 35 kA and 0.5 ms. The scheme of TPEMF presented above provided the pulsed electromagnetic pressure P^{PEMF} to the local area of a weld at a simultaneous passing of electric current through that area [9].

The effect of P^{PEMF} initiated the localized fields of tensile deformations in the treated metal, the interaction of which with plastic welding compressive deformations facilitated the decrease in the level of residual stresses. The effect of electric current provided the increase in ductile properties of metal and the reduction of its resistance to deformation.

The EDT was performed during passing of pulsed current through the contact area of the copper electrode *2*, being a part of the electrode device, with the surface of welded joint 1 (Figure 1, *b*). The electrode device included a planar multi-turn inductor *L* of diameter D_e = 100 mm, and the electrode *2*, rigidly connected to the disc *3* of a non-ferromagnetic material. The interaction of magnetic field of the inductor and the eddy currents induced by it in the disc *3* results in generation of electrodynamic force, which transfers pressure P^{EDT} through the electrode *2* to the contact area simultaneously with passing of pulsed current through it. The commutation of electric circuit consisting of capacity, inductance of the inductor and active resistance of the conductors, was realized by the control key *K*. The EDT was performed at the values of U_{ch} = 500 V and C_{ch} = 6600 μF and I_d^{PEMF} and t_d^{PEMF} were, respectively, 3.1 kA and 1.0 ms [10]. The effect of EDT, as well as in the case of TPEMF, is determined by summing the two effects, the first of which is the pulsed pressure P^{EDT} preset by passing PEC through the inductor *L*, disc *3* and electrode *2*, the value of which reaches 20 kN at U_{ch} = 500 V. The second is the electric current of a specified density which spreads from the contact area. The treatment of

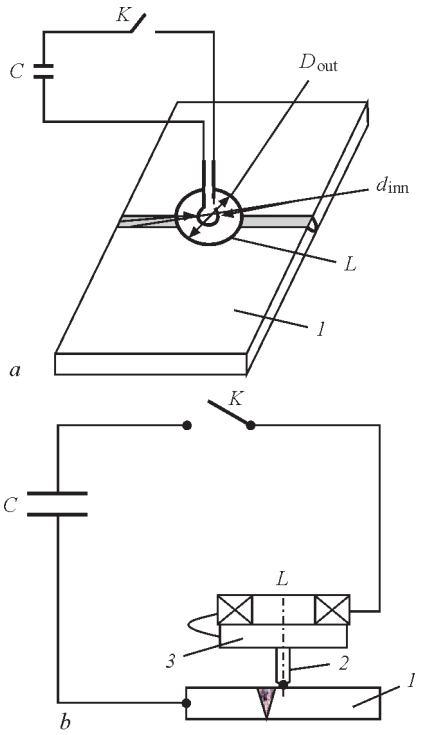

Figure 1. Scheme of discharge circuit: *a* — TPEMF [8]; *b* — EDT (see description in the text)

weld was performed according to the scheme, similar to that realized at TPEMF: the inductor was moved along the fusion line at the pitch of 5–7 mm after each PEC. In general, the mechanism of influence of P^{EDT} on welded joint is similar to that realized at TPEMF.

The difference of EDT from TPEMF is in the fact that in the first case to the treated metal a load is applied, concentrated in the zone of current-conducting end of the electrode *2* (Figure 1, *b*), and in the second — the load is distributed over the surface of the inductor *L* contacting with the treated metal (Figure 1, *a*).

To evaluate the influence of TPEMF and EDT on the stressed state of AMg6 alloy without account for the welding stresses, the treatment of plates of the base metal of 360×500×4 mm sizes was performed. TPEMF and EDT were carried out in the center of the plates by single PEC at the modes applied for treatment of welded joints. In the process of treatment of specimens the evaluation of Joule heating [9], initiated by passing PEC and PEMF through the treated material, was made. In case of TPEMF, for evaluation of changes in temperature, temporary distribution of current density and stressed state of the plate without a weld the numerical modeling was applied using finite element method.

During EDT the change in the temperature of Joule heating in the zone of electrodynamic effects was registered using thermocouples [11].

For TPEMF and EDT of welded plates the specialized assembly devices were used providing position-

ing of the inductor and a guaranteed contact of the electrode with the treated surface. The stressed state of welded plates was determined using the method of electron speckle interferometry based on the measurement of displacements, arising at the elastic unloading of metal volume in the investigated points on the surface of specimens caused by drilling blind holes. [12].

Results of experiments and their discussion. The analysis of results of evaluation of change in values of the temperature of surface of plates T_{surf} under the inductors L (Figure 1, *a*) at TPEMF, as well as in the zone of contact interaction of the electrode *2* (Figure 1, *b*) in the EDT zone, showed influence of Joule heating on the stressed state of specimens at the methods of treatment described above is almost absent. Thus, the peak values of T_{surf} at TPEMF did not exceed 25 °C [8], while at EDT — 30 °C [11], which has no significant influence on the stressed state of AMg6 alloy [10].

The evaluation of change in PEC density with time, i.e. j in the welded plate over the period of its action t at TPEMF and EDT, was carried out (Figure 2). The dependence $j = f(t)$ at TPEMF was determined by numerical method realized in the finite element formulation. The distribution of $j = f(t)$ at TPEMF, presented in curve *1* [8], has the form of attenuated sinusoid, which is characteristic for the discharge circuit with active resistance (the role of which is performed by welded specimen), which is composed of the capacitor C and inductance L. The values of j during the whole period of discharge of the capacitor are within the range of 1–4 kA/mm^2. This indicates the fact that at TPEMF the reduction in resistance of material to deformation takes place as a result of electroplastic effect (EPE) [9]. The EPE is determined as a specific action of PEC at $j \geq 1$ kA/mm^2, initiating changes of plastic properties of the material due to interaction of conductance electrons with the defects of crystal lattice (dislocations), thus increasing their mobility [13]. This creates conditions for development of inelastic deformations (microshears) in the area of defects of crystalline structure, leading to relaxation of residual stresses of the first type at the macrolevel.

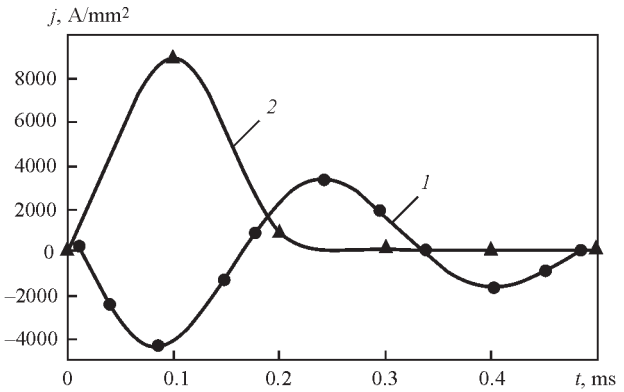

Figure 2. Distribution of current density in the annealed plate of AMg6 alloy δ = 4 mm after TPEMF [8] (curve *1*) and EDT (*2*)

The distribution of j at EDT was registered in the phase of increment of electrode effect on the treated surface of the plate. The unipolar character of the dependence $j = f(t)$ at EDT (curve *2*), calculated according to the methods, shown in the [11], is preset by configuration of discharge circuit and is determined by joint effect of dynamic load at indentation of electrode into the treated material, as well as by direct passing of PEC through it in the period of discharge cycle. Moreover, if at contact-free TPEMF, where the pressure of P^{TPEMF} is realized only by electrodynamic forces and PEC passes through the constant cross section of the plate, then at EDT the change of current in the area of contact interaction with the treated surface of electrode occurs, directly depending on the change of P^{EDT} in time. The change in the area of electrical contact of electrode with the plate is determined by the laws of elastic-plastic contact of interaction of the system «sphere-plane» at a zero initial gap [14]. The temporary ratios of values of pulsed current and contact area of electrode, determining the change of j at EDT, are presented in the work [11]. At the initial stage of increment of pulsed current, corresponding to the period of time t = 0–0.1 ms (curve *2*), the area of electrical contact of the pair «electrode-metal» is minimal, which causes an increment of values of j up to 9.0 kA/mm^2. With increase in contact area to the maximum value at the time t = 0.1–0.6 ms, the value j monotonously decreases to 0.15 kA/mm^2.

Analyzing the distribution $j = f(t)$ at EDT in curve *2*, it can be concluded that at the initial phase of indentation of electrode at t = 0–0.2 ms the EPE also takes place, the influence of which is minimal in the period of t = 0.2–0.5 ms. The efficiency of EDT, as is mentioned above, is determined by the combined effect of current and dynamic components of the process. Thus, the dynamic load creates conditions for breakthrough of barriers by dislocation factions, and a direct passing of PEC of high density provides propagation of dislocations in a directed flow of conduction electrons, which corresponds to the concept of electron-dislocation interaction [9]. In detail the mechanism of effect on the conductive materials at EDT is described in the work [15].

At the comparison of curves *1* and *2* in Figure 2 it can be seen that considering the fact that the influence of EPE on the structure and ductility of the material directly depends on the value j [9], the contribution of EPE to relaxation of stresses at EDT is more expressed, than at TPEMF. This is connected with peculiarities of passing PEC in the discharge circuits used

at both types of treatment. Thus, the absolute value of current density at TPEMF is not more than 4 kA/mm^2, whereas at EDT it reaches 9 kA/mm^2. Moreover, for TPEMF the bipolar PEC and for the EDT the unipolar one are characteristic, which affects the efficiency of electric pulsed effects. Thus, in the work [16] it is shown that at the same amount of electricity and amplitude of PEC, passed through the loaded specimen, the bipolar pulses cause a lower relaxation (jump) of stresses, than unipolar ones. This, according to the authors' opinion, is caused by the fact that the successive PEC of different polarity counteract each other initiating the movement of dislocations in the opposite directions due to which the resultant of the Burgers vector is lower than that at the unipolar PEC.

The comparative evaluation of distributions of tangential stresses σ_θ after TPEMF and EDT was carried out on the surface of the annealed plates of AMg6 alloy (Figure 3). The scheme of applying the effect of TPEMF and EDT to the plate as well as location on the specimen of cross-section, where σ_θ was determined, is shown in Figure 3, *a*. The diagram of σ_θ after TPEMF [8] (Figure 3, *b*, curve *1*) has a form of a sinusoid with two zones of tension balanced by the compression zone located between them. The first zone of tension with a maximum value of σ_θ = = 7 MPa was located at the area l = 0–8 mm of the plate cross-section, located under the center of the inner hole of the inductor. The second zone of tensile stresses with the maximum value σ_θ = 18 MPa, was located in the area of the plate l = 24–45 mm from the center of the inductor. The zone of compressive stresses with the maximum value σ_θ = –35 MPa, was located in the area l = 8–24 mm from the center of the hole. The maximum effects fell on the area of section of the plate surface located below the generatrix of the inner cylindrical surface of the inductor L of d_{inn} diameter. Analyzing the distribution of σ_θ in curve *1*, it can be concluded that TPEMF (at the preset process parameters) facilitates compressive stresses, reaching not more than 0.25–0.3$\sigma_{0.2}$ in AMg6 alloy.

The distribution of stresses after EDT [11] (Figure 3, *b*, curve *2*), is characterized by compression area with the maximum value to σ_θ = –160 MPa, localized in the zone of contact interaction of electrode *2* (Figure 1, *b*) with the treated surface. The compression zone is balanced by a monotonically decreasing field of tensile stresses with the peak value σ_θ = 60 MPa, located at the 15 mm distance from the longitudinal axis of the electrode. Analyzing the distribution of σ_θ shown in curve *2*, it can be concluded that EDT stimulates compressive stresses in the AMg6 alloy, close to the value of $\sigma_{0.2}$ for AMg6 alloy. The distribution of longitudinal (relatively to the weld axis) σ_x component of residual welding stresses in the central cross section of plates before and after TPEMF and EDT, is shown in Figure 4. It is seen from Figure that before treatment the maximum values σ_x are close to the conditional yield strength $\sigma_{0.2}$ of AMg6 alloy. Comparing the appearance of diagrams σ_x before (curve *1*) [7, 8], as well as after TPEMF (curve *2*) [8] and EDT (curve *3*) [7], it can be seen that the pulsed effects influence the distribution of stresses in the treated section.

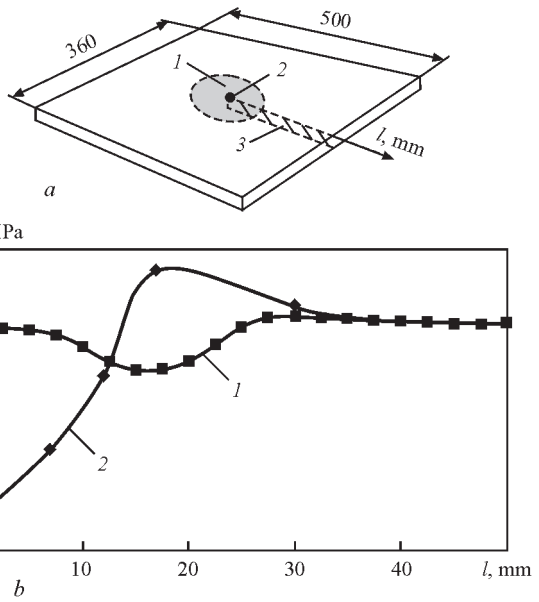

Figure 3. Tangential stresses σ_θ in the annealed plate of AMg6 alloy δ = 4 mm after TPEMF [8] and EDT [11]: *a* — investigated plate (*1* — zone of TPEMF effect; *2* — EDT; *3* — section in which σ_θ was determined); *b* — distribution of σ_θ after TPEMF (curve *1*), after EDT (2)

Analyzing the distribution of σ_x presented in curve *2*, it can be seen that the area of effective influence at TPEMF is comparable with the inner diameter of planar inductor, the value of which is 15 mm. The arrangement of inductor was preset in such a way that the highest density of power lines of TPEMF fell on

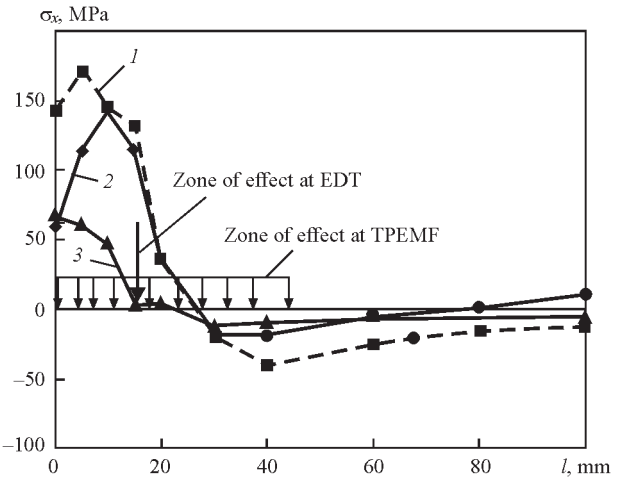

Figure 4. Distribution of welding residual stresses σ_x in the plate of AMg6 alloy δ = 4 mm without treatment (curve *1*), after TPEMF [8] (*2*) and EDT (*3*)

Values of electric and mechanical parameters of TPEMF and EDT

Type of treatment	Charge capacity C_{ch}, μF	Charge voltage U_{ch}, V	Discharge current I_d, kA	Charge power E_{ch}, J	Stress before treatment σ_0, MPa	Stress after treatment σ_{tr}, MPa	Decrease in stress $\Delta\sigma$, MPa	Specific power of treatment $E_s/\Delta\sigma$, J/MPa
TPEMF	600	3000	35.0	2700	148	52	96	28.1
EDT	6600	500	3.0	825	130	5	125	6.6

the weld metal, which determined the maximum efficiency of treatment of the mentioned area. So, the value σ_x in the weld zone reduced to 50 MPa, which makes 35 % of values of stresses before TPEMF. At the distance from the center of the weld for 5 mm the values σ_x make 65 % of initial ones, and at the distance of 15 mm the TPEMF almost does not influence the distribution of σ_x. From the comparison of curves *1* and *2* in Figure 4 it follows that the effectiveness of TPEMF on welded joint is monotonously decreased towards edges of the inner diameter of the inductor. Thus, if is accepted the area of tension diagram $S_{\sigma+}$ on the curve 1 (Figure 4) as over 100 %, than as the result of TPEMF (curve *2*) the value $S_{\sigma+}$ is reduced by 23 %.

Analyzing the distribution of σ_x after EDT (curve *3*) it can be seen that the influence of the latter on decrease in stresses is more expressed as compared to the effect of TPEMF. The efficiency of effect at EDT is obviously determined by the character of concentrated energy input into the treated metal (unlike the distributed effect at TPEMF) and the ratio of value P^{EDT} and amplitude of pulsed current. Thus, after EDT the reduction of tensile σ_x occurs in the area of effect (arrow in Figure 4) from 120 to 5 MPa. The character of distribution of σ_x after EDT is connected with the fact that in the discharge cycle the electrodynamic effect initiates the wave of tensile deformation in the near-weld zone [15], the interaction of which with residual stresses of weld causes a localized plastic deformation, which determines the character of σ_x distribution after treatment of the plate. The EDT of butt welded joint of AMg6 alloy causes a decrease in residual welding stresses in the treatment zone to the values close to zero. Therefore, the value of $S_{\sigma+}$ as a result of EDT (curve *3*) is reduced by 76 %.

The comparative evaluation of power consumption, required for reduction of stresses as a result of a single pulsed effect, realized at the two described types of treatment, was carried out. As the evaluation characteristic, the specific stored energy E_s of the capacitor was used, consumed for reducing the level of stressed state Δ_σ per one MPa — E_s/Δ_σ. The values of Δ_σ for TPEMF and EDT were preset on the basis of maximum of values σ_x, registered before treatment σ_0 and after σ_{tr} in the area of pulsed effect (Figure 4):

$$\Delta\sigma = \sigma_0 - \sigma_{tr}, \text{ MPa}. \quad (1)$$

The calculation of values E_s was performed using the expression for the stored energy of the capacitor [4]. The values of electrical and mechanical parameters for the described effects, used for evaluation of E_s/Δ_σ are presented in the Table.

Analyzing the data of the table, it can be seen that the value of the stored energy of EDT, consumed for reduction of residual welding stresses in the AMg6 alloy per one MPa, is four times lower than the similar value at TPEMF. This is an essential factor in selecting the type of treatment of long welded joints, where the number of effects can be hundreds and thousands.

It is necessary to mention the technological features of TPEMF application, that can be seen when comparing the values of U_{ch} for two types of treatment. This is connected, first of all, with the use of high voltage (over 1000 V) at TPEMF for inductors power supply, which results in increasing cost of electrotechnical equipment, possible undesirable electrophysical phenomena (breakdown of electrical insulation, spark processes and etc.). In the use of TPEMF it is assumed that the inductor is a consumable element of the equipment complex. Taking into account the most of positive results on redistribution of welding stresses after TPEMF, presented in Figure 4, it would be appropriate to carry out investigations on optimization of the design of inductor and treatment modes, aimed at intensification of TPEMF effect on welded joints of structural materials.

Among the disadvantages of EDT a high degree of localization of pulsed current effect should be mentioned, which requires a great number of electrode movements along the weld line as compared to TPEMF. The further investigations on improving the efficiency of EDT should be directed both to expanding the zone of influence of effect of discharge current, as well as to the development of technological measures for improving the contribution of EPE to the pulsed effect, aimed at regulating the stressed state of welded joints. Moreover, for two types of treatment it is relevant to increase their power characteristics, aimed at transformation of tensile stresses into compressive ones.

Based on the carried out work it can be concluded that the two considered methods are characterized by a significant potential for the control of residual

stress-strain state of welded joints, which implies carrying out further investigations on their improvement.

Conclusions

1. The comparative evaluation of efficiency of control of residual stresses of welded plates of AMg6 alloy was carried out at treatments using pulsed electromagnetic field (TPEMF) and pulsed current (EDT), performed with planar inductors.

2. It was established that TPEMF and EDT allow reducing the initial level of welding stresses in the area of pulsed effects, respectively, by 65 and 100 %.

3. It was established that the value of the stored energy of EDT, consumed for reduction of welding residual stresses in AMg6 alloy per one MPa, is four times reduced than the similar value at TPEMF.

4. It was shown that unlike EDT, the use of TPEMF, is connected with the use of high voltages (over 1000 V) for the power supply of inductors, which results in increase in the cost of electrical equipment, possible undesirable electrophysical phenomena (breakdown of electrical insulation, spark processes, etc.).

5. It was shown that TPEMF and EDT are characterized by a significant potential for the control of residual stress-strain state of welded joints, which involves carrying out further investigations for their improvement.

1. Trufyakov, V.I. (1973) *Fatigue of welded joints*. Kiev: Naukova Dumka.
2. Trufyakov, V.I., Mikheev, P.P., Kuzmenko, A.Z. (1980) Influence of scale factors and residual welding stresses on rate of fatigue crack propagation. *Problemy Prochnosti*, **6**, 20–22, 30.
3. Petuchkov, V.G., Kudinov, V.M., Fadeenko, Yu.I. (1993) *Explosion treatment of welded joints of metal structures*. Moscow: Metallurgiya.
4. Antonov, Yu.A., Ragozin, Yu.I. (2001) Pulse method of residual stress relieving. *Fizika i Khimiya Obrab. Materialov*, **3**, 91–95.
5. Tang, F., Lu, A.L., Mei, J.F. et al. (1998) Research on residual stress reduction by a low frequency alternating magnetic field. *J. of Materials Processing Technology*, **74**, 255–258.
6. Stepanov, G.V., Babutsky, A.I. (2007) Modeling of stress relaxation under action of high density pulse current. *Problemy Prochnosti*, **2**, 113–120.
7. Lobanov, L., Pashchin, N., Pivtorak, V. et al. (2014) Application of local current pulses for determination and control of residual stresses. *Advanced Materials Research*, **996**, 386–391.
8. Stepanov, G.V., Babutsky, A.I., Mameev, I.A. et al. (2011) Redistribution of residual welding stresses due to treatment by pulse electromagnetic field. *Problemy Prochnosti*, **3**, 121–131.
9. Baranov, Yu.V., Troitsky, O.A., Avramov, Yu.S. (2001) *Physical principles of electroplastic treatment and new materials*. Moscow: MGIU.
10. Lobanov, L.M., Pashchin, N.A., Cherkashin, A.V. et al. (2012) Efficiency of electrodynamic treatment of aluminium alloy AMg6 and its welded joints. *The Paton Welding J.*, **1**, 2–6.
11. *UDK 658.562:* Report (final) of research activity on project R 7.3.1: To develop the technology and equipment for prompt non-destructive determination of residual stresses in welded structures based on application of local current pulse and electron speckle interferometry. Nat. Registr. 011U003481. Kiev: PWI.
12. Lobanov, L.M., Pivtorak, V.A., Savitsky, V.V. et al. (2006) Procedure for determination of residual stresses in welded joints and structural elements using electron speckle interferometry. *The Paton Welding J.*, **1**, 24–29.
13. Kravchenko, V.Ya. (1966) Effect of directed electron flow on moving dislocations. *Zh. Experimentalnoj i Teoreticheskoj Fiziki*, **51**, Issue 6(12), 1677–1688.
14. Johnson, K. (1989) *Mechanics of contact interaction*. Moscow: Mir.
15. Lobanov, L.M., Pashchin, N.A., Mikhoduj, O.L. et al. (2012) Effectiveness of various variants of electrodynamic treatment of AMg6 alloy and its welded joints. *The Paton Welding J.*, **12**, 26–31.
16. Troitsky, O.A., Kalymbetov, P.U. (1981) Dependence of electroplastic effect in zinc on isolated pulse duration. *Fizika Metallov i Metallovedenie*, 51(Issue 5), 1056–1059.

Received 30.06.2016

doi.org/10.15407/tpwj2016.10.03

PREDICTION OF LIMITING AMPLITUDES OF CYCLE STRESSES OF WELDED JOINTS WITH STEADY RESIDUAL STRESSES

V.A. DEGTYAREV
G.S. Pisarenko Institute for Problems of Strength, NASU
2 Timiryazevskaya Str., 01014, Kiev, Ukraine. E-mail: ips@ipp.kiev.ua

In the work the method for determination of diagrams of limiting amplitudes of the cycle of welded joints with steady residual tensile stresses is proposed based on the results of tests of small specimens, which can be considered as an express method for calculation of characteristics of fatigue resistance of welded joints when there is no possibility to carry out full-scale investigations and the appropriate computational dependences are presented. The analysis of literature data for different types of welded joints showed satisfactory correlation of experimental and calculated values of fatigue limits of welded joints of low-carbon and low-alloyed steels of a low strength. It was established that all the diagrams of limiting amplitudes of the cycle of welded joints with steady residual stresses are finished on the line, where each point at different mean stresses of the cycle corresponds to the minimum limiting amplitude of the cycle of welded joint with its value of limiting steady residual stress, which provides realization of limiting stresses of cycle. It was shown that if at the low values of steady residual stresses the relative reduction in fatigue limits of butt welded joints of steels of different strength is occurred almost for the same value, then with their increase, the reduction of fatigue limit of steel with higher mechanical characteristics is more significant. 23 Ref., 1 Table, 3 Figures.

Keywords: *amplitude of cycle stresses, mean stress of cycle, yield strength, steady residual stress, fatigue limit, diagram of limiting amplitudes of cycle*

Numerous investigations indicate, that among the whole number of factors which determine the load-carrying capacity of welded metal structures of different purpose, welding residual stresses (RS) play a significant role [1, 2]. In the greatest extent the influence of tensile RS on the fatigue limits is revealed at symmetric loading cycle and is considerably reduced due to a more significant relaxation with the increase in the level of operating stresses or the ratio of asymmetry cycle R_σ [3–5]. As far as the reduction of RS occurs mainly during several tens of cycles of loading to a specified value, then the set value of residual stresses σ^s_{res} plays the main role in decreasing the fatigue limit of welded joint [6, 7], the method of determination of which is presented in the work [8]. This should be reflected on the character of diagrams of limiting stresses of the cycle (DLSC) [8] or limiting amplitudes of the cycle (DLAC). If for welded joints without RS the limiting amplitude σ_a depends on the mean stress of the cycle σ_m, then for all the types of welded joints of different strength with high RS such dependence is not observed. As the determination of diagrams is based, as a rule, only on the stresses from external load, not accounting for RS, then the determination of DLAC of welded joints, containing different level of σ^s_{res}, can be important for artificial control of residual stresses during prediction of limiting state of welded metal structures. Undoubtedly, the most valid data can be obtained during tests of full-scale elements of metal structures containing the different level of σ^s_{res}. However, due to considerable material costs a number of experimental investigations of influence of the level σ^s_{res} on fatigue resistance of welded joints is extremely limited. Therefore, the development of the method for determination of DLSC or DLAC of welded joints with RS according to the results of tests of small specimens is urgent. Earlier, in the work [9] the method for determination of fatigue limits of welded joints with high RS was proposed based on the results of tests of small specimens considering the established fact of intersection of diagrams of limiting stresses of cycle. In the works [8, 10] the determination of diagrams of limiting stresses of the cycle of welded joints with different value of initial RS was proposed based on the results of small specimens tests and the level of limiting initial residual stress was calculated which provides realization of the limiting cycle of stresses. At the same time the methods proposed until now can not provide an unambiguous answer, where the diagrams of limiting amplitudes of the cycle of welded joints with different value of steady residual stresses are finished and why they are parallel to the diagram of limiting amplitudes of the cycle of specimens without RS. Moreover, the proposed methods did not find experimental confirmation for different types of weld-

© V.A. DEGTYAREV, 2016

ed joints, and it is unclear whether they can be applied to welded joints with different mechanical properties. In this regard, in the present work the calculated method for determination of limiting amplitudes of cycle of welded joints with different levels of steady residual tensile stresses was grounded based on the results of tests of small specimens without RS at their comparison with experimental data and the cause was revealed explaining why diagrams of limiting amplitudes of the cycle of welded joints with different value σ^s_{res} are finished on the line having the same value of minimum limiting amplitude of cycle, independent of the mean stress of cycle.

Analysis of obtained results. During tests at a single value R_σ the diagram of limiting amplitudes of cycle of welded specimens without residual stresses (Figure 1, line *1*) is usually represented in the form:

$$\sigma_a = \sigma_{-1} - \psi_\sigma \cdot \sigma'_m, \quad (1)$$

where σ_{-1} is the fatigue limit of welded joint at a symmetric cycle of stresses; σ_m is the actual value of mean stress of cycle; ψ_σ is the coefficient of sensitivity to the asymmetry of the cycle of stresses, which is determined at a known value of ultimate strength of the material σ_t by the ratio of σ_{-1}/σ_f.

According to this dependence the limiting amplitude of stresses σ_a depends on the mean stress σ_m. It should be noted that in the present work the influence of the theoretical coefficient of stress concentration was not considered because of determination of DLSC or DLAC, accepted in the work [11], only on the action of nominal stresses. The analysis of results of tests of different types of welded joints with high residual stresses, obtained experimentally, shows that σ_a does not depend on σ_m in this case (line *3*). [4] With the growth of mean stress or the asymmetry coefficient of the cycle, the difference between the limiting amplitudes of welded specimens with residual stresses and without them is reduced and approximately in the point, corresponding to the yield strength σ_y of the material, the lines 1 and 3 are intersected [8, 12]. In this case the limiting amplitude reaches its minimum value σ^l_a at the mean stress σ_{mY} (y, A) and has the same value for welded joints without RS and with them. Thus, the value σ^l_a may be determined using calculation method at the known value of fatigue limit of welded joint without RS in the following form:

$$\sigma^n_a = \sigma_{-1} - \psi_\sigma \cdot \sigma_{mY}. \quad (2)$$

Taking into account that $\sigma^l_a = \sigma_Y - \sigma_{mY}$ having substituted it to (2), it can be written that

$$\sigma_{mY} = \frac{\sigma_Y - \sigma_{-1}}{1 - \psi_\sigma}. \quad (3)$$

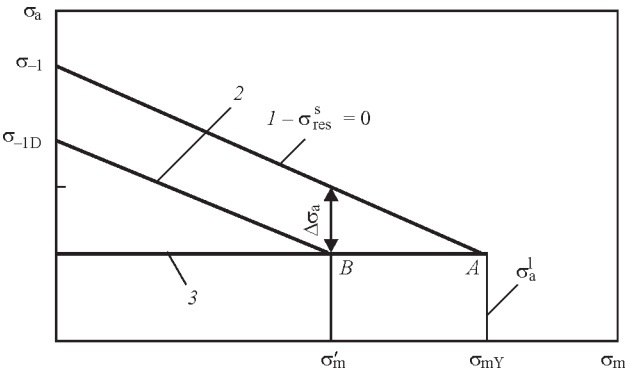

Figure 1. Scheme for determination of diagrams of limiting amplitudes of cycle of welded joints with steady residual stresses: *1* — diagram of limiting amplitudes of cycle of welded specimens without residual stresses; *2* — calculated diagram of limiting amplitudes of cycle of welded specimens with steady residual stress; *3* — diagram of minimum limiting amplitudes of cycle

Thus, the dependence for determination of σ^l_a can be represented as

$$\sigma^l_a = \frac{\sigma_{-1} - \psi_\sigma \sigma_Y}{1 - \psi_\sigma}. \quad (4)$$

The earlier analysis of literature data [12] showed, that if we present the results of investigations of different types of welded joints of low-carbon and low-alloyed steels with the steady residual stresses σ^s_{res} in the form of the sum of the limiting amplitude of the cycle σ_{RD} of such a joint and the steady residual stress, which is considered as a static component, i. e. ($\sigma_{R\Sigma}$ = $= \sigma_{RD} + \sigma^s_{res}$), and the mean stress, respectively, in the form of $\sigma_{m\Sigma} = \sigma_m + \sigma^s_{res}$, then independently of the level of residual stress all the points are satisfactorily lie on DLSC of welded joints without residual stresses, described by the dependence of Goodman [11]

$$\sigma_{max} = \sigma_{-1} + (1 - \psi_\sigma)\sigma'_m. \quad (5)$$

Moreover, when the sum of the initial residual stresses and stresses from external load, i. e. the fatigue limit, does not reach the yield strength of the material, the steady RS correspond to the initial ones and in this case the summed stresses are located at the inclined area of a diagram. After $\sigma_{R\Sigma}$ reaches the yield strength of the material, the relaxation of the initial RS to the steady level (maximum level) occurs and, in spite of the different values σ^s_{res}, obtained depending on the stresses from external load, the realization of a single limiting cycle of stresses is provided. In this case, the results of tests of specimens with different value of the steady residual stresses can be appropriately described by the equation in the form:

$$\sigma_{R\Sigma} = \sigma_{-1} + (1 - \psi_\sigma) \cdot (\sigma'_m + \sigma^s_{res}). \quad (6)$$

In the absence of RS the equation (6) acquires the form (5). It should be noted that the given expression is valid under the condition that the influence of the steady residual stress and mean stress from the ex-

ternal load on the fatigue resistance of welded joints is identical. Consequently, the sensitivity of welded joints with different value of steady residual stresses to the loading asymmetry must also be the same. In addition, one should bear in mind that the expression for determination of steady residual stress bears an idealized character and provides an approximate calculation [8]. It is connected with the fact that during cyclic deformation, when total stresses, as a rule exceed the elastic limit of material as a result of accumulation of inelastic deformations, the cycle-by-cycle reduction of the initial RS occurs. Therefore, to determine it more accurately, the additional experimental information or information about inelastic deformation of the investigated material [13] or the diagrams of the limits of cyclic creep at the preliminary specified tolerance for residual deformation, providing reduction of RS to the predetermined value, are required [14]. However, in practice the widespread use of the mentioned dependence is connected with the accessibility of rapid determination of values included in it.

The fact of presence of a single diagram allows, firstly, selecting the required modes of loading the welded structure to achieve the preset σ^s_{res} in it, and, secondly, determining the diagrams of limiting stresses of the cycle or limiting amplitudes of the cycle of welded joints with the preset value σ^s_{res} based only on the stresses from external load using the results of tests of welded joints without RS. Taking into account that $\sigma_{aD} = \sigma_{R\Sigma} - \sigma_{m\Sigma}$, the dependence for determination of DLAC of welded specimens with a preset value of steady residual stresses (Figure 1, line *2*) can be written as

$$\sigma_{aD} = \sigma_{-1} - \psi_\sigma \cdot (\sigma'_m + \sigma^s_{res}), \quad (7)$$

or

$$\sigma_{aD} = \sigma_{-1}(1 - \frac{\sigma'_m + \sigma^s_{res}}{\sigma_?}). \quad (8)$$

In this case, the inclined area of the diagram after the joint solution of equations (1) and (7) is displaced to the value $\Delta\sigma = \psi_\sigma \sigma^s_{res}$ in parallel relatively to DLAC of welded specimens without RS.

The mean stress from the external load, under the action of which the preset value σ^s_{res} remains in welded specimen, can be easily determined by solving the equation (7) relatively to σ_m, taking into account that $\psi_\sigma = (\sigma_{-1} - \sigma^l_a) / \sigma_{mY}$

$$\sigma'_m = \frac{\sigma_{-1} - \sigma_{aD}}{\psi_\sigma} - \sigma^s_{res}. \quad (9)$$

Particularly interesting is the answer to the question, where DLAC of welded joints with the preset value σ^s_{res} is finished. After conversion of the equation (2) relatively to σ_{mY} and the combined solution of equations (2) and (9) we shall obtain finally that the mean stress for welded specimens with the steady residual stress, which in this case will be limiting, and thus $\sigma_{aD} = \sigma^l_a$ is displaced along the line 3 to the value $\Delta\sigma_m = \sigma_{mY} - \sigma_m = \sigma^s_{res}$ (p·B). Thus, each point at this straight line at different mean stresses of the cycle corresponds to the minimum limiting amplitude of the cycle of welded joint with its value of limiting steady residual stress, which provides finally the realization of the limiting cycle of stresses.

As an example, in the Table for different types of welded joints made of steels of different strength, the literature data are given experimentally obtained on the basis of 2×10^6 cycles of fatigue limits at a symmetric loading cycle at different values σ^s_{res} and their calculated values. The Table presents also the experimental values of fatigue limits of welded joints without residual stresses. The comparison of results of calculated evaluation of the influence of steady RS on fatigue limits of welded joints according to the proposed methods and experimental data showed a good correlation for welded joints of low-carbon and low-alloyed steels of a low strength. It is seen that the difference is within the range of 3–11 MPa, which corresponds to the error of 6–20 %. Concerning the welded joint of low-alloyed steel 10KhSND, it is seen that due to a low fatigue limit, a small difference in the calculated and experimental values leads to a noticeable error. Moreover, the analysis of Table data showed that for high-strength steels (14KhMDFR) the proposed methods of calculation lead to a significant error. This is apparently connected with the fact that, having an elongated character of the diagrams of limiting amplitudes in welded joints of such steels, such processes are probably developed at the increase in mean stress with the accumulation of cycles, which can increase not only the strength of metal, but also increase the limiting value of stresses amplitude in this case. In this regard, the diagrams of limiting stresses or amplitudes may have a hyperbolic character [23]. It shows once again that hypothetical dependences of the type of Smith or Hay, describing the behavior of diagrams of the investigated materials, which are often used in the literature, should be considered as approximate, not reflecting the whole complexity and multifactorial nature of fatigue of the welded joints. Nevertheless, the analysis of the results allows concluding that under certain difficulties in carrying out fatigue tests or absence of experimental data the presented methods can be used as an express method for calculation determination of fatigue characteristics of welded joints of low-carbon and low-alloyed steels with a different value σ^s_{res}.

Comparison of experimental and calculation values of fatigue limits of different types of welded joints produced of different strength materials (MPa)

Steel, type of joint	σ_y, MPa	σ^s_{res}, MPa	σ^l_a, MPa	σ_m, MPa	σ^e_{-1}, MPa	σ^p_{-1}, MPa	Δ	Reference
St. 3, cruciform	300	0 127	21.5 –	278.5 151.5	40 28.5	31.5	–3	[15]
M16S, butt	237	0 160	72 –	165 0	116 76	72	4	[16]
14KhMDFR, butt	600	0 450	20 –	580 0	110 70	40	30	[17] [4]
Low-carbon, butt	300	0 230	56 –	244 15	108 69	59	10	[8]
09G2S, with deposits	317	0 150	60 –	257 107	120 95	85	10	[18]
Low-carbon with transverse fillet welds	240	0 175	68 –	172 0	80 60	68	–8	[19]
St.3, welding-on of transverse stiffeners	260	0 220	40 –	220 0	80 40	38	2	[20] [4]
10KhSND, welding-on of transverse stiffeners	442	0 410	30 –	412 0	99 20	30	–10	[21] [4]
09G2S, butt	339	0 270	64 –	276 0	136 75	64	11	[22] [4]
09G2, butt	343	0 160	67 –	276 –	155 99	105	–6	[9]
St. 3(killed), overlapped with flange weld and welding around the contour	230	0 195	27 –	203 –0	54 35	28	7	[1] [4]
Note. Upper value is for specimens without residual stresses, lower value is for specimens with steady residual stresses.								

To determine the asymmetry coefficient of cycle at which the residual stresses are relaxed completely, it is enough to write that

$$\sigma_{RD} = \frac{2\sigma^l_a}{1 - R_\sigma} = \sigma_Y. \quad (10)$$

Substituting the expression (2) to (10), after some transformations it can be established that intersection of diagrams of limiting amplitudes of the cycle of welded joints without residual stresses and with the steady level of residual stresses (Figure 1, lines *7* and *3*) will occur at

$$R = 1 - \frac{2(\sigma_{-1} - \psi_\sigma \sigma_{mY})}{\sigma_Y}. \quad (11)$$

It is easy to determine the asymmetry coefficient of the cycle, at which intersection of diagrams of limiting amplitudes of the cycle of welded joints with the set value of residual stresses occurs with the line *3*, knowing that $\sigma_{aD} = \sigma^l_a$ and $\sigma_{RD} = \sigma_{aD} + \sigma_m = \sigma_Y - \sigma_{mY} + \sigma_m$. Substituting the expression (7) to (10), it can be written that

$$\sigma_Y - \sigma_{mY} + \sigma'_m = \frac{2(\sigma_{-1} - \psi_\sigma \sigma^s_{res} - \psi_\sigma \sigma'_m)}{1 - R}. \quad (12)$$

After some transformations we will obtain that

$$R = 1 - \frac{2(\sigma_{-1} - \psi_\sigma \sigma_{mY})}{\sigma_Y - \sigma^s_{res}}. \quad (13)$$

Thus, the higher the value σ^s_{res}, the lower the value R_σ at which intersection of diagrams of limiting amplitudes of the cycle of welded joints occurs with the line *3*. It should be noted that the degree of influence of RS on fatigue resistance of welded joints depends not only on their level, but also on the parameters of external load as well as mechanical characteristics of the used materials. The mentioned calculated ratios allow evaluating not only the influence of RS on fatigue limits, but also calculating the fatigue strength of welded elements of metal structures at artificial regulation of residual stresses in them.

As an example of calculation according to the proposed methods, Figure 2 presents a series of diagrams of limiting amplitudes of the cycle of butt welded joints of low-carbon steel St.3 (killed) (σ_y = 300 MPa) and low-alloyed steel 09G2S (σ_y = 340 MPa) with different level of steady residual stresses. It is seen that the diagrams are parallel not only between themselves but also DLAC of welded joints without RS. Moreover, their displacement relatively to each other occurs for the value equal to $\Delta\sigma_a = \psi_\sigma \sigma^s_{res}$. All the diagrams are finished at the points located on a straight line *6*, which is parallel to the mean stress of the cycle. It means that regardless of the level of the steady residual stresses, all the diagrams of limiting amplitudes of the cycle have the same value of the minimum limiting amplitude σ^l_a equal to 56 MPa for low-carbon and 64 MPa for low-alloyed steels at different value of mean stress of the cycle, and it does not contradict to the literature data [10]. In this connection it can be noted that in reality the mentioned

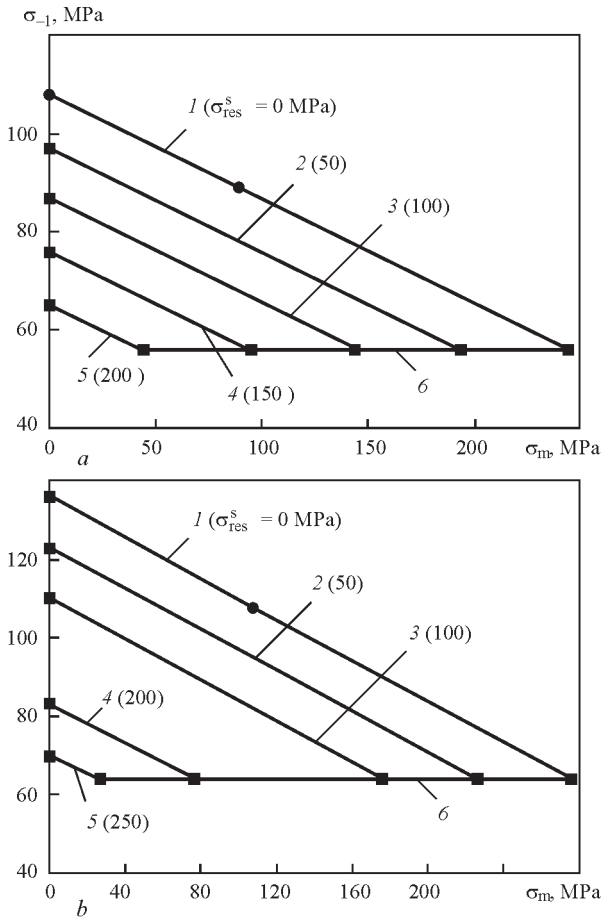

Figure 2. Diagrams of limiting amplitudes of cycle of butt welded joints of low-carbon steel St. 3 (killed) (*a*) and low-alloyed steel 09G2S (*b*): *1* — without residual stresses; *2–5* — with specified level of residual stresses; *6* — diagram of minimum limiting amplitudes of cycle (●, ■ — experimental and calculated values of fatigue limits, respectively)

straight line *6* is not the diagram of limiting amplitudes of the cycle of welded joints with high RS, as it is usually called at the present time in the literature [4] but most probably the diagram of minimum limiting amplitudes of the cycle (DMLAC), where each point on the mentioned straight line is nothing else than a totality of fatigue limits of welded joint with its value of limiting steady residual stress, which provides the realization of the limiting cycle of stresses. Regarding the diagrams of limiting stresses of the cycle, then it is better to call such a straight line as the diagram of minimum limiting stresses of the cycle with its value of limiting σ^s_{res}.

The sensitivity of butt welded joints of steels of different strength to the value σ^s_{res} is illustrated in Figure 3. Taking into account the experimental and calculated data, the Figure presents the dependences of changes in their fatigue limits at symmetric loading cycle on the value of steady residual stresses in relative coordinates. From the analysis of Figure it follows that at low values σ^s_{res} the relative reduction of fatigue limits of welded joints σ_{-1D} occurs almost

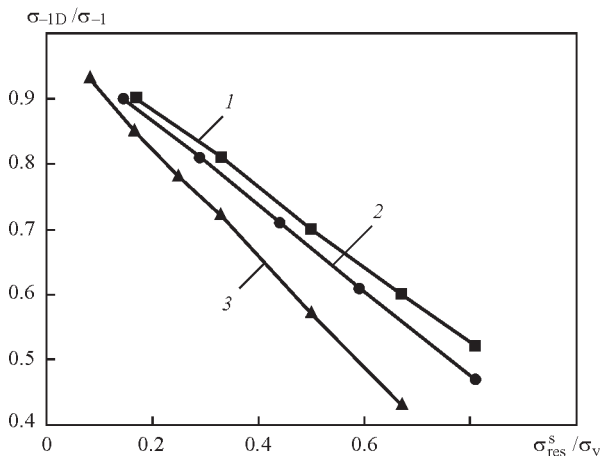

Figure 3. Influence of steady residual stresses on fatigue limits of butt welded joints: *1* — low-carbon steel St. 3(killed) (σ_y = = 300 MPa); *2* — low-alloyed steel 09G2S (σ_y = 340 MPa); *3* — low-alloyed high-strength steel 14KhMDFR (σ_y = 600 MPa)

to the same value. However, with increase in σ^s_{res}, the reduction of fatigue limit of welded joints of steel with higher mechanical characteristics is more significant as a result of which the curves diverge. For example, at the value σ^s_{res} equal to 0.5 σ_y, the reduction in fatigue limit of welded joint of low-carbon and high-strength steel occurs at 30 and 43 %, respectively. If the twice reduction of fatigue strength of welded joint of steel 14KhMDFR is achieved at the value σ^s_{res} equal to 0.6 σ_y, then for the welded joint of steel St. 3(killed) it is achieved almost at 0.85σ_y. It can be noted that the practical value of the Figure consists in the presented possibility to determine the selection of steel at the presence of steady residual stresses in the elements of metal structures of the known value without additional labor consuming investigations of large-sized specimens.

Thus, the presented methods can be considered as an express method for calculation of characteristics of fatigue resistance of welded joints, containing different level of steady residual stresses when there is no possibility for full-scale experimental investigations.

Conclusions

1. The method for determination of diagrams of limiting amplitudes of cycle of welded joints of low-carbon and low-alloyed steels of low strength with the steady residual stresses was proposed and experimentally confirmed.

2. The regularity of change in fatigue limits of butt welded joints of different strength steels was established based on their mechanical characteristics and steady residual stress.

1. Duchinsky, B.N. (1956) Endurance of components of welded bridge structures in fluctuating and alternate stresses. In: *Ex-*

amination of strength of welded bridge structures. Issue 20. Moscow: Transzheldorizdat.
2. Okerblom, N.O. (1950) *Welding stresses in metal structures*. Moscow; Leningrad: Mashgiz.
3. Hobbacher, A. Recommendations on fatigue of welded components. *IIW Doc. X-1539-94-XV-845–94*.
4. Trufyakov, V.I. (1973) *Fatigue of welded joints*. Kiev: Naukova Dumka.
5. Bajkova, I.P. (1969) Influence of external tensile load on welded strains and stresses. *Svarochn. Proizvodstvo*, **6**, 3–5.
6. Ryakhin, V.A., Moshkarev, G.N. (1984) *Service life and stability of welded structures of construction site and road making machines*. Moscow: Mashinostroenie.
7. Dawson, R. (1980) Vibration stress relieving and study of its efficiency. *Teoreticheskie Osnovy*, 102(**2**), 1–9.
8. Trufyakov, V.I., Kudryavtsev, Yu.F., Mikheev, P.P. (1988) On effect of residual stresses on fatigue resistance of welded joints. *Avtomatich. Svarka*, **2**, 1–4.
9. Shulginov, B.S., Degtyarev, V.A., Matveev, V.V. (1984) On limit cycle stresses of welded joints with high residual stresses. *Problemy Prochnosti*, **3**, 58–61.
10. Trufyakov, V.I., Mikheev, P.P., Kudryavtsev, Yu.F. (1988) Change of fatigue resistance of welded joints under action of residual stresses. In: *Proc. of 3rd All-Union Symp. on Residual Technological Stresses* (Kutaisi, October, 1988). Moscow: In-te for Problems in Mechanics, 358–364.
11. Serensen, S.V., Kogaev, V.P., Shnejderovich, R.M. (1975) *Load-carrying capacity and strength calculations of machine parts*. Moscow: Mashinostroenie.
12. Degtyarev, V.A., Shulginov, B.S. (2008) Assessment of limit cycle stresses for welded joints with high residual stresses by testing results of small-sized specimens without residual stresses. *Problemy Prochnosti*, **2**, 66–81.
13. Troshchenko, V.T., Tsybanev, G.V., Gryaznov, B.A. et al. (2009) Fatigue of metals. Influence of surface state and contact interaction. In: *Strength of materials and structures*, Vol. 2. Kiev: IPS.
14. Degtyarev, V.A., Vlasenko, V.I. (1992) Application of complex diagram of limit cycle stresses for vibration treatment purpose. *Tyazholoe Mashinostroenie*, **8**, 27–30.
15. Navrotsky, D.I. (1961) *Strength of welded joints*. Moscow: Mashgiz.
16. Trufyakov, V.I. (1956) About the role of residual stresses in reduction of endurance of welded joints. *Avtomatich. Svarka*, **5**, 90–103.
17. Myunze, V.Kh. (1968) *Fatigue strength of steel welded structures*. Moscow: Mashinostroenie.
18. Trufyakov, V.I., Gushcha, O.I., Trotsenko, V.P. (1976) Change of residual stresses in stress concentration zones at cyclic loading of welded joints. *Problemy Prochnosti*, **12**, 14–17.
19. (1991) *Guidelines*. Engineering safety. Probabilistic method of calculation of welded structures fatigue. Standard RD 50-694–90. Valid from 01.07.91. Moscow: Standart.
20. Kudryavtsev, I.V., Naumchenkov, N.E. (1976) *Fatigue of welded structures*. Moscow: Mashgiz.
21. Popova, M.M. (1978) Fatigue resistance of 14Kh2GMR steel welded joints. Metal structures of crane and examination of conveyors. *Transact. LPI*, **362**, 70–74.
22. Eregin, L.P., Naumchenkov, N.E. (1971) Static and fatigue strength of butt welded joints of 09G2S steel made on ground and roll scale. *Svarochn. Proizvodstvo*, **11**, 36–39.
23. Oding, I.L. (1962) *Admissible stresses in machine-building and cyclic strength of metals*. Moscow: Mashgiz.

Received 10.05.2016

doi.org/10.15407/tpwj2016.10.04

INFLUENCE OF HIGH-FREQUENCY MECHANICAL VIBRATIONS OF THE ITEM ON STRUCTURE AND WEAR RESISTANCE OF KH10R4G2S DEPOSITED METAL

G.V. POKHMURSKAYA[1], **M.M. STUDENT**[2], **A.A. VOJTOVICH**[3], **A.Z. STUDENT**[2] and **A.R. DZYUBIK**[3]

[1]Technical University of Chemnitz
09107, Chemniz. E-mail: pokhmurska@mb.tu-chemnitz.de
[2]G.V. Karpenko Physico-Mechanical Institute, NASU
5 Nauchnaya Str., 79601, Lviv, Ukraine. E-mail: student-m-m@ipm.lviv.ua
[3]«Lviv Polytechnic» National University
12 Stepan Bandera Str., 79013, Lviv, Ukraine. E-mail: andrsibox@gmail.com

The paper presents the results of studies of the effect of high-frequency (100 Hz) mechanical vibrations on microstructure and wear resistance of metal, deposited with PP Kh10R4G2S wire and OSTs45M flux. It established that when horizontal vibration is used, deposited metal solid solution, uniformly saturated with fine iron-chromium borides (FeCr)B, prevails in the structure. Homogeneous structure improves wear resistance by 2.0–2.5 times. 9 Ref., 1 Table, 5 Figures.

Keywords: *surfacing, flux-cored wire, vibration, microstructure, fatigue life, wear pattern*

Earlier conducted studies revealed that the form and size of carbide inclusions influence deposited metal performance [1]. Deposits produced with flux-cored wires (FW) of Fe–Cr–B–C system of hypereutectic composition are characterized by precipitation of carboboride dendritic axes of the first and second orders in the microstructure [2–4]. Pointed shape of hard inclusions, however, is a source of stress concentration, from which microcracks initiate, which, in its turn, leads to lowering of weld metal load-carrying capacity. It was also found previously [5, 6] that both mechanical characteristics of weld metal and its wear resistance are significantly increased at application of vibration during the surfacing process [7, 8]. The aim of this study was to optimize the amplitude of mechanical vibrations in the substrate during deposition to ensure high values of hardness and wear resistance of the deposited metal.

Deposited layers were produced on a substrate of mild steel St3sp under a layer of OSTs45M flux (composition in wt.%: 44 SiO_2, 44 MnO, <2.5 MgO, 6–9 CaF_2, <6.5 CaO, <2 Fe_2O_3, <0.15 S, <0.15 P) using flux-cored wire PP Kh10R4G2S. FW diameter was 2.6 mm with 25 % fill factor.

Samples of 300×150×10 mm size were surfaced. Their horizontal or vertical vibration was carried out with a frequency of 100 Hz at the amplitude of 70 and 300 μm. Horizontal vibration was applied across the deposited bead. Before surfacing, welding consumables were dried at 250 ° temperature for 2.5 hours. Beads were deposited with ABS suspended head with DC power supply (PSO 500 generator). Surfacing parameters were as follows: current of 420 A, arc voltage of 30–32 V, FW feed rate of 73 m/h, arc travel speed of 21 m/h, bead overlapping of 30 %.

Phase analysis was performed in X-ray diffractometer D8 Discover using Co-radiation. Microstructure was examined in electron microscope EVO 40 XVP. Axio Visio software was used for quantitative estimate of the dimensions of structural components in the deposited layers; inclusion area was compared with unit area of the microsection in the longitudinal plane.

Modulus of elasticity was measured by dynamic indentation with 50 g load. Scratch test (penetration depth, tangential force) was also carried out at 40 g load with dwell time under load of 40 s, and scratch length of 956 μm. Direction of scanning was across the bead.

Wear resistance of deposited layers at abrasive wear with loose abrasive was evaluated according to GOST 23.208–79. In particular, dried quartz sand with particle size of 200–1000 μm was continuously fed into the zone of rubber disc contact with the sample. Friction velocity was 0.3 m/s, and the force of its pressing to the sample was 2.4 kN. Abrasive wheel with CM 2 ceramic binder was used to determine the deposited layer wear by fixed abrasive. Linear velocity of friction was 0.8 m/s, load in linear contact zone was 1.5 kN. Length of the test path was 720 m. Impact wear was assessed at impact force of 12 kJ, using a sphere of 25 mm diameter from ShKh15 steel,

© G.V. POKHMURSKAYA, M.M. STUDENT, A.A. VOJTOVICH, A.Z. STUDENT and A.R. DZYUBIK, 2016

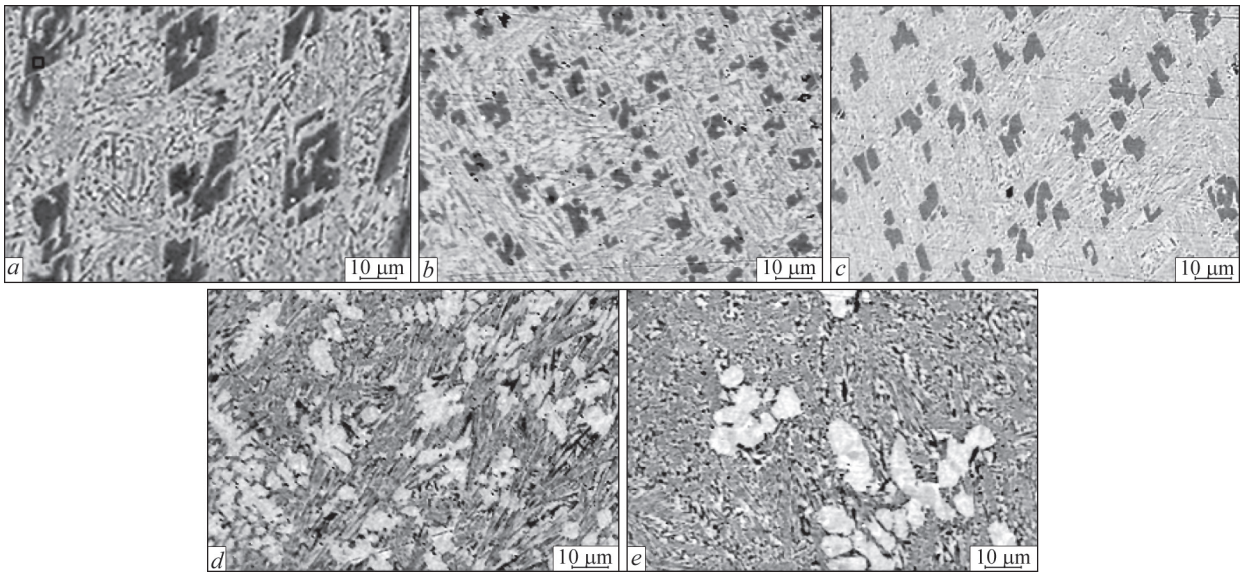

Figure 1. Microstructure in bead crest of metal deposited with PP Kh10R4G2S wire: *a* — without vibration; *b*, *c* — at vertical vibration; *d*, *e* — at horizontal vibration; at amplitude of 70 μm (*b*, *d*), 300 μm (*c*, *e*)

which hit the tested surface with a frequency of 40 s^{-1}. Experiment duration was 3600 s. Sample weight loss was determined with an accuracy of up to $2 \cdot 10^{-4}$ g in electronic scales.

Results and their discussion. Composition of the layers deposited without vibration included such phases as ferrochrome (FeCr), ferroboron (Fe_2B) and iron-chrome boride (FeCr)B [9] (Figure 1).

Metallographic examinations showed that vibration influences the size and shape of hard inclusions. On the crests of beads formed without vibration, the size of the area of isolated inclusions of (FeCr)B phase is 10–150 μm^2 (Figure 2, *a*). Surfacing samples using vertical vibration with the amplitude of 300 μm reduced the size (Figure 2, *b*) of borides (FeCr)B, the spread of their area was 10–30 μm^2. Application of horizontal vibration during surfacing revealed that hypereutectic structural components are refined even more. In particular, at maximum amplitude of 300 μm a significant refinement of iron-chromium borides (FeCr)B was clearly recorded, the size of the area of their isolated inclusions being 2–5 μm^2 (Figure 2, *c*). Furthermore, at horizontal vibration of a sample, formation of FeCr matrix phase in the form of unequiaxed grains was found in the deposited layer microstructure (Figure 1, *d, e*). At oscillation amplitude of 70 μm, their width and length ratio on the crests of the beads was 10–40 μm (Figure 1, *d*), and at the amplitude of 300 μm, these dimensions decreased to 5–30 μm (Figure 1, *d*). Presence of a small amount of FeCr matrix grains without inclusions enables relaxation of stresses, induced in subsequent operation of the deposited metal (Figure 2).

Dynamic indentation of the metal deposited with additional vibration, was performed to assess its mechanical properties. It was found that the greatest resistance to indenter penetration is in good agreement with the fine-grained microstructure on the bead crest and high density of hard (FeCr)B particles. Moreover, at horizontal vibration with the amplitude of 300 μm, the modulus of elasticity was equal to 331 GPa, which is significantly higher than the value obtained on samples deposited with application of vertical vibration (297 GPa), and without its application (295 GPa). This result may be an indication of the influence of mechanical vibrations on the level of weld metal po-

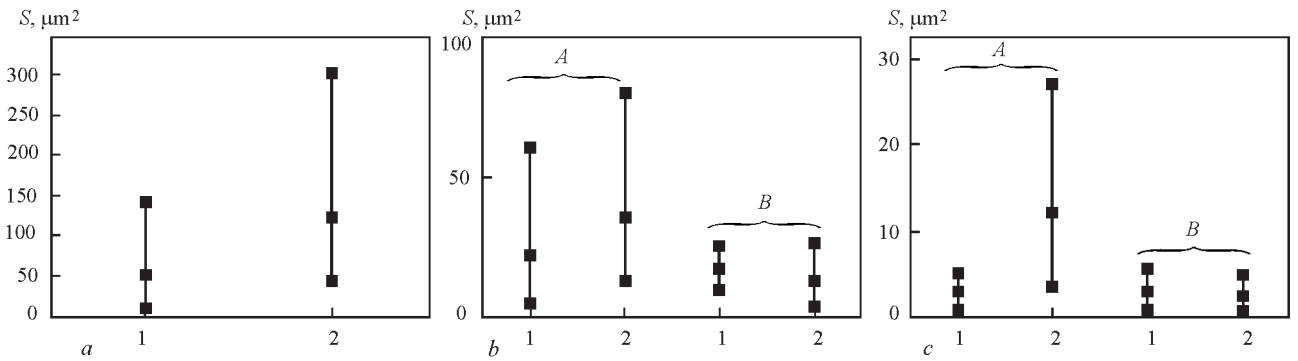

Figure 2. Change of area *S* of inclusions (1.6Fe + 0.4Cr)B; *a* — without vibrations; *b*, *c* — at vertical and horizontal vibration: *1* — on bead crest; *2* — in their overlapping zone; *A*, *B* — at the amplitude of 70 and 300 μm, respectively

Wear of samples with deposited layers, g

Parameter	Without vibration	Horizontal vibration		Vertical vibration	
Amplitude, μm	0	70	300	70	300
Wear with fixed abrasive	0.035	0.030	0.015	0.10	0.150
Wear with loose abrasive	0.020	0.015	0.01	0.045	0.035
Impact wear	0.009	0.0005	0.0007	0.005	0.004

rosity. After all, if we take into account the values of the modulus of elasticity, then at maximum amplitude of horizontal vibration, metal density turns out to be the highest. This is also confirmed by the reaction force of the material (tangential force) during indenter passing (scratch method) along the bead crest. Tendency to increase of deposited metal fracture resistance with increase of horizontal vibration amplitude is preserved, while at vertical vibration, it decreases, on the contrary. The large spread of tangential force values shows the low fracture resistance of deposited metal under the conditions of cutting in the presence of fine particles of iron-chromium borides of 10–30 μm^2 in the microstructure of the deposited layers at maximum amplitude of vertical vibration. In the deposited layers produced without vibration, the spread of tangential force values is slightly less than in the deposited metal at vertical vibration. This suggests that under cutting conditions, a larger size of the area (10–150 μm^2) of hard inclusions has a positive effect. At horizontal vibration of 300 μm amplitude, the spread of tangential force values is the smallest, due to a highly homogenous solid solution and small dimensions of hard inclusions. The magnitude of the force of resistance to material fracture increases closer to the zone of overlapping of the deposited layers (Table).

In addition, evaluation of the impact of vibration during surfacing on metal wear resistance was performed by the loss of mass of samples through wear of the deposited surface by fixed and loose abrasive, as well as under shock loading conditions. When testing by fixed abrasive, it was established that for samples deposited without the vibration, the loss amounted to 0.035 g, and at horizontal vibration with the amplitude of 70 and 300 μm it was 0.03 and 0.015 g, respectively. However, at vertical vibration of samples, weight losses increased with increase of vibration amplitude (see Table). The nature of damage of the deposited layers after friction also agrees well with the obtained results of mass wear. At wearing by fixed abrasive, we found fairly deep parallel grooves and traces of crumbled out borides (FeCr)B on the friction surface, produced without vibration (Figure 3, *a*). They easily cracked into pieces, because of friction, and were removed from the contact spot, leaving deep grooves. So, this is what led to low wear resistance of deposited metal.

At horizontal vibration amplitude of 300 μm, there is practically no cleavage from spallation of hypereutectic borides on the surface of the zone of metal contact with abrasive wheel (Figure 3, *b*). However, shallow, nonuniformly distributed traces of friction were observed on deposited layer surface. This is consistent with the nonuniformity of variation of the

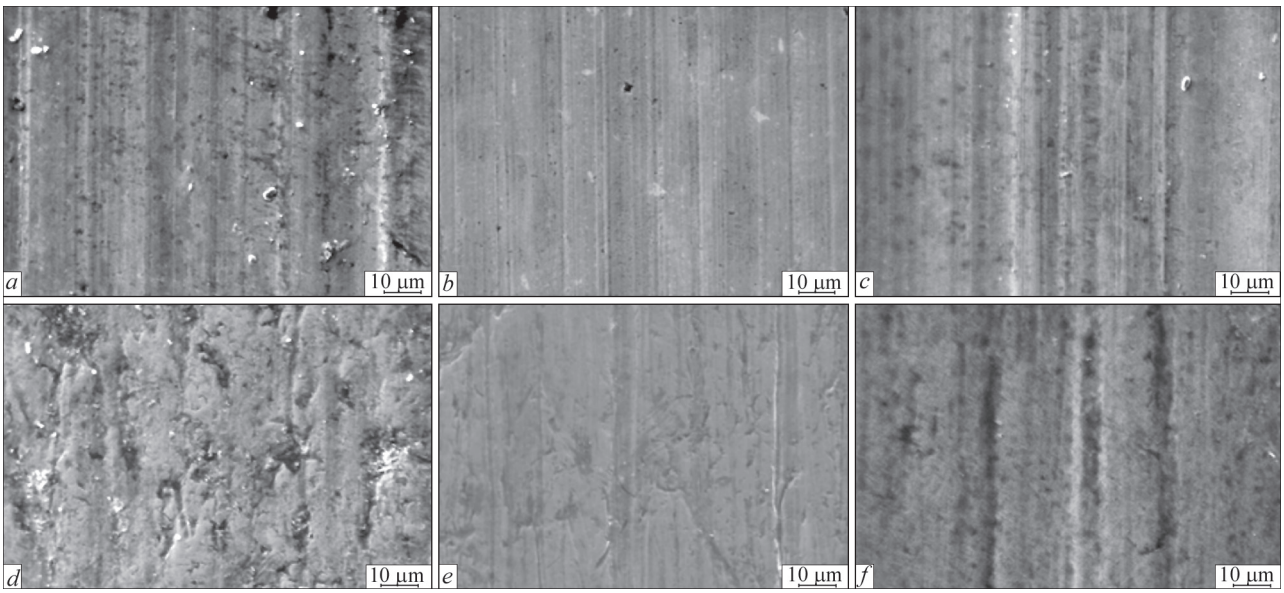

Figure 3. Morphological features of friction surfaces at wear of metal deposited with PP Kh10R4G2S wire without vibration (*a*, *d*) and with horizontal (*b*, *e*) and vertical (*c*, *f*) vibration of samples at 300 μm amplitude, during testing with fixed (*a*–*c*) and loose abrasive (*d*–*e*)

deposited metal microhardness, and presence of soft ferrite matrix grains in the structure. The latter contributes to stress relaxation in the contact zone and, thus, prevents chipping out of hard borides, which exactly cause deep damage of the friction surface.

In the case of surfacing with vertical vibration, deep and wide parallel traces of wear, and traces of chipping out of hypereutectic borides were detected on the friction surface (Figure 3, *c*). Constant increment of wear through deepening of the grooves by boride particles, which in this case acted as microcutters, is, probably, connected with it. Thanks to systematic orientation of borides in the direction of friction, new borides are gradually released from the eutectic matrix as the wheel goes deeper into the material. In this case, they have a negative impact on wear because of the cutting effect. When testing by loose abrasive of layers deposited without vibration, chipping out of hard borides becomes the main wear mechanism (Figure 3, *d*). Here, loose abrasive largely contributes to this chipping out. However, spalled borides leave virtually no characteristic parallel friction traces on the surface. Stiffness of the rubber wheel is, probably, insufficient to create the necessary force of pressing the abrasive to the deposited surface. As a result, spalled parts of borides together with quartz sand are removed from the zone of friction and no longer influence the wearing process. Application of horizontal vibration at surfacing promotes precipitation of inclusions of iron-chromium borides (FeCr)B in the metal structure. They are tightly held by ferritic matrix of FeCr and this makes it difficult to remove them. Therefore, wear is reduced, and shallow dents from ferrochromium boride inclusions and only here and there — grooves formed by them, are observed on the surface.

Study of the influence of vertical vibration on wear by loose abrasive showed that its negative impact persists. Wear surface of deposited layers at vibration amplitude of 300 μm is characterized by numerous traces of hard boride chipping out. Because of local cutting effect, they leave relatively deep grooves on the friction surface (Figure 3, *f*). However, if we compare the reliefs of wear surfaces of the layers deposited without application of vibration and after vertical vibration, it becomes obvious that the determining feature of wear is not the depth of the grooves from friction in the contact zone of the wheel with the metal, but the area of traces and resistance to spallation of hypereutectic borides from the eutectic matrix. Thus, the larger the size of borides and the lower the resistance to their spalling from the matrix, the more intensive is the deposited metal wear, when tested by loose abrasive (Figure 4).

Also analyzed was the nature of damage on the surfaces of bead crests during impact testing. In metal deposited without vibration, significant damage to the crest surfaces was recorded (Figure 4, *a–c*), which began as a result of plastic deformation. Violation of cohesive bond between the hard borides and the ductile matrix caused spallation of first coarse, then fine borides, and then separate parts of FeCr matrix (Figure 4, *a*).

Stresses arising in the vicinity of concentrator tips, formed by (FeCr)B-inclusions, were quite sufficient for crack initiation. It is possible that similar cracks can propagate also in-depth the deposited layer, as deposited material hardness was equal to *HRC* 55–57. With longer duration of testing, the density of arrange-

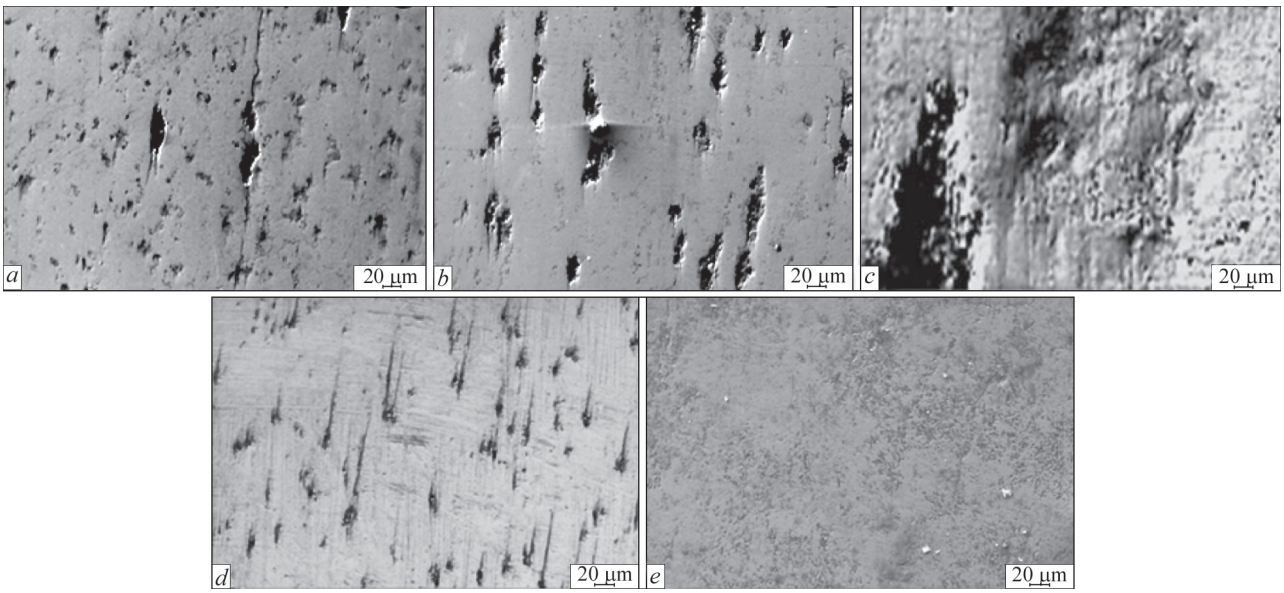

Figure 4. Morphological features of surfaces at application of impact loads: *a–c* — without vibration; *d, e* — at vertical vibration; *d, e* — at vibration amplitude of 70 and 300 μm, respectively

ment of sphere impact traces on the surface of the deposited layer became greater. In this case, the partitions between the closest pits were destroyed, releasing coarse (FeCr)B borides from the matrix (Figure 4, *b*). At this stage, fine Fe_2B borides became involved in the fracture. Violation of the cohesive bond with the matrix in them created fine pores in the deposited layer, which contributed to gradual further metal wear (Figure 4, *c*). Here, deep, clearcut pits on worn surfaces of bead crests show the selectivity of the wearing process and its association with larger-sized borides.

Data on weight loss of the samples after impact wear indicate that the use of vibration during surfacing increases deposited layer wear resistance (Table). The features of its influence on damage of deposited metal surface were analyzed. Since at application of vertical vibration with a low amplitude of 70 μm spread of iron-chromium boride area decreased significantly (10–60 μm^2) (see Figure 2, *b*), wear of the surface on bead crest took place by the same mechanism as without vibration. Wear localization was increased, as finer borides were chipped out, the adherence of which to the matrix is significantly stronger. Note the orientation of bands of pits caused by boride spallation, across the weld beads, which is associated with the direction of heat removal during molten pool solidification. As cracking is an effective method of stress relaxation in the deposited layer, the bridges between these pits were easily destroyed (Figure 4, *d*). However, the main contribution to wear was made not by cracks, but by spalled borides. When vibration was used during surfacing, boride area per unit area of the microsection is substantially smaller (see Figure 2, *b*).

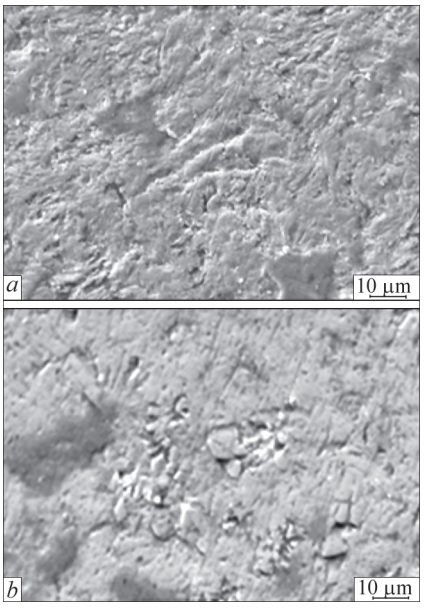

Figure 5. Morphology of wear surface on bead crest in layers, deposited with PP Kh10R4G2S wire, at horizontal vibration of amplitude: *a* — 70; *b* — 300 μm

Therefore, the value of losses from wear should also be reduced. This is consistent with the results of determination of the amount of wear by the weight method (see Table).

At increase of vertical vibration amplitude to 300 μm, signs of general, relatively shallow wear were detected on the bead crest (Figure 4, *d*). This is due to dispersion of strengthening Fe_2B phase. Local wear elements with cracking were observed only occasionally, but these fragments were not the deciding factor. As a special feature, we noted loss of defect orientation that was observed, when other deposition conditions were used. It hinders crack growth at breaking up of the bridges between the pits, and is evidence of a strong cohesion of wear-resistant phases and the matrix.

Application of horizontal vibration changed the phase state and morphological structure of the deposited layer. FeCr rounded grains and dispersed hard particles of iron-chromium borides (FeCr)B appeared. Such structural-phase composition qualitatively changes the nature of the action of load impact. The determinant factor, responsible for metal wear on bead crests, is the ability of the deposited layer to plastically deform, and relax the stresses occurring during impact wear tests. Traces of plastic deformation of deposited metal matrix are a characteristic feature of its surface relief after testing (Figure 5 *a, b*). In the case of bead relief, one can see spallation of its thin layers occurring at later stages of wear, as a result of plastic deformation of deposited metal surface (Figure 5, *a*). As traces of fine impurities were observed underneath them, it can be concluded that the reason for this is the loss of cohesive bond of fine inclusions with the matrix followed by spallation of work-hardened layer from the base (Figure 5).

Wear of weld metal produced at horizontal vibration amplitude of 300 μm occurs by the same mechanism, as at lower vibration amplitude. However, the number of areas where chipping out is promoted by plastic deformation, is reduced, and their localization is increased (Figure 5, *b*). It is typical of metal on the bead crest and is associated with low density of ductile FeCr phase and high dispersity of hard (1.6Fe + 0.4Cr)B phase (cross section of 1–5 μm^2). Note also the lowest cracking susceptibility of surface layers of all the considered variants of deposit formation.

Therefore, the surface layer of metal, obtained using horizontal vibration, is characterized by a high capacity for stress relaxation through plastic deformation and a low cracking susceptibility. This accounts for its high wear resistance in impact tests, which is the result of structural and phase transformations,

changes in the morphology and size of reinforcing phases in the structure of the deposited metal.

Conclusions

Microstructure of layers deposited with flux-cored wire PP Kh10R4G2S by automatic submerged-arc process with OSTs45M flux, using vertical and horizontal vibration at a frequency of 100 Hz and vibration amplitude of 70, 300 μm was studied. Application of vibration in the surfacing process provided refinement and rounding of the strengthening (FeCr) B phase.

It is found that the layers deposited at horizontal vibration at the amplitude of 300 μm in bead crest zone, are characterized by high capacity for stress relaxation through plastic deformation of surface layers and a low susceptibility to cracking, that explains their high resistance in impact tests.

1. Zhou, Y., Yang, Y., Qi, X. et al. (2012) Influence of La_2O_3 addition on microstructure and wear resistance of Fe–Cr–C cladding formed by arc surface welding. *J. of Rare Earths*, 30(**10**), 1069.
2. Yuksel, N., Sahin, S. (2014) Wear behavior-hardness-microstructure relation of Fe–Cr–C and Fe–Cr–C–B based hardfacing alloys. *Materials and Design*, 58, 491–498.
3. Katsicha, C., Badisch, E., Manish, R. et al. (2009) Erosive wear of hardfaced Fe–Cr–C alloys at elevated temperature. *Wear*, 267, 1856–1864.
4. Pokhmurska, G.V., Student, M.M., Lanets, O.S. et al. (2015) Effect of vibration during surfacing of protective layer on its macrostructure and shock-abrasive wear. *Fizyko-Khimichna Mekhanika Materialiv*, Issue 3.
5. Govindarao, P., Srinivasarao, P., Gopalakrishna, A. et al. (2012) Effect of vibratory welding process to improve the mechanical properties of butt welded joints. *Int. J. of Modern Engineering Research (IJMER)*, 2(Issue 4), 2766–2770.
6. Husein, A.R., Abdul, N.A., Talib, R.A. (2011) Improvement of mechanical welding by using induced harmonic vibration. *J. of Applied Sci*., 11(**2**), 348–353.
7. Wanga, S., Li, H., Chenb, X. et al. (2010) Improving microstructure and wear resistance of plasma clad Fe-based alloy coating by a mechanical vibration technique during cladding. *Materials Sci. and Engineering, A*, 528, 397–401.
8. Pulka, Ch.V., Shably, O.N., Senchishin, V.S. et al. (2012) Influence of vibration of parts on structure and properties of metal in surfacing. *The Paton Welding J*., **1**, 23–25.
9. Vojtovich, A.A., Pokhmurska, G.V., Student, M.M. et al. (2015) Peculiarities of formation and fracture of deposited layers from flux-cored wires of Fe–Cr–B–C system at shock loads. *Problemy Trybologii*, **4**, 114–123.

Received 11.03.2016

doi.org/10.15407/tpwj2016.10.05

COMPARISON OF PROCEDURES FOR EVALUATION OF EFFECT OF WELDING THERMAL CYCLE ON IMPACT TOUGHNESS OF HAZ METAL OF WELDED JOINTS FROM LOW-ALLOY STEELS

V.D. POZNYAKOV, L.I. MARKASHOVA, S.L. ZHDANOV, E.N. BERDNIKOVA, A.V. ZAVDOVEEV and **A.A. MAKSIMENKO**
E.O. Paton Electric Welding Institute, NASU
11 Kazimir Malevich Str., 03680, Kiev, Ukraine. E-mail: office@paton.kiev.ua

One of the most important indices of mechanical properties, which together with other factors determine the quality and working capacity of the welded joints, is impact toughness. Impact toughness is characterized by material capability to absorb mechanical energy in process of deformation and fracture under impact load effect. This paper carries a comparative evaluation of effect of welding on impact toughness of HAZ metal of specimens, produced from bead-on-plate tests, and reference ones, treated on welding thermal cycle, from steel 10G2FB. It is determined that effect of the welding thermal cycles on impact toughness indices of HAZ metal of welded joints from steel 10G2FB is ambiguous. Rapid decrease of *KCU* and *KCV* values is observed at $w_{6/5} < 6$ °C/s cooling rates. Increase of cooling rate provides for rise of HAZ metal impact toughness and in some cases it reaches *KCU* and *KCV* values of base metal. Therefore, it is a good correlation of the values of impact toughness between the specimens, treated on welding thermal cycle, and specimens, produced from welded joints. It is insignificant difference in nature of their fracture. 7 Ref., 2 Tables, 6 Figures.

Keywords: *low-alloy steel, impact toughness, welding thermal cycle, bead-on-plate test, heat-affected zone, structure, fracture surface*

One of the most important indices of mechanical properties, which together with other factors determine the quality and working capacity of the welded joints, is impact toughness. Impact toughness is characterized by material capability to absorb mechanical energy in process of deformation and fracture under impact load effect [1].

Since different areas of the welded joints (weld metal, heat-affected zone) can, respectively, vary on chemical composition, structure and properties then impact toughness is determined for each of indicated areas. Sampling, manufacture and impact bend testing of the specimens is carried out on GOST 6996–66. A notch, depending on purpose of the test, is located along weld metal, along fusion zone and in different areas of near-weld zone at some distance from fusion line. The notch can be of V- or U-shape. In accordance with this, impact toughness has *KCV* or *KCU* indices. Mostly, such an approach is used in impact bend testing of welded joints at certification of engineering welding processes and welders as well at final stage of checking the developed welding procedures.

Somewhat other methods are used in scientific-research and experimental works on study the welding effect on base metal, including evaluation of this effect on impact toughness of metal of heat-affected zone (HAZ).

One of them, namely «Bead-on-plate test method for determination of allowable modes of arc welding and surfacing» (GOST 13585–68) is used for evaluation of change of base metal mechanical properties, promoted by welding thermal cycle directly in HAZ adjacent to fusion zone as well as other areas of HAZ [2]. An essence of this method lies in deposition of beads on solid or composite plates of examined steels at different heat input and further determination of impact toughness and strength properties of HAZ. At that, the data on effect of heat input on impact toughness of metal in HAZ complete resolidification area is of the most interest. In this case, the notch on the specimens is made in such a way so as its bottom locates on a bead axis below the fusion line at not more than 0.5 mm distance to base metal side. The peculiarity of indicated specimens is the fact that in the impact bend testing only beginning of fracture proceeds in the controlled zone, while its propagation proceeds along the base metal. At that, the lower welding heat input is the larger amount of base metal will be involved in fracture. Based on this, it can be assumed that bean-on-plate test procedure should be sufficiently good in describing a capability of HAZ metal to

© V.D. POZNYAKOV, L.I. MARKASHOVA, S.L. ZHDANOV, E.N. BERDNIKOVA, A.V. ZAVDOVEEV and A.A. MAKSIMENKO, 2016

fracture nucleation resistance. However, accuracy of information in a question how such metal will resist fracture propagation raises doubts. In particular, it is related to the cases when relatively small welding modes are used in bead-on-plate deposition, thus promoting small HAZ width, as well as when the indices of impact toughness of steel significantly exceed impact toughness of HAZ metal.

Effect of welding on base metal can be also evaluated using a method at which thermal action on metal is carried out without application of welding (GOST 23870–79) [3–6]. In this case, the billets (ingots of specific size) from studied steel are heated and cooled on mode, comparable with welding thermal cycle (WTC). For this, the billets are heated to set temperature by means of passing current and then forced cool. Such action on metal provides formation in it of approximately the same structure as in HAZ metal of the welded joints subjected to similar thermal action in welding. Since for WTC simulation the whole section in the middle of the billets is heated and cooled uniformly, then it can be supposed that metal impact toughness in different areas of this section will be sufficiently close. Thus, the results of specimen testing can provide more reliable information on capability of HAZ metal of that or another steel to fracture propagation resistance in impact bending.

Taking into account mentioned above, the aim of present work lies in carrying out a comparative evaluation of welding effect on impact toughness of HAZ metal of specimens, produced from bead-on-plate test and base metal billets treated on WTC, by example of one of low-alloy steels.

Investigation procedures. Plates of 250–450 mm width and 600 mm length were used for bead-on-plate test method. They were cut in such a way that bead direction in further deposition coincides with rolling direction. Before welding an average part of the plate, designed for bead deposition, was cleaned from scale and corrosion to general width of 80 mm (40 mm in each side from a deposition axis).

The bead was deposited along longitudinal symmetry axis of the plate (Figure 1) on modes providing change of cooling rate in 600–500 °C ($w_{6/5}$) temperature range from 3 to 30 °C/s. Such metal cooling intensity in HAZ overheating area is typical for the majority of arc welding processes, i.e. automatic submerged arc, gas-shielded mechanized and manual welding with stick electrodes. The parameters of welding modes and corresponding rates of cooling of HAZ metal of bead-on-plate tests are given in Table 1.

Bead deposition was carried out in a jig by Sv-08GA wire of 4 mm diameter using AN-348 flux with reverse polarity direct current at 27 °C ambient temperature. No wire oscillation was allowed. After bead deposition was finished the plate remained in the jig till complete cooling of the specimen.

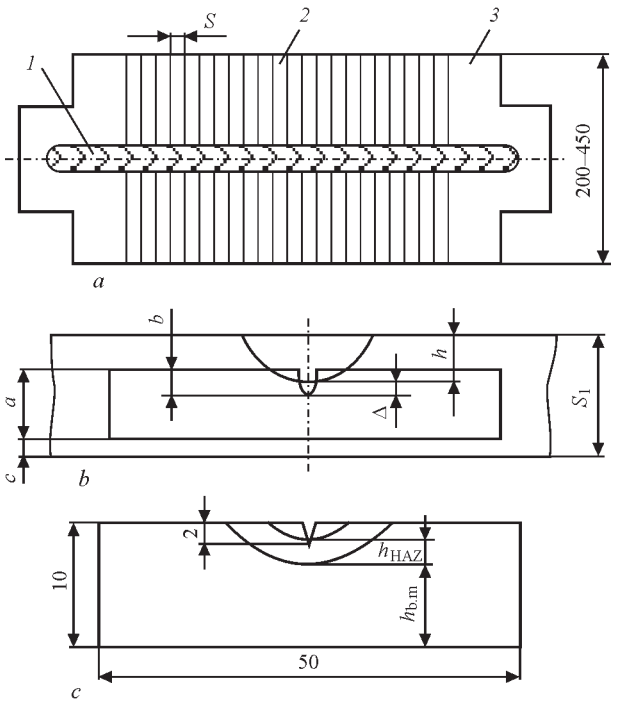

Figure 1. Bead-on-plate test with deposit (*a*), scheme of cutting the specimens for impact bend testing (*b*) and designation of areas of welded joint, which are included in impact specimen (*c*): *1* — deposited bead; *2* — compound bars; *3* — run-on plate; *h* — area with deposited metal; h_{HAZ} — HAZ area; $h_{b.m}$ — base metal area

The specimens for mechanical tests were made from the plates prepared and deposited using the method indicated above. These specimens should correspond to the requirements of GOST 13585–68, therefore the microsections were made from bead-on-plate tests at the initial stage. They were used for determination of bead parameters (bead width, bead reinforcement, penetration depth and HAZ parameters). This allowed determining a thickness of metal layer, which should be removed before specimens manufacture.

Bars of 13×13×150 mm size made from studied steel were used for investigations applying billets treated on welding thermal cycle. Their heat treatment was carried out on MSR-75 unit, developed at the E.O. Paton Electric Welding Institute. Heating of the bars was carried out by passing current up to 1200–1300 °C temperature (corresponds to HAZ metal overheating

Table 1. Modes of deposition and cooling rate for HAZ metal of bead-on-plate tests from 18.7 mm thick plate

I_w, A	U_a, V	v_w, m/h	Q_w, kJ/cm^2	$w_{6/5}$, °C/s
580–600	34–38	12.9	50.6	3
580–600	34–38	20.0	35.7	6
580–600	34–38	23.7	28.6	10
380–400	30–32	20.0	20.4	20
380–400	30–32	23.7	17.0	30

area of welded joints) at 170–200 °C rate. At this temperature they were hold approximately during 2 s and then were cooled. Copper jaws of the unit were cooled using flowing water for providing bars' cooling at $w_{6/5}$ from 2.5 to 7.5 °C/s. More intensive rates of specimen cooling were reached as a result of additional blowing of the specimens by inert gas that allowed variation of $w_{6/5}$ from 8 to 30 °C/s due to change of value of gas consumption.

Additionally, HAZ metal impact toughness was evaluated based on results of testing of the specimens produced from butt joints of 18.7 mm thickness with V-groove preparation (C21 on GOST 2564–80 and 14771–76), made by manual coated electrode welding and mechanized CO_2 welding. In this case cutting of the specimens and making of a notch was carried out on GOST 6996–66.

Manual arc welding was performed by ANP-10 grade electrodes of 4 mm diameter on the following mode, i.e. I_w = 160–170 A; U_a = 24–25 V; v_w = 8.5–9.0 m/h, which provided intensity of cooling of welded joint HAZ metal with $w_{6/5}$ = 30 °C/s rate. Flux-cored wire Megafil 821R of 1.2 mm diameter and the next mode were used for mechanized welding, namely I_w = 180–200 A, U_a = 28–30 V, v_w = 13.5–15.0 m/h. At that, the cooling rate at HAZ metal area made 21 °C/s. In all cases welding was carried using reverse polarity direct current.

The rate of heating and cooling of the specimens was controlled using chromel-alumel thermal couple of 0.5 mm diameter, and evaluated on results of processing of oscillograms, recording of which was made using 117/1 oscillograph in temperature — time coordinates.

Specimens of 10x10x55 mm size (type VI with round notch and type IX with acute notch on GOST 6996–66) were made for determination of impact toughness of HAZ metal from beat-on-plate tests and billets treated on WTC. The specimens were mechanically cut. The specimens were cooled by emulsion in order to prevent metal heating.

Testing of the specimens was carried out at 20 and –40 °C temperature (not less than three specimens at each temperature). Impact toughness was determined in area of complete resolidification of HAZ metal (KCU_{+20}, KCU_{-40}, KCV_{+20}, KCV_{-40} J/cm^2).

Structures of fracture surface of the specimens were examined with the help of scanning electron microscope of SEM 515 grade of Philips Company (the Netherlands).

Results of investigations and their discussion. High-strength structural niobium and vanadium micro-alloyed steel having 18.7 mm thickness and the following composition (wt.%) was selected as an object for investigation: 0.08 C; 0.25 Si; 1.57 Mn; 0.19 Mo; 0.05 Nb; 0.05 V; 0.032 Al; 0.006 N; 0.007 S; 0.013 P. In as-delivered condition (controlled rolling) steel has the following mechanical properties: σ_y = 531–581 MPa; σ_t = 610–660 MPa; δ_5 = 24.8–26.3 %; ψ = 62.0–64.8 %, KCU_{+20} = 340–350 J/cm^2; KCU_{-40} = 280–320 J/cm^2; KCV_{+20} = 300–330 J/cm^2, KCV_{-40} = 190–210 J/cm^2.

It is determined that steel impact toughness is changed under the effect of welding thermal cycle based on results of testing the specimens, produced

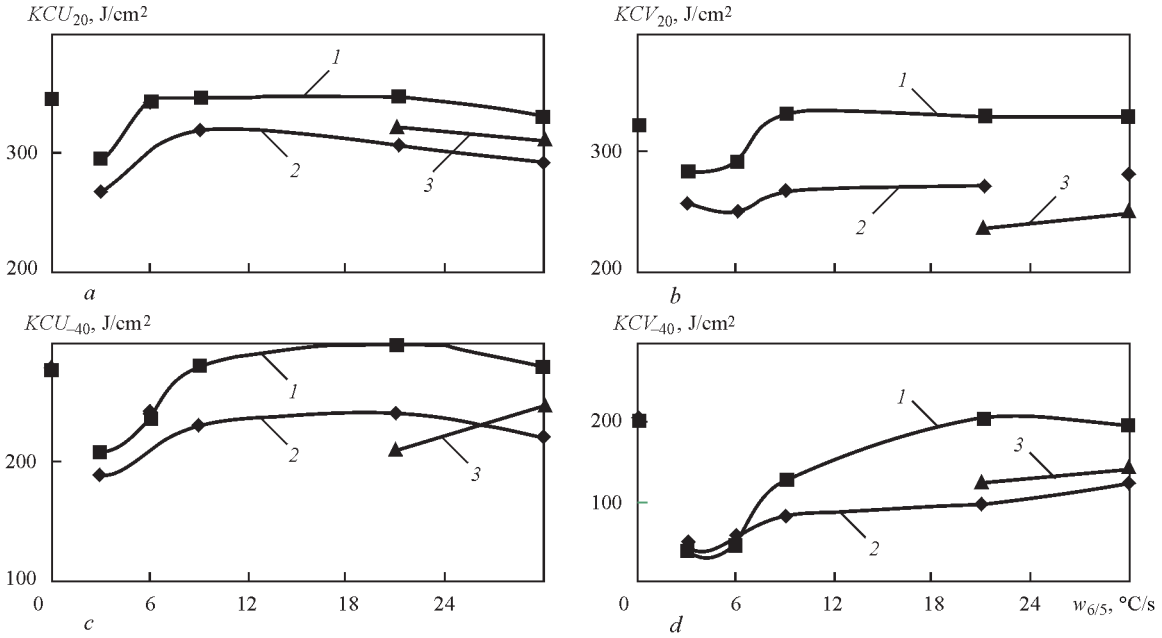

Figure 2. Effect of cooling rate on impact toughness of specimens, produced from bead-on-plate tests (*1*); WTC-treated billets (*2*); welded joints (*3*) (values of impact toughness indices of base metal are given in point $w_{6/5}$ = 0)

Table 2. Nature of fracture and size of microrelief elements of fracture surfaces in zone of main crack propagation

Fracture nature		Welded joint	WTC simulation	Bead-on-plate test	Base metal
Ductile	V_a, %	5–7	5	100	95
	d_p, μm	1–3	1–3	1–10	1–10
	D_p, μm	–	–	20–70×70–250 (av. 45×160)	10–70×20…–150 (av. 40×85)
Brittle intergrain	V_a, %	95	95	–	5
	D_f, μm	10–20	20–60	–	10–25
Secondary microcracks	L_{cr}, μm	5–10	5–30	–	–

from bead-on-plate tests, from welded joints as well as from heat-treated billets of studied steel. It is usually reduced (Figure 2) in relation to base metal.

The most obvious reduction of impact toughness indices of metal in HAZ overheating area is observed in the case when deposition of plates (in production of bead-on-plate tests) was carried out on modes providing high heat input (Q_w = 50.6–35.7 kJ/cm^2; $w_{5/6}$ = = 3–6 °C/s), and billet heat treatment is done on welding thermal cycles, providing indicated cooling rate of metal in 500–600 °C temperature range. It should be noted that under such cooling conditions the indices of impact toughness of specimens, produced from bead-on-plate tests, and billets treated on welding thermal cycle are sufficiently close.

Decrease of welding heat input provides for rise of $w_{6/5}$ (Table 1) and increase of indices of impact toughness of HAZ metal. The most obvious increase of *KCU* and *KVC* indices (virtually till the base metal level) is observed in the case, when the investigations were carried out using the specimens, produced from bead-on-plate tests, deposition of which was carried out on modes providing $Q_w \leq 28.6$ kJ/cm^2 ($w_{6/5} \geq 10$ °C/s). Under the same cooling conditions the impact toughness of specimens, treated on WTC, is also rises, however, in all cases it is lower than that of the specimens, produced from base metal and bead-on-plate tests.

As indicated in work [7], variation of impact toughness indices of 10G2FB steel as a result of effect of welding thermal cycles on it is related with a change of phase-structural composition of HAZ metal, namely, with formation in it of coarse grain ferrite-bainite structure at $w_{6/5} \leq 10$°C/s and fine-grain bainite structure at $w_{6/5} \geq 10$ °C/s.

In order to explain the differences between the impact toughness indices of the specimens, produced from bead-on-plate tests, and bars, treated on WTC, it is necessary to consider what areas of welded joint are included in impact specimens and what are their relationship in fracture zone.

The following can be noted as for the specimens, produced from the bars treated on WTC. Since the middle part of the specimen, where the notch was subsequently made, was uniformly heated and cooled in process of heat treatment, it had homogeneous on composition structure formed in it. Respectively, in this case, fracture of the specimen took place along the metal which has approximately similar mechanical properties. As it is schematically shown in Figure 1, the impact specimen, produced from bead-on-plate tests, partially consists of a layer of deposited metal, HAZ and base metal. The deposited metal does not participate in specimen fracture, since it includes the notch. Since impact loads fall on HAZ and base metal, then fracture of the specimen takes place directly along this areas.

We are to consider a variation of relationship of area width, corresponding to HAZ (h_{HAZ}) and base metal ($h_{b.m}$) depending on welding heat input. Such data are shown in Figure 3. They indicate that relationship between h_{HAZ} and $h_{b.m}$ makes 0.9 in zone of fracture of impact specimens, produced from bead-on-plate tests, deposition of which is carried out using large heat input. Respectively, in this case, fracture of the specimen will mainly take place along HAZ metal as in the specimens treated on welding thermal cycle. Therefore, it is not surprisingly that the indices of impact toughness of the specimens, produced from bead-on-plates and heat-treated billets, virtually match.

HAZ width reduces with decrease of welding heat input ($w_{6/5}$ rise). In this connection $h_{HAZ}/h_{b.m}$ relationship is also reduced. At $Q_w \leq 28.6$ kJ/cm^2

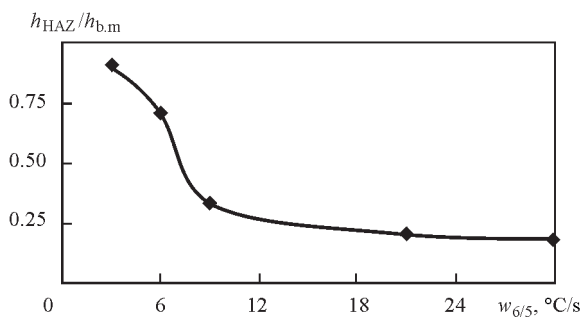

Figure 3. Effect of cooling rate of bead-on-plate tests on relationship between width of areas of HAZ metal (h_{HAZ}) and base metal ($h_{b.m}$), taking part in fracture of impact specimens

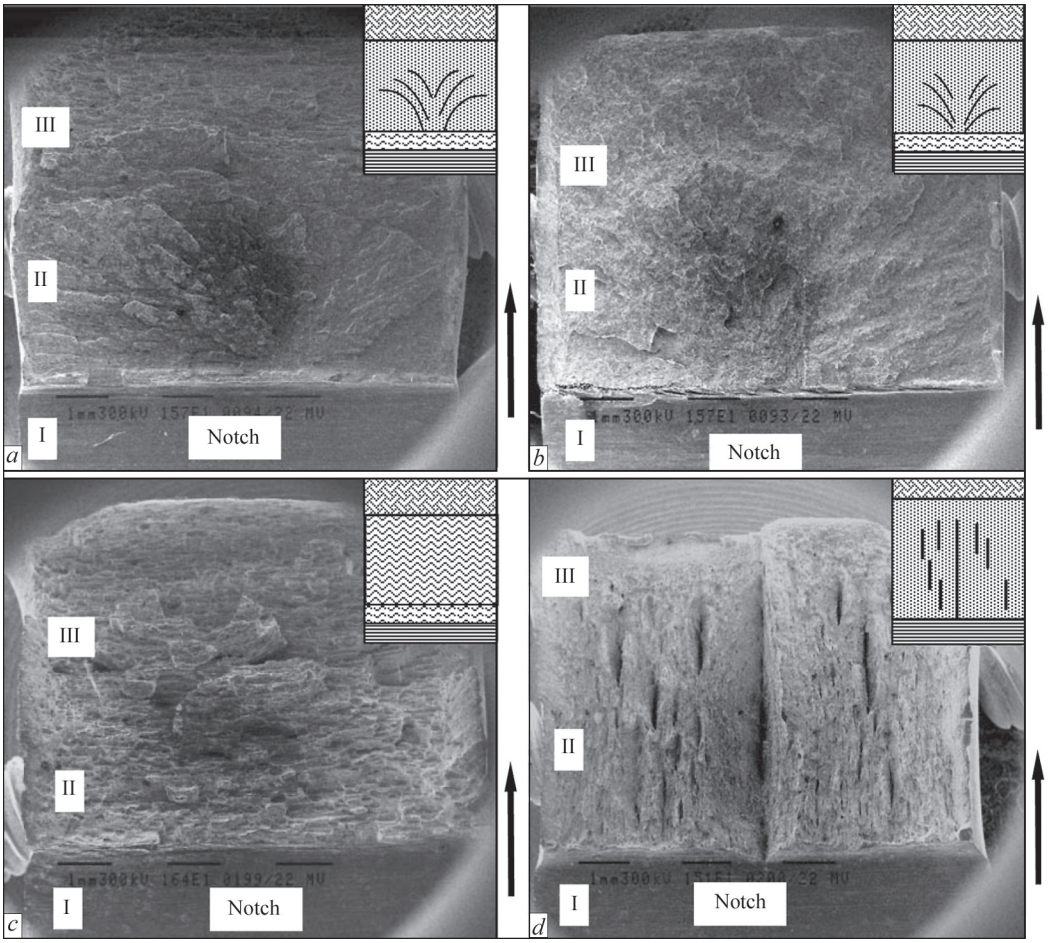

Figure 4. General view of break surface on fracture zones of specimens, produced from: welded joint (*a*); billets treated on WTC (*b*); bead-on-plate test (*c*); base metal (*d*), ×16 (schematic presentation of the breaks are in the upper right part of the picture) (see designations in the text)

($w_{6/5} \geq 10$ °C/s) a fraction of HAZ in specimen fracture reduces virtually to 25 %. Respectively, the main fracture of impact specimens took place on base metal. This, apparently, can be an explanation of the fact that the indices of impact toughness of specimens, produced from bead-on-plate tests, welding of which was carried out at lower modes, are comparable with impact toughness indices of base metal.

As for fracture of the specimens, produced from welded joints, then they mainly fracture on HAZ metal. At that, all HAZ areas were involved in fracture, namely high-temperature as well as low-temperature. Therefore, the impact toughness indices of such specimens are significantly differ from *KCU* and *KVC* indices of the specimens, produced from bead-on-plate tests, and have relatively good correlation with similar properties of heat-treated specimens.

The dependence of obtained results is verified by the fractographic examinations of the specimen fractures. Their aim lied in comparison of fracture nature (transcrystalline and intercrystalline; brittle; quasi-brittle; ductile or mixed) of welded joint metal on fracture zones (I — zone of fracture necleous near notch; II — main crack propagation; III — zone of break) as well as analysis of fracture structure of welded joints taking into account parameters of microrelief elements of fracture surface: size of chip facets d_{fac}, pits of ductile constituent (disperse d_p, coarse D_p) length of secondary cracks l_{cr}. General view of specimen fractures is given in Figure 4. The arrows show fracture direction.

Since zone I (near notch) and zone III (break) in all investigated specimens are characterized by similar ductile type of fracture, further they are not studied in details. It is appeared to be more reasonable to carry out a comparative analysis in zone of main crack propagation (II), where significant difference in fracture nature was observed.

Analysis of specimen fracture showed that according to macrorelief the fracture surfaces in zone II of the specimens, produced from WTC treated billets, and one from welded joints, are similar. In both cases the radial scars (Figure 4, *a*, *b*) propagating from fracture nucleus match with general direction of crack propagation.

Further examination of micropeculiarities of the fracture surfaces in zone of main crack showed that fracture of the specimens, produced from welded joints, and ones from WTC treated billets, can be

characterized as brittle intergrain chip (Table 2; Figure 5; Figure 6, *a*, *b*) with local areas of ductile constituent (disperse pits of d_p = 1–3 μm size, volume fraction V_f ~ 5 %). Such details of microrelief as the areas of ductile constituent indicate a local plastic deformation, i.e. development of a brittle chip in adjacent grain can take place with obvious plastic deformation in a transient zone.

Analysis of fracture nature of the specimens, produced from welded joints, showed that size of the chip facets on fracture surface makes d_{fac} ~ 10–20 μm, size of single secondary microcracks l_{cr} ~ 5–10 μm (Figure 6, *a*).

Secondary microcracks of 5–10 μm length were also observed on fracture surface of the specimens, produced from WTC treated billets. However, the chip facets in such specimens are 2–3 times larger, than in the specimens, produced from welded joints, they achieve 20–60 μm size, approximately (Figure 6, *b*). It can be explained by the fact that fracture of the specimens, produced from WTC treated billets, takes place on metal with coarse grain, which is typical for HAZ overheating area of welded joint, and along all HAZ areas in the specimens, made from welded joints.

Fracture of the specimens, produced from bead-on-plate tests and base metal, takes place completely in another way. Analysis of fracture of these specimens

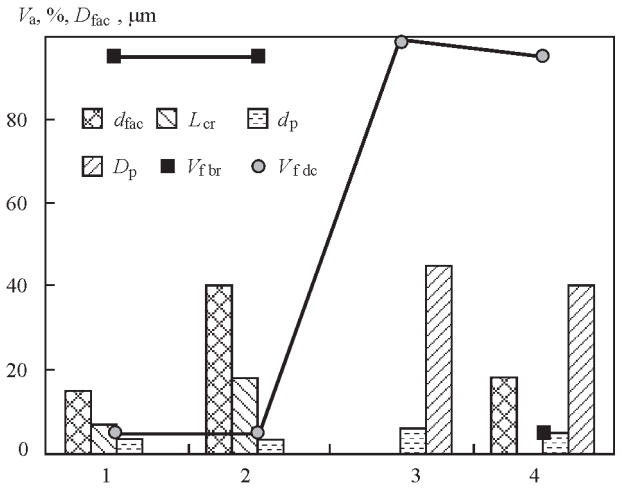

Figure 5. Change of volume fraction of brittle ($V_{f.br}$, %) and ductile ($V_{f.dc}$, %) fracture, size of facets (d_{fac}, μm) of brittle intergrain chip and pits (d_p, D_p, μm) of ductile fracture, length of secondary cracks (L_{cr}, μm) in fracture of specimens, produced from: welded joint (*1*); billets treated on WTC (*2*); bead-on-plate test (*3*); base metal (*4*)

showed that a ductile pit type of fracture (Figure 6, *c*, *d*) is observed on their surface in both cases. The difference lies only in the fact that fiber fracture surface of the specimens, produced from bead-on-plate tests, is characterized by expressed splitting on displaced levels in transverse direction of main crack propagation (Figure 4, *c*), and fracture of the base metal has a fiber-banded structure in longitudinal direction (Figure 4, *d*). Apparently, it is related with the fact that the

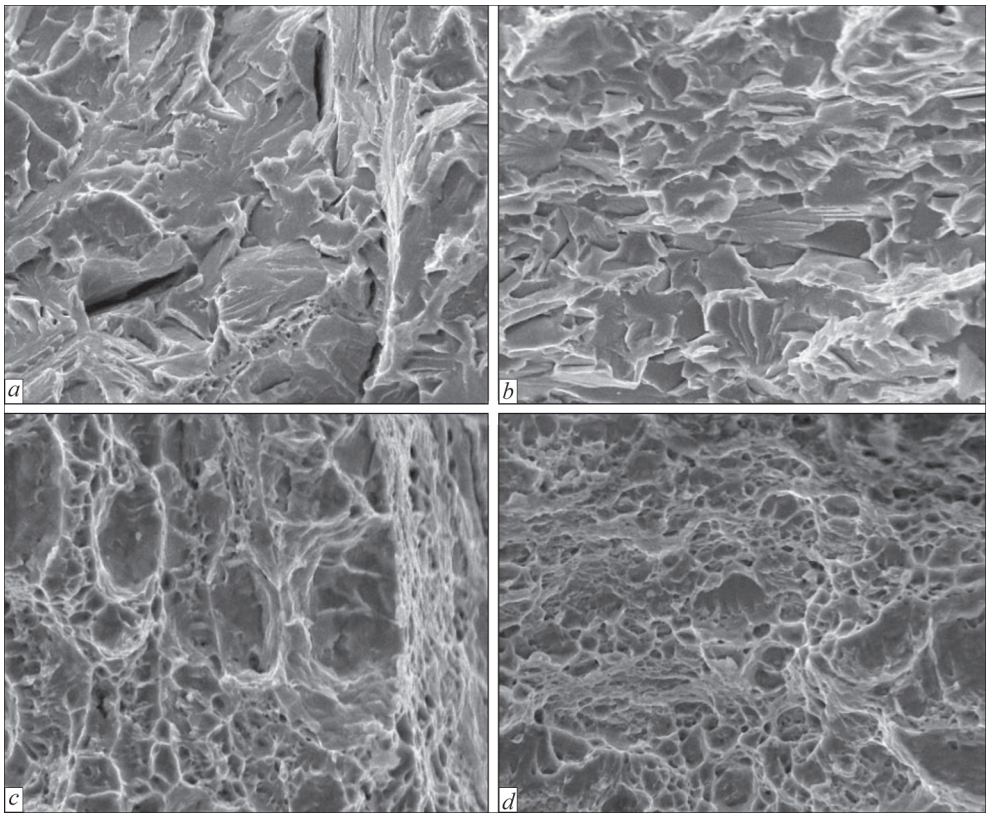

Figure 6. Nature of fracture in main crack zone: *a*, *b* — brittle transcrystalline chip in fracture of specimens, produced from welded joint (*a*), and treated on WTC method (*b*); *c*, *d* — ductile fracture of specimen from bead-on-plate test (*c*) and base metal (*d*), ×1550

specimens, produced from bead-on-plate tests, and base metal, were cut in directions different in relation to rolling. It is not surprisingly, that a fracture nature of such specimens is approximately similar, since, according to mentioned above, and, as can be seen from Figures 1 and 3, development of the main crack in the specimens, produced from bead-on-plate tests, welding of which was carried out at low heat input, mainly takes place along the base metal.

Conclusions

1. Effect of welding thermal cycles on impact toughness indices of HAZ metal of welded joints from 10G2FB steel is ambiguous. Rapid decrease of *KCU* and *KCV* values is observed at cooling rates $w_{6/5} < 6$ °C/s. Increase of cooling rate provides for rise of impact toughness of HAZ metal and in some cases it reaches *KCU* and *KCV* values of base metal.

2. Reduction of welding heat input promotes for increase of cooling rate $w_{6/5}$ of HAZ metal of bead-on-plate tests, and decreases the width of this area in the joint.

3. Low rates of cooling of HAZ metal ($w_{6/5} <$ °C/s), typical for welding processes, carried out at increased heat input ($Q_w > 35$ kJ/cm^2), promotes for fracture of the specimens mainly on HAZ metal, and *KCU* and *KCV* indices of the specimens, produced from bead-on-plate tests and treated on welding thermal cycle, have insignificant difference.

4. Fracture of the specimens, produced from bead-on-plate tests, with rise of $w_{6/5}$ to 10 °C/s and above ($Q_w < 30$ kJ/cm^2) mainly takes place along the base metal. Due to this the difference between the indices of impact toughness of the specimens, produced from bead-on-plate tests, and one from billets treated on welding thermal cycle, becomes noticeable.

5. A good correlation is found for the values of impact toughness between the specimens, produced from welded joints and billets treated on welding thermal cycle. Fracture nature of such specimens varies insignificantly.

1. (1991) *Metals science and heat treatment of steel*: Refer. Book. Ed. by M.L.Bernshtejn, A.G. Rakhshtadt. Vol.1: Methods of testing and research. Moscow: Metallurgiya.
2. Emelyushin, A.N., Sychkov, A.B., Sheksheev, M.A. (2012) Examination of weldability of high-strength pipe steel of K56 strength grade. *Vestnik Magnitogorskogo Gos. Tekhn. Un-ta im. G.I. Nosova*, Issue 3, 26–30.
3. Gulakov, S.V., Nosovsky, B.I., Novokhatskaya, A.S. et al. (2008) Method and equipment for simulation of welding(surfacing) thermal cycle. *Visnyk Pryazov. Derzh. Tekhn. Un-tu*, Issue 18, Pt 1, 179–183.
4. Stolyarov, V.I., Efimenko, L.A., Elagina, O.Yu. et al. (2008) Weldability of high-strength pipe steels for large diameter gas pipes. *Probl. Chyorn. Metallurgii i Materialoveneniya*, **3**, 39–47.
5. Nazarov, A.V., Yakushev, E.V., Shabalov, I.P. et al. (2014) Comparison of weldability of high-strength pipe steels microalloyed with niobium, niobium and vanadium. *Metallurgist*, 57(Issue 9), 911–917.
6. Efimenko, L.A., Elagina, O.Yu., Vyshemirsky, E.M. et al. (2010) Evaluation of influence of technological and service parameters on life and safety of assembly welded joints of stop valves. *Khimicheskoe i Neftegazovoe Mashinostroenie*, **2**, 42–45.
7. Poznyakov, V.D., Markashova, L.I., Maksimenko, A.A. et al. (2014) Effect of cyclic load on microstructure and cold resistance of 10G2FB steel HAZ metal. *The Paton Welding J.*, **5**, 2–9.

Received 26.10.2016

doi.org/10.15407/tpwj2016.10.06

EFFECT OF SURFACING TECHNOLOGY ON CORROSION RESISTANCE OF DEPOSTED METAL AS APPLIED TO CONDITIONS OF SERVICE OF HYDRAULIC EQUIPMENT PARTS*

Yu.M. KUSKOV[1], **V.A. ZHDANOV**[1], **V.A. TISHCHENKO**[1], **M.M. STUDENT**[2] and **N.R. CHERVINSKAYA**[2]
[1]E.O. Paton Electric Welding Institute, NASU
11 Kazimir Malevich Str., 03680, Kiev, Ukraine. E-mail: office@paton.kiev.ua
[2]G.V. Karpenko Physical-Mechanical Institute, NASU
5 Nauchnaya Str., 79601, Lvov, Ukraine

Corrosion resistance of metal of 30Kh20MN and 30Kh22MN types, produced by submerged arc surfacing using different techniques and technologies of surfacing was investigated. The feasibility of increasing the corrosion resistance of the deposited metal by proper selection of the surfacing technology was found. The best results on corrosion resistance were obtained in a pulsed surfacing using flux-cored wire at its feeding with 0.5 Hz pulse. The results of investigations can be used in restoration of worn-out parts and manufacture of the new ones of hydraulic equipment. 6 Ref., 2 Tables, 5 Figures.

Keywords: *submerged arc surfacing, technology of surfacing, pulsed feeding of wire, deposited metal, corrosion*

Many parts of equipment, installed in salt and coal mines and used in public services, are operated under the complex conditions of abrasive wear and corrosion effect. The most known representatives of these parts are the rods, plungers of hydraulic equipment, in particular, of mine hydraulic props of mechanized piles and supporting shields of tunneling machines. To increase the service life of these parts, their working surfaces are already protected during manufacturing by using galvanic coatings, mainly of chromium type. The thickness of the deposited layer is usually 5–50 μm, and hardness (for chrome) is *HV* 800–1000. In spite of their high wear-resistant and anti-corrosion properties the galvanic coatings are not durable and their density and, respectively, resistance to corrosion and wear are decreased with time.

Figure 1 shows the corrosion damages on chrome-plated surface of the rod after service in a coal mine. It should be also noted, that deposition of galvanic coatings on the working surface is ecologically dangerous process, which is refused in many industrialized countries.

One of the methods, allowing restoration of rods and plungers and return of hydraulic machines into service is the submerged arc surfacing (Figure 2).

The earlier experiments on surfacing, as well as investigations on modeling of deposited metal behavior in different synthetic media (in particular, water of coal mines) showed that metal of martensite-ferrite class of 30Kh20MN and 30Kh22MN types possesses good protective properties (depending on service conditions). Hardness of this deposited metal can be regulated in the ranges of *HRC* 35–48. However, in some cases during the service process and even at a long storage of deposited products in open rooms the dark circular

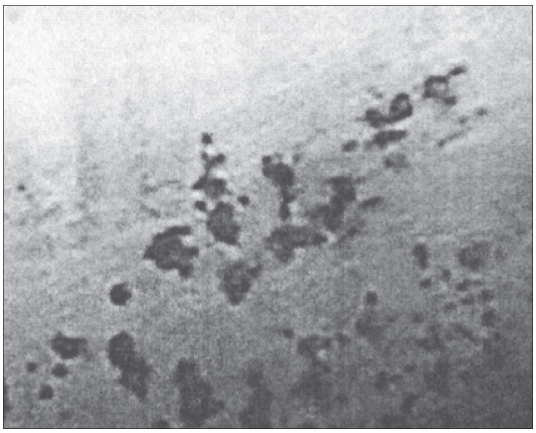

Figure 1. Corrosion damages on chrome-plated surface of rod after service in a coal mine

*On the materials of the work performed in the frames of the target program of the NAS of Ukraine «Problems of live and service safety of structures, constructions and machines» (2013–2015).

© Yu.M. KUSKOV, V.A. ZHDANOV, V.A. TISHCHENKO, M.M. STUDENT and N.R. CHERVINSKAYA, 2016

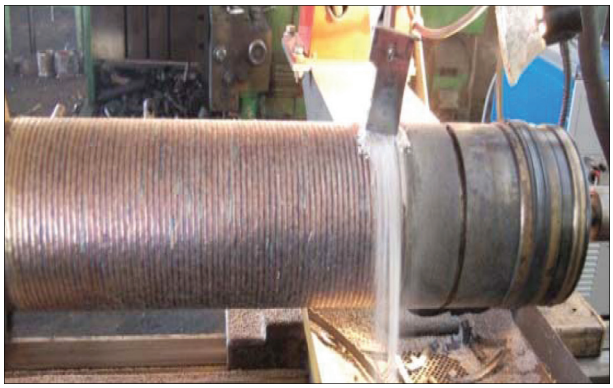

Figure 2. Process of submerged arc surfacing of plunger of mine hydraulic props

bands, corresponding to zones of overlapping beads, deposited by a helical line, appeared on the deposited surfaces. Probably, this is connected with that the metal of zone of overlapping the neighboring beads is located in a hazardous region of temperatures (680–780 °C). And, depending on time of duration in this region the conditions of proceeding the diffusion processes are changed with a possible formation of chemical and structural heterogeneity in metal [1, 2] and, respectively, by reduction in its resistance to corrosion.

Coming from that the metal of 30Kh20MN and 30Kh22MN types is characterized by rather high values of service properties, it was decided to provide their optimum level by testing these metals using surfacing by different technological procedures. Moreover, this approach to the selection of metal being deposited was stipulated by its relatively simple chemical composition as compared, for example, with the metal 08Kh20N10G7T, recommended for surfacing of mine props, and has lower content of expensive nickel by one order (at more than twice increased hardness). At the first stage of investigations the following surfacing procedures, as optimum ones, were selected:

- surfacing in one layer with a large overlapping of beads for 1/2 of their width. In accordance with work [1], such technique of surfacing can improve the structure and chemical homogeneity;

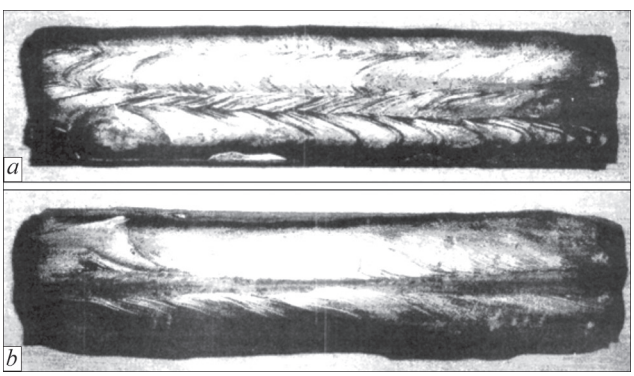

Figure 3. Specimens deposited by flux-cored wire PP-Np-30Kh20MN in one (*a*) and three (*b*) layers

Table 1. Conditions and results of a pulsed surfacing of single-layer metal 30Kh20MN

Specimen	Pulse of wire feeding, Hz	Hardness of deposited metal *HRC*
11	2.5	50–52
22	3.3	53–56
33	1.1	51–52
44	0.5	48–50

- surfacing in three layers with a misaligned overlapping of beads. Taking into account that the wear of working surface usually does not exceed 2 mm, the surfacing in three layers allows producing thickness for more than 2 mm, but in this case the heating of lower layers is more uniform. The drawback of this technology is the surfacing of excess metal with its subsequent removal by the mechanical treatment;
- surfacing with a pulsed feeding of the flux-cored wire. The pulsed electrode wire feeding is performed by using a mechanism, based on a quasi-wave converter [3]. From the data of works [4, 5] the reduction in heat input into the deposited metal occurs due to a pulsed feeding of the electrode wire and the more favorable structure is formed.

As far as during surfacing of rods and plungers it is necessary to provide a minimum penetration of the base metal (this is especially important in making a single-layer surfacing) and minimum thickness of the deposited metal, then the diameter of the flux-cored wire is accepted to be 2.2 mm. As a base metal the steel 40Kh was selected in the form of a sheet of 40 mm thickness. It was supposed that results, obtained in surfacing of horizontal surface of the specimen, will correspond to the results of a circumferential surfacing of cylindrical parts at a precise keeping of the parameters of the surfacing process conditions. Surfacing in a conventional condition: I = 250 A, U = 30 V, v_s = 18 m/h; in a pulsed condition: pulse of wire feeding is 0.5–3.3 Hz, U = 30 V, I = 250 A, v_s = 15 m/h, AN-26 flux.

The appearance of specimens, deposited by flux-cored wire PP-AN205 (PP-Np-30Kh20MN) at conventional and pulsed modes is given in Figures 3 and 4. The conditions of surfacing (pulses, Hz) and hardness of a single-layer deposited metal 30Kh20MN at a pulsed feeding of the flux-cored wire are given in Table 1.

Testing of specimens of deposited metal on corrosion resistance was performed in unit SVA-1BM of G.V. Karpenko PhMI. Corrosion processes were studied by using potentiostats PI-50-1 and IPC-Pro. For potentiostat IPC-Pro the program IPC 2000 was used, which is applied for hardware complex «Potentiostat IPC-Pro + PC IBM PC».

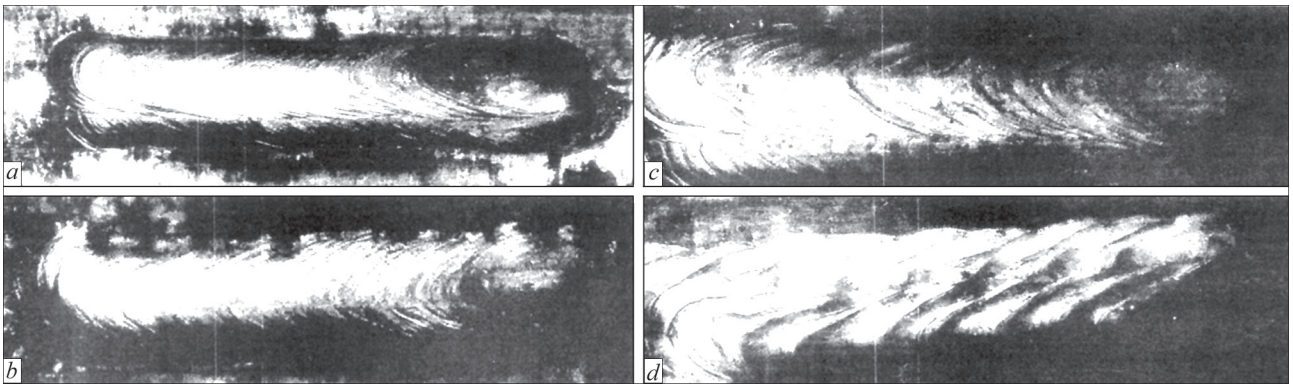

Figure 4. Specimens deposited by flux-cored wire PP-Np-30Kh20MN with superposition of pulses of its feeding: *a* — 2.5; *b* — 3.3; *c* — 1.1; *d* — 0.5 Hz

Table 2. Values of corrosion (before and after polarization tests) of single-layer metal 30Kh20MN, deposited in a pulsed mode

Values of corrosion	Specimen			
	11	22	33	44
E_{stab}, mV	–415	–473	–457	–582
E_{corr}, mV	–379	–463	–466	–441
$i_{corr} \cdot 10^{-3}$, mA/cm^2	3.06	4.99	3.8	1.44
Note. Evaluation of specimen surface quality after 10-day soaking in NaCl solution showed that traces of corrosion are observed on specimens 11, 22 and 33, while the traces of corrosion are not observed on specimen 44.				

To study the processes, occurring as a result of contact of materials being studied and corrosion medium, the method of voltammeter measurements was applied, allowing revealing the specifics of proceeding the electrochemical reactions on the surface of the material studied in the process of its interaction with a preset corrosion medium. In this case the basic characteristic, by which the systems «material-medium» was evaluated, was a polarization curve. This is dependence of current density i on potential E of

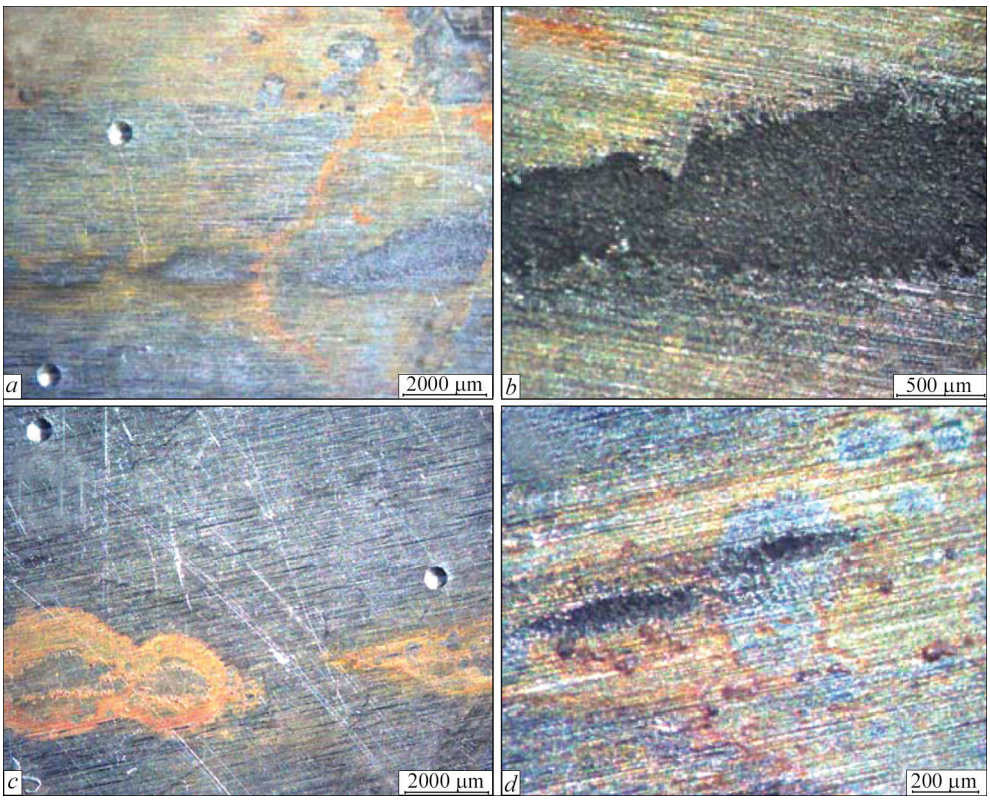

Figure 5. Surface of specimens, deposited in a pulsed mode, after corrosion tests: *a*, *b* — specimen 22 ; *c*, *d* — 44

the studied surface. The polarization curves were taken in a potentiodynamic mode, maximum reflecting the pattern of real processes proceeding on the studied surface [6]. Electrode processes of investigated specimens, being working electrodes, in corrosion medium were measured as compared with saturated chloride-silver electrode. An auxiliary electrode was a platinum grid. Rate of potential scanning was 2 mV/s.

The investigations were carried out in electrochemical cell in medium of 3 % water solution of NaCl. Before the polarization tests the specimens were soaked in this solution for 10 days.

The best results on corrosion resistance were obtained on specimens deposited in a pulsed mode at the value of 0.5 Hz. The effect of the pulse value on proceeding the corrosion process is given in Table 2.

Figure 5 shows the surfaces of specimens 22 and 44 after polarization tests. As is seen from Figure 5, *b* after the polarization tests the significant corrosion damages of surface of specimen 22 are observed. On the surface of specimen 44 the minimum local zones of damage can be detected at a large magnification (Figure 5, *d*). Thus, the value of a pulse of wire feeding in surfacing can have a great influence on corrosion processes in the deposited metal.

Conclusions

1. The feasibility of improvement of deposited metal corrosion resistance by a proper selection of technique and technology of surfacing by the same surfacing material was found.

2. The best values of corrosion resistance of the deposited metal of C–Cr–Ni–Mo system are attained in a single-layer pulsed submerged arc surfacing with a flux-cored wire at the 0.5 Hz pulse of its feeding.

3. Results of carried out investigations can be applied in restoration of hydraulic equipment worn-out parts and manufacture of new ones, in particular rods and plungers.

1. Kondratiev, I.A., Vasiliev, V.G., Dzykovich, I.Ya. (1996) Investigation of structure heterogeneity of 35V9Kh3SF type deposited metal and its influence on serviceability of built-up mill rolls. *Avtomatich. Svarka*, **6**, 17–20.
2. Palchuk, N.Yu. (1954) Effect of heating in manual welding on intercrystalline corrosion of welds of 18-8 type steels. *Ibid*., **3**, 41–49.
3. Lebedev, V.A. (1996) Control of rate and pitch of pulse electrode wire feed in mechanisms based on quasi-wave converter. *Ibid*., **6**, 34–37.
4. Lebedev, V.A., Tishchenko, V.A. (2013) Examination of heat-affected zone in mechanized surfacing with mode modulation. *Remont, Vosstanovlenie, Modernizatsiya*, **10**, 29–34.
5. Kryukov, A.V., Pavlov, N.V., Zelenkovsky, A.A. (2013) Peculiarities of welding with pulse electrode wire feed. *Tekhnologiya Mashinostroeniya*, **7**, 30–31.
6. Zhuk, N.P. (1976) *Course of theory of corrosion and protection of metals*. Moscow: Metallurgiya.

Received 22.12.2015

doi.org/10.15407/tpwj2016.10.07

DEPOSITION OF PROTECTIVE COATINGS ON COPPER PLATES OF CCM MOLDS BY THE METHOD OF AUTOVACUUM BRAZING

M.A. POLESHCHUK, M.G. ATROSHENKO, A.V. SHEVTSOVA and **A.L. PUZRIN**
E.O. Paton Electric Welding Institute, NASU
11 Kazimir Malevich Str., 03680, Kiev, Ukraine. E-mail: office@paton.kiev.ua

Possibility of applying a protective layer in the form of a thin metal sheet on flat copper panels of CCM molds by autovacuum brazing was verified on models. 08Kh18N10T steel and nickel were used as protective sheets. Peel strength of bimetal brazed joints between the layers was studied, and bending tests were also performed. A sound brazed seam without defects in the form of pores or cracks was produced between the copper plate and 08Kh18N10T steel sheet 2 mm thick. Peel strength of protective steel layer was equal to 300 MPa, on average. Obtained results allow recommending the method of autovacuum brazing for deposition of protective coatings from 08Kh18N10T steel on flat panels of molds. 9 Ref., 6 Figures.

Keywords: *CCM molds, protective coatings, autovacuum brazing, brazed joints, metallography, mechanics*

The major amount of steel produced in the world is poured into water-cooled copper molds, which are replaceable components of continuous casting machines (CCM). During CCM operation, the mold inner surface undergoes abrasive wear, because of friction of solidifying steel crust of the poured billet against the copper water-cooled wall. Particularly intensive and non-uniform wear is observed on the walls of molds designed for producing billets of rectangular or square section in radial-type CCM. Such molds are usually made to consist of separate flat panels with individual cooling. Working surface of some of them can reach one square meter. The service life of such a mold is determined by admissible wear of working surface and can be up to one hundred melts [1].

Service life of CCM molds can be extended in two ways: recovery repair of worn panels or deposition of a protective metal or metal-ceramic coating on their working surface, having higher wear resistance than that of copper.

CCM mold panels are subjected to current repair as required. A layer of copper of thickness greater than that of formed defects, is removed from the working surfaces of cooled copper plates by machining uniformly over the entire plane. During panel operation such repair is repeated several times, until copper plate thickness is reduced to maximum permissible size. Such copper plates can be subjected to reconditioning repair, during which a copper layer is deposited onto their working surface by fusion or friction stir welding process up to restoration of initial thickness [2, 3].

In work [4] it is shown that the method of autovacuum brazing (AVB) can be effectively used for reconditioning repair of copper plates of CCM mold panels. This method allows relatively easily applying the restorative copper layer on working surface of copper plates of a large area without distortion or buckling of the latter, that is inherent to other techniques. Brazed seam between the copper layers (base and restorative) is not inferior to copper proper as to strength, and its thermal resistance has practically no influence on the process of heat transfer through the copper plate [4].

In this work, AVB method was used for deposition of protective coatings of metals with higher wear resistance than that of copper, on thick copper cooled plates of molds. The objective of the study was assessment of principal possibility of producing this type of brazed joint and determination of its mechanical properties.

Proceeding from the concepts of the mechanisms of operation of CCM water-cooled molds, let us formulate the main requirements to the properties of protective coatings. They should be dense and wear-resistant; should have good adhesion to copper over the entire wall surface; and minimum thermal resistance to heat flow from molten steel to cooling water.

At present protective coatings from nickel, chromium, steels or ceramics are deposited by electrolytic [1, 5], detonation [5, 6], explosion [7] and other methods. Unfortunately, none of these methods produces a protective coating, the properties of which fully satisfy all the above requirements. So, for instance, with electrolytic or detonation methods, it is impossible to produce a dense coating with good adhesion to copper. This may lead to erosion damage of the coating or its spallation. At cladding of mold copper wall surface with a steel plate by explosion welding, air is trapped in individual regions of the joint. Such air cavities in this location essentially increase thermal resistance to heat flow from the molten metal to cooling water through the wall that is inadmissible in mold operation.

In our opinion, all the above-mentioned requirements to protective coating of the panel wall will be

© M.A. POLESHCHUK, M.G. ATROSHENKO, A.V. SHEVTSOVA and A.L. PUZRIN, 2016

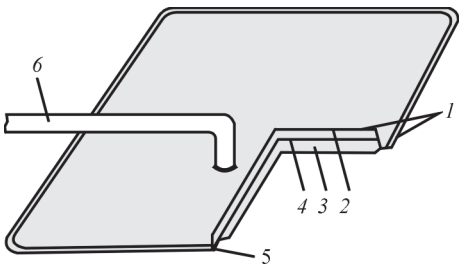

Figure 1. Assembly for brazing: *1* — cassette halves; *2* — protective coating; *3* — base metal, simulating mold panel; *4* — braze alloy; *5* — sealing seam; *6* — vacuum tube

the most completely satisfied by rolled sheet from wear-resistant metal, for instance, from certain grades of steel or nickel, brazed to the copper plate over the entire surface. Such a coating can be deposited on the mold panel during its manufacture or during repair. The complexity of the task is due to the need to have a sound brazed seam over the entire area of the joint of thick copper with wear-resistant sheet.

08Kh18N10T steel and nickel as corrosion-resistant materials with higher wear resistance than that of copper were selected as protective coating for the experiments. 08Kh18N10T steel has thermal expansion factor close to that of copper. This factor is important to achieve the required strength and performance of the brazed joint. In case of application of a less expensive sheet from carbon steels as protective coating, generation of stresses in the brazed seam is inevitable, because of an essential difference in thermal expansion of such steels and copper, that may lead to its failure.

Development of basic technology of AVB of protective coatings was performed experimentally by brazing test packages of 100×100 mm size by the procedure described in [4]. The packages were assembled from three layers: base metal, simulating mold panel, protective layer and braze alloy between them. Copper of grade M-1 of 7 mm thickness, was used as the base metal, and protective layers were made from stainless steel 08Kh18N10T 2 mm thick, or sheet nickel 4 mm thick. The braze alloy was foil of beryllium bronze BrB2 which has shown itself well in brazing multilayer copper packages. Foil of 0.2 mm thickness, was placed in two layers.

Packages pre-assembled for brazing, were placed into special cassettes, creating a closed volume. The cassettes consisted of two similar stamped parts. The material for manufacturing the cassettes was 1 mm thick sheet from 08Kh18N10T steel, which at brazing temperature ensured package compression by atmospheric pressure uniformly over the entire surface. Filled cassettes were welded around the perimeter by argon-arc welding with vacuum-tight weld.

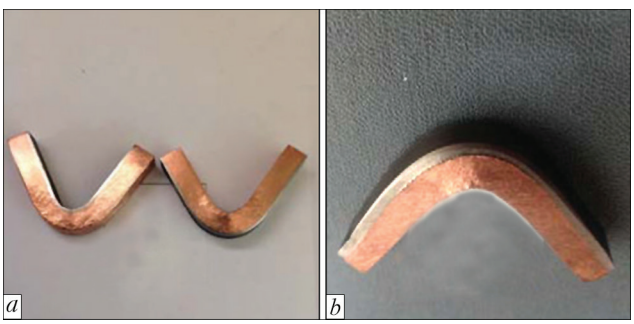

Figure 2. Samples after bending test: *a* — copper-steel (*left* — protective layer inside, *right* — outside); *b* — copper–nickel

A tube was welded into the cassette for pumping down. General view of the cassette is shown in Figure 1.

Prepared cassettes were placed flat on the table in the heat-treating furnace, vacuum tube was brought outside through a hole in the door, a compound pressure and vacuum gauge, and a backing pump through a gate valve, were connected to it. Before brazing, a rarefaction of 10^{-1} was created inside the cassette, and then the gate valve was closed. Heat furnace was heated up to brazing temperature of 1040 °C with isothermal exposure for 30 min. Cassettes were cooled with the furnace.

After brazing, the cassettes were cut, and samples for investigations were prepared from the removed packages.

First of all, bending test of the samples was conducted to assess the quality of the brazed joint. Samples measuring 80×10 mm cut out through the entire thickness of the brazed joint, were tested. The samples were bent at 90° inwards, with the protective layer facing inside and outside (Figure 2).

On copper–steel 08Kh18N10T samples no delamination, cracks or tears were found, either in the first or in the second case in the joint zone. Test results indicate good quality of copper–steel 08Kh18N10T brazed joint, produced with BrB2 braze alloy.

After testing the copper-nickel sample with protective layer on the outside (Figure 2, *b*), a delamination occurred in the bending zone. Because of unsatisfactory result of this test, sample bending with protective layer inside was not performed.

Peel testing of brazed bimetal samples was carried out according to the procedure and on samples described in [4]. This procedure is not standard and the normative documents do not provide the values that would define the minimum acceptable peel strength limit for bimetals or layered monometals based on copper. However, this characteristic is important and determines the quality of the brazed joint and performance of the entire item. Thus, the obtained during testing limit values of bimetal peel strength were compared with ultimate tensile strength of monolithic solid copper samples of the same size, made from a copper sheet, similar to base metal prior to brazing. Ultimate tensile strength of monolithic samples was 450 MPa, that of copper–steel 08Kh18N10T bimetal was 301.5 MPa, that of copper–nickel bimetal was 108 MPa. All these data are the averaged results of tests on three samples of each type.

In our opinion, bond strength of copper–steel 08Kh18N10T bimetal obtained with BrB2 braze alloy is high enough to ensure the bimetallic item per-

Figure 3. Microstructure (×500) of copper–steel 08Kh18N10T brazed joint (unetched state)

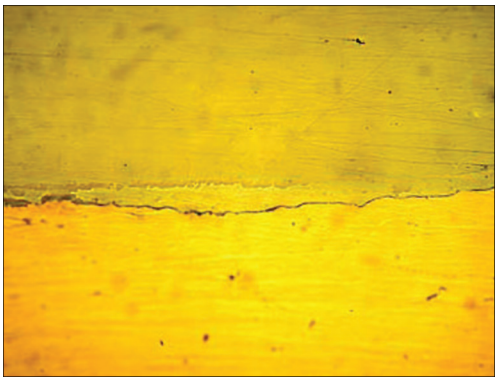

Figure 5. Microstructure (×500) of copper–nickel brazed joint (unetched state)

formance. To clarify the reasons for the unsatisfactory results of mechanical testing of copper–nickel brazed joint, comparative metallographic analysis of copper–nickel and copper–steel 08Kh18N10T samples was performed. For this purpose, unetched and etched ground samples were studied in NEOFOT 32 microscope at different magnifications. Etching of the samples was carried out in two stages. At the first stage, the sample was etched in an aqueous solution of sulfuric acid, chromic anhydride and sodium chloride to reveal the copper structure. At the second stage, electrochemical etching in chromic anhydride was performed to reveal the structure of stainless steel and nickel.

No clearcut brazed seam is observed in unetched copper–steel 08Kh18N10T microsection (×500) (Figure 3). Zone of contact of braze alloy and stainless steel with the size of projections and depressions of 2–15 μm, is visible over the entire length of the microsection. The contact zone has no defects such as pores or cracks. All this testifies to the high quality of the brazed joint along the entire length of the studied section.

The width of diffusion zone on steel 08Kh18N10T is equal to 10–50 μm.

After etching a distinct brazed seam of 60–80 μm width is observed (Figure 4). It has finer grain than the copper base metal.

Measurement of microhardness in the brazed joint zone showed that its value is 990–1480 MPa and that of copper base metal is 602–713 MPa.

After etching of steel 08Kh18N10T one can see that the size of its grains decreases towards the boundary with the brazed seam from 40 (in the main part of protective coating) to 5–12 μm. Microhardness of steel 08Kh18N10T at the boundary is equal to 2480–2540 MPa, and that in the rest of the steel is 2200–2280 MPa. Weld width is 60–80 μm; diffusion zone from the side of steel 08Kh18N10T is 10–50 μm, so that the total width of the transition zone of brazed joint is in the range of 70–130 μm.

No pores or cracks were observed, when studying bimetal copper–nickel joint on unetched microsection at ×500 magnification. In the area of contact of nickel — BrB2 mutual dissolution of metals (nickel and copper) took place to form a solid solution area 5–15 μm wide (Figure 5).

On the boundary of nickel with the seam, a broken but not dissolved nickel oxide film in the form of interlayers and inclusions, is visible. A brazed seam (BrB2) of the width from 25 to 50 μm is observed after copper etching (Figure 6). Seam microhardness is 89±20 MPa.

After electrolytic etching, grains of 100×80 μm size with a microhardness of 1390±200 MPa are observed in the layer of nickel. Nickel region adjacent to the brazed seam, has a recrystallization zone of 25 μm width with grain size of 7–15 μm. Microhardness of this zone is 2290±150 MPa, which is 1.6 times higher than nickel hardness (Figure 6, *b*). Such an increase in microhardness is associated with grain refinement in this region.

The brazed seam width is 25–50 μm, that of recrystallization zone from the nickel side is about 25 μm. Thus, the total width of the transition zone of this brazed joint is in the range of 25–75 μm. Lower

Figure 4. Microstructure of copper–steel 08Kh18N10T brazed joint after etching at different magnifications: *a* — ×100; *b* — ×1000

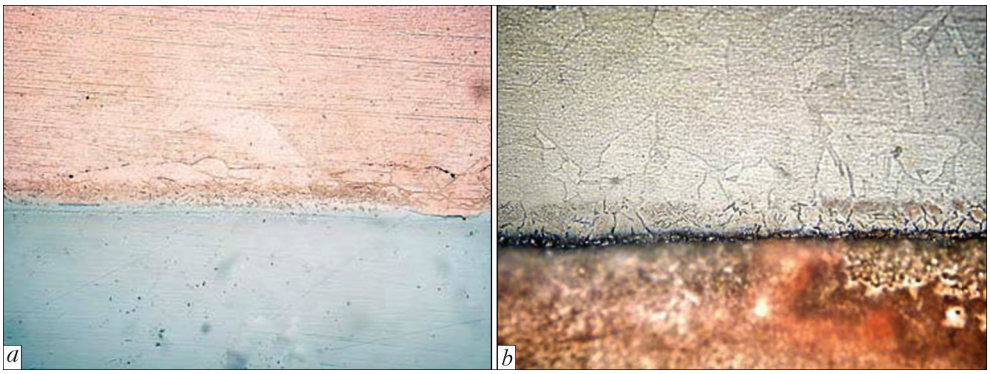

Figure 6. Microstructure of copper–nickel brazed joint after etching: *a* — ×1000; *b* — ×200

values of peel strength in nickel-coated samples as compared to samples coated by steel 08Kh18N10T, can be explained by presence of undissolved particles of oxide film on nickel surface and in the seam.

Assessing the overall results of the above experimental studies, we can say that a sound joint of the copper plate with the protective layer has so far been obtained by AVB process only for a sheet of steel 08Kh18N10T. This joint has no pores, cracks, or tears and the peel strength limit of 08Kh18N10T steel sheet at separation from copper reaches 300 MPa on the average. Such strength value is almost twice higher than the requirements of GOST 10885–85, which specifies the strength characteristics of steel bimetals [8].

During operation CCM molds are among the most heat-loaded industrial units, cooled by water. The specific heat flux transferred from molten steel to water in the mold upper part in the area of liquid metal meniscus can reach 1.8 MW/m^2. This value is reduced with greater distance from the metal surface, and at the bottom of the mold it does not exceed 0.46 MW/m^2.

Such a change in the specific heat flux is due to appearance of additional thermal resistance in its path below the liquid metal meniscus, which is created by the crust of solidifying future workpiece. Furthermore, a gas gap forms between this crust and the mold wall. This crust thickness increases continuously and at the outlet of the mold it is equal to 15–18 mm [9].

The protective coating applied to the copper wall in the form of a metal sheet, and the brazed seam also create additional thermal resistance in the heat flux path. However, a protective layer applied to the mold copper wall influences the process of heat transfer only in the upper part of the mold in the region of liquid metal meniscus, where the solidified crust of the future billet is practically absent. Calculations show that protective coating of steel 08Kh18N10T 1 mm thick reduces the specific heat flux in the meniscus region by no more than seven percent [9]. Since the area of this zone is much smaller than the area of the walls of the entire mold, it can be assumed that the protective coating applied to the copper wall of the mold by AVB has practically no effect on heat transfer process of the entire unit.

Conclusions

1. It is experimentally proved that AVB method can be used to produce sound joints of thick copper plates with a sheet of steel 08Kh18N10T.

2. Defectfree brazed seams of copper–steel 08Kh18N10T bimetal with high mechanical properties were produced using foil of bronze BrB2 as braze alloy.

3. AVB method allowed achieving peel strength limit of 08Kh18N10T steel sheet of 300 MPa at separation from the copper plate, which is higher than GOST requirements for corrosion-resistant steel bimetals.

4. Obtained results allow us recommending autovacuum brazing for application of protective coatings on working surfaces of CCM mold panels.

5. The protective coating applied by AVP method on copper walls of the mold has almost no effect on the process of heat transfer throughout the unit.

1. Markushin, A.A., Kuklev, A.V., Ajzin, M.Yu. (2005) *Radial slab mold with parallel-plate ducts and nickel coating of walls*. Moscow: Metallurgizdat.
2. Abramovich, V.R. (1988) *Fusion welding of copper and copper-based alloys*. Moscow: Mashinostroenie.
3. Nikityuk, Yu.N., Grigorenko, G.M., Zelenin, V.I. et al. (2013) Technology of restoration repair of slab moulds of MCCB by friction stir surfacing method. *Sovremennaya Elektrometallurgiya*, **3**, 51–55.
4. Grigorenko, G.M., Puzrin, A.L., Atroshenko, M.G. et al. (2015) Autovacuum brazing in repair of copper panels of MCCB moulds. *The Paton Welding J.*, **9**, 45–49.
5. Masato, T. (2009) Moulds of MCCB of steel from Mashima kosan. In: *Proc. of Int. Sci.-Pract. Seminar on Electrocladding and Thermal Spraying*. Ekaterinburg, 20–24.
6. Korobov, Yu.S. (2009) Improvement of service life of metallurgical equipment using thermal spraying. In: *Proc. of Int. Sci.-Pract. Seminar on Electrocladding and Thermal Spraying*. Ekaterinburg, 56–71.
7. Kudinov, V.M., Koroteev, A.Ya. (1978) *Explosion welding in metallurgy*. Ed. by E.S. Karakozov. Moscow: Metallurgiya.
8. *GOST 10885–85:* Sheet hot-rolled two-ply corrosion-resistant steel (OKP 09 950) Introd. 01.07.86: Minchermet SSSR, 1986.
9. Evteev, D.P., Kolybalov, I.N. (1984) *Continuous casting of steel*. Moscow: Metallurgiya.

Received 19.04.2016

doi.org/10.15407/tpwj2016.10.08

INDUCTION DEVICE FOR HEAT TREATMENT OF WELDED JOINTS OF RAILWAY RAILS

E.A. PANTELEJMONOV and **R.S. GUBATYUK**
E.O. Paton Electric Welding Institute, NASU
11 Kazimir Malevich Str., 03680, Kiev, Ukraine. E-mail: office@paton.kiev.ua

The paper studies the design peculiarities of induction device for heat treatment of welded joints of railway rails and gives the results of its testing. The device uses the inductors with magnetic cores and matching transformers, developed and manufactured at PWI. The inductors are located opposite one another from rail sides. Inductive wire of the inductor is divided for two parallel conductors, which follow the shape of rail surface, surround part of running surface, inner edge of rail head, rail web and part of rail flange with increased air gaps in area of rail web and blades. The magnetic cores are located over rail head running surface, inner edges of head, web and lower surface of rail flange. Testing of induction device at 2.4 kHz current frequency showed uniform distribution of temperature field in rail section and absence of overheating of rail blades. Heating of rail zone of 50–55 mm width to 850–910 °C temperature took 140 s. Nominal power of supply source is 90 kW. 7 Ref., 4 Figures 4.

Keywords: *rails, rail welded joints, heat treatment, induction heating, inductor*

Heat treatment of the welded joints of railway rails, produced with resistance butt welding, is used for providing structural zonal homogeneity after welding, balance of hardness of metal of rails head, elimination of unfavorable diagram of internal residual stresses of welded joint metal [1, 2]. A process of heat treatment includes heating of welded joint zone and further quenching of running surface of rail head by means of forced cooling with air-water mixture or compressed air. Currently, heat treatment of the welded joints of rails is carried out, mainly, using induction units of UIN-001 type of different modification. The main elements of the unit are a system of inductors, control block, quenching block and high-frequency power source of 100 kW power and current frequency 8.0–16.0 kHz. The system of inductors includes two similar electrically connected multirun inductors without magnetic cores. The heating temperature for heat treatment of welded joints of rails of R65 type at UIN-001 unit makes 850–950 °C, heating time is 240 s from welding heat and 360 s from workshop temperature [3, 4].

One of the ways to increase efficiency of induction heating equipment for heat treatment of the welded joints of rails is improvement of inductor design. A task of the inductors is to reduce the of time of welded joints heating in order to increase efficiency of rail bar production lines, provide uniform distribution of temperature field along rail section and eliminate rail elements overheating.

It is known that the magnetic cores [5, 6] promote increase of level of electromagnetic coupling of current in the inductors with eddy-currents being inducted in the heated part, and, respectively, rise of efficiency and coefficient of power of inductor-part induction system. Application of the magnetic cores in the inductors allows distributing power delivered to the welded joint taking into account difference in mass of metal of head, web and flange of the rail as well as solving the problem of head center heating and place of transfer of the rail flange into the web due to the peculiarities of heating of complex shape parts with high frequency currents.

Present work describes the peculiarities of inductor design and gives the results of testing of the induction device for heat treatment of the welded joints of railway rails. The inductors with magnetic cores and matching transformers, developed and manufactured

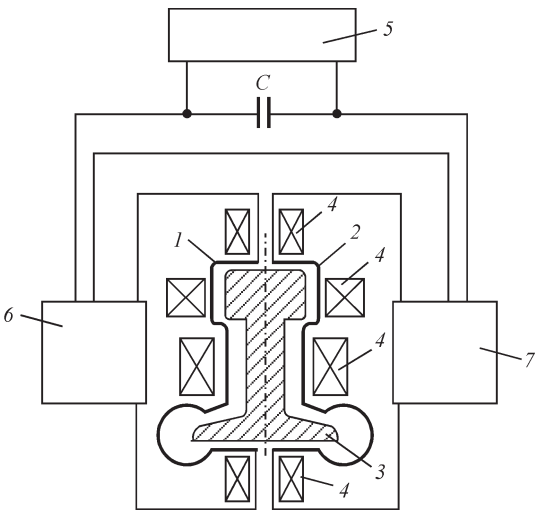

Figure 1. Scheme of induction device (descriptions *1–7* see in the text)

© E.A. PANTELEJMONOV and R.S. GUBATYUK, 2016

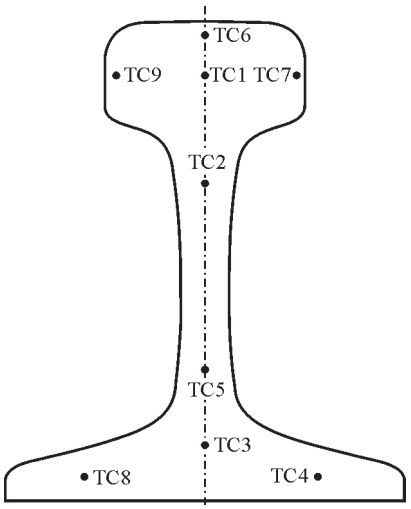

Figure 2. Scheme of location of thermal-electric converters TC1–TC9 in rail section (see designations in the text)

at PWI, are used in the device. Nominal frequency of current is 2.4 kHz.

Induction device (Figure 1) consists of inductors *1* and *2* of similar design. The inductors are located opposite one another from rail *3* side surfaces. Inductive wire of the inductor is divided for two parallel conductors, follow the shape of rail surface, surround part of running surface, inner edge of rail head, rail web and part of rail flange with increased air gaps in area of rail web and blades. Conduct buses of the inductors over the head running surface are equipped with the channels for passing a pyrometer beam. The different length magnetic cores *4* are installed over the head running surface, inner edges of rail head, web and lower surface of rail flange [7]. Matching transformers *6* and *7* are used for connection of inductors to thyristor frequency converter *5*.

Efficiency of the induction device was investigated in heating of zone of R65 type rail. Infrared pyrometer Optris CSLT15 was used for measurement of temperature on running surface of rail head. A distance from pyrometer to running surface makes 130 mm. Temperature of metal in rail section was controlled with chromel-alumel thermal-electric converters TC1–TC9 (TC1 — along symmetry axis at 20 mm

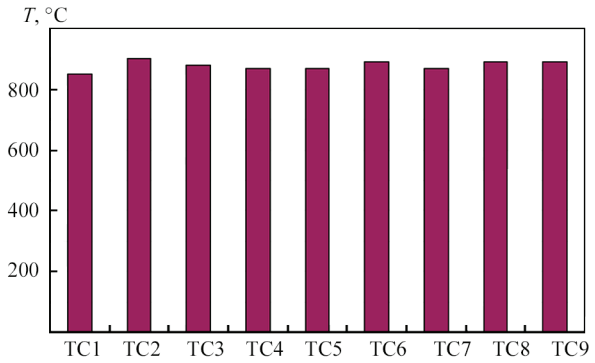

Figure 4. Histogram of temperature in points of rail section during 140 s heating time

depth from running surface; TC2, TC3, TC5 — along symmetry axis at 120, 20 and 50 mm distance, respectively, from flange lower surface; TC4 and TC8 — at 10 mm depth from flange lower surface and 32 mm from blade edges; TC6 — along symmetry axis at 3 mm depth from running surface; TC7, TC9 — in center of inner edges at 3 mm depth) (Figure 2).

Tests of the induction device showed that heating of rail zone from 20 °C temperature to temperature on head running surface 850 °C (Figure 3, *a*) was carried out for 60 s. The nominal power of frequency converter is 90 kW. Width of heat affect zone makes 50–55 mm. The rate of heating of head running surface to temperature of magnetic transformation point makes around 17.5 °C/s. The rate of heating on head running surface reduces to 1 °C/s with metal loss of magnetic properties and rise of depth of current penetration. The time of heating reduces to 40 s in heating of rail zone from 250 °C temperature to temperature on head running surface 850 °C/s (Figure 3, *b*) and nominal power of frequency converter 90 kW. Heating of rail zone from 250 °C temperature was simulated by a process of heat treatment of the welded joints of rails from welding heat in process lines of rail bar production.

Distribution of the temperature field in rail section in heating of rail zone from 20 °C during 140 s are reflected by dependencies, given in Figure 4. Temperature of head inner edges is 870–890 °C (TC7,

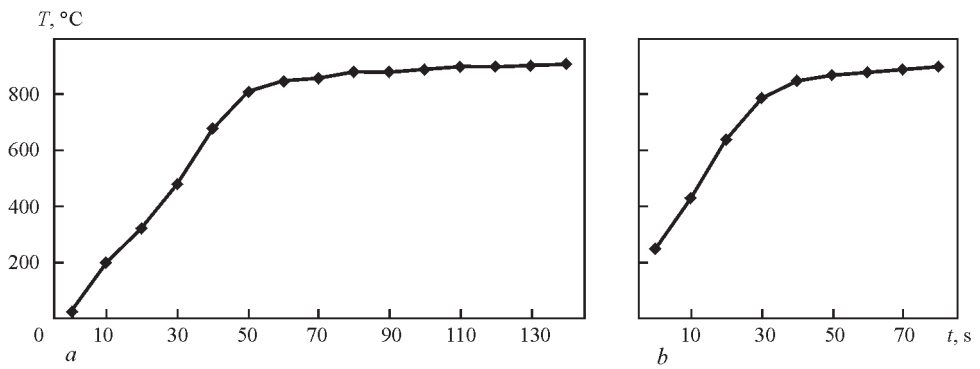

Figure 3. Time dependencies of temperature on running surface of rail head in heating of rail zone from 20 (*a*) and from 250 °C (*b*)

TC9), that of web makes 870–890 °C (TC2, TC5), it is 880 °C (TC3) at 20 mm depth from lower surface of flange along rail symmetry axis and 870–890 °C for rail flange (TC4, TC8). Time of holding of head running surface at temperature more than 850 °C is around 80 s. A temperature difference between running surface (Figure 3, *a*) and center of head (TC1, Figure 1) is not more than 50–60 °C. No overheating of rail blades is present. The temperature in place of flange to rail web transfer is 880–890 °C (TC3, TC5).

Conclusions

1. The induction device for heat treatment of the rail welded joints includes the inductors with magnetic cores and matching transformers, developed and manufactured at PWI. The inductors differ by design of inductive wire and location of magnetic core relatively to rail elements.

2. Uniform distribution of the temperature field in rail section and absence of rail blades overheating were reached in process of testing of the induction device at current frequency 2.4 kHz. Heating of the rail zone of 50–55 mm width to 850–910 °C temperature was performed for 140 s. Nominal power of supply source is 90 kW. It is necessary to note a reduction of time of heating in comparison with ITTZ-250/2.4 and UIN-001 units, which are used for heat treatment of the welded joints of rails under track and workshop conditions.

1. Genkin, I.Z. (2003) Heat treatment of rail welded joints in induction units. *The Paton Welding J*., **9**, 38–41.
2. Nesterov, D.K., Sapozhkov, V.E., Levchenko, N.F. et al. (1990) Heat treatment of rail steel using induction heating. *Metallovedenie i Termicheskaya Obrabotka Metallov*, **8**, 30–34.
3. Rezanov, V.A., Fedin, V.M., Bashlykov, A.V. et al. (2013) Differential quenching of rail welded joints. *Vestnik VNIIZhT*, **2**, 28–33.
4. Fedin, V.M. (2005) Development of new technological equipment for restoration of used rails. *Ibid*., **4**, 22–25.
5. Slukhotsky, A.E., Ryskin, S.G. (1974) *Inductors for induction heating*. Leningrad: Energiya.
6. Pismenny, A.S., Pantelejmonov, E.A., Prokofiev, A.S. et al. (2000) Design of an inductor with a magnetic core for heating flat surfaces. *The Paton Welding J*., **11**, 41–45.
7. Pantelejmonov, E.A. *Induction device for heat treatment of rail welded joints*. Pat. 109123 UA. Int. Cl. K C 21D1/10. Publ. 10.08.2016.

Received 04.06.2016

doi.org/10.15407/tpwj2016.10.09

ASH115M2 MACHINE FOR ELECTROSLAG WELDING OF VERTICAL, INCLINED AND CURVILINEAR BUTT JOINTS

G.V. ZHUK[1], **A.V. SEMENENKO**[1], **I.I. LYCHKO**[2], **S.M. KOZULIN**[2] and **Anat.V. STEPAKHNO**[3]
[1]SC «EDTB of the E.O. Paton Electric Welding Institute of the NAS of Ukraine»
15 Kazimir Malevich Str., Kiev, Ukraine. E-mail: dktbpaton@gmail.com
[2]E.O. Paton Electric Welding Institute, NASU
11 Kazimir Malevich Str., 03680, Kiev, Ukraine. E-mail: office@paton.kiev.ua

Design features of a modern machine for electroslag welding of vertical, inclined and curvilinear butt joints are described. It enables manufacturing unique metal-intensive items. 5 Ref., 2 Figures.

Keywords: *electroslag welding, vertical and curvilinear joints, control system, travel mechanism, guide rail, drive carriages*

In May, 2016 specialists of SC «EDTB of the E.O. Paton Electric Welding Institute of the NAS of Ukraine» [1] and PJSC «PPWE of the E.O. Paton Electric Welding Institute of the NAS of Ukraine» (Kiev) [2] introduced two electroslag welding machines ASh115M2 in a metallurgical enterprise (Figures 1, 2).

At this moment electroslag welding is not as common, as, for instance, submerged-arc or gas-shielded welding.

It is applied in manufacture of unique metal-intensive items, which are not mass-produced. Leading foreign manufacturers of welding equipment do not offer electroslag welding equipment in their catalogs, so that it is difficult to say, whether they are manufacturing such equipment. There are no manufacturers of modern electroslag equipment in the CIS territory. Only such well-known apparatuses as A-535 and AD-381 are proposed.

New ASh115M2 machines are designed for electroslag welding of vertical, inclined and curvilinear butt joints with curvature radius $R > 4000$ mm and angle of inclination of ±25° from the horizontal, as well as butt joints of sheet structures with one-sided forced formation of the weld.

Ash115M2 machine includes:

- electroslag unit with control panel — 1 pc;
- guide rail with supports – 1 set;
- frame with spool for electrode wire — 2 pcs;
- control panel — 1 pc;
- welding current source — 2 pcs.

Electroslag unit with control panel is a mounting self-propelled heavy-type apparatus, fitted with all the required mechanical and electromechanical correctors, as well as sensors for making high-quality welds. It is designed so that it could be disassembled

Figure 1. Welding of converter support half-ring

© G.V. ZHUK, A.V. SEMENENKO, I.I. LYCHKO, S.M. KOZULIN and Anat.V. STEPAKHNO, 2016

into four main components, which can be easily and quickly put together. These are travel mechanism, suspension, oscillator and control panel.

Travel mechanism is fitted with special press-down rollers (they also act as wheels for the drive carriage), which allow fastening and removing it in any part of the guide rail without disassembling the unit. Such a design greatly facilitates for welders fastening the unit on the guide rail in site and its removal after completion of operations. Previously, in all the units the drive carriages were fastened and removed from the start or end of the guide rail. This increased the time of unit mounting and created a lot of inconvenience for the operator.

Owing to a new mechanism of rotation, the unit enables making position circumferential butt joints, during which process the welding operator changes the spatial position of the nozzles.

The guide rail is a flexible strip of spring steel with involute rack at the end face. It consists of several parts, abutted to each other (length is determined by the length of the future weld). The rail is fastened on supports which are welded to the item by erection welds.

Frames with electrode wire spool (two pieces) are placed separately near the unit. To avoid sharp inflections of wire conduits when making extended welds, it is necessary to envisage a lifting platform for lifting the spools with welding wire and the welding operator.

SU331 system was developed to control the technological process of electroslag welding of items, which provides control of all the machine mechanisms and the two welding sources VDU-1202P.

SU331 system is based on programmable controller of CJIM type of Omron (Japan). Modern frequency inverters of Omron V1000 type are applied to control asynchronous electric motors of the unit.

Specification of ASh115M2 machine

Welded item thickness, mm	80–200
Electrode wire diameter, mm	3
Number of electrode wires, pcs	2
Electrode wire feed rate, not more than, m/h	250
Rated welding current per one electrode (at 100 % duty cycle), A	1000
Rated voltage and frequency of the mains	380 V, 50 Hz
Travel speed, not more than, m/h	10
Welding speed, m/h	0.4–6.0
Transverse oscillation speed, m/h	20–75
Nozzle dwell time at pool edge, s	1–9
Adjustable electrode spacing, mm	50–150
Oscillation range, not more than, mm	100
Ranges of adjustment of electrode «dry» extension, mm	40–120
Ranges of adjustment of angles of electrode inclination to slag pool surface	±25°
Flow rate of water (shop line) for shoe cooling, l/min	25
Correction of nozzles across the gap, mm	±20
Transverse correction of the shoe, mm	±25

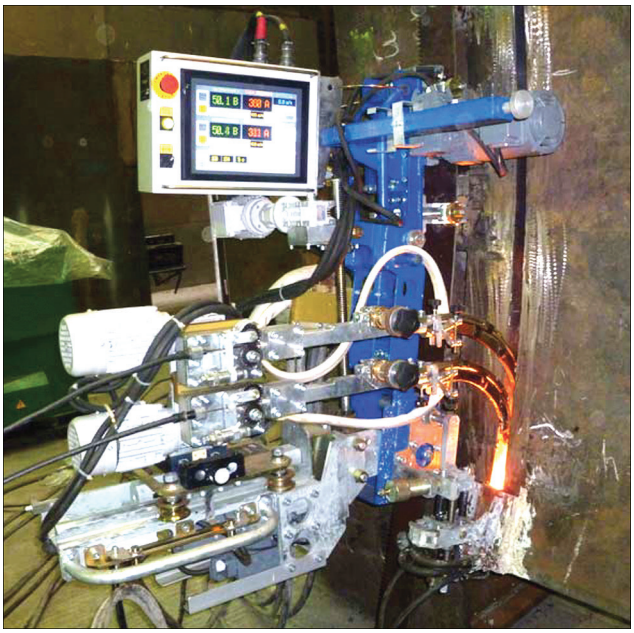

Figure 2. Appearance of ASh115M2 unit

During control system development, special attention was given to ergonomics and operator comfort.

Convenient control panel with colour sensor display of Omron NS12 type allows the operator monitoring and setting the welding parameters, as well as controlling the operation of machine mechanisms. Technological and emergency messages are displayed in addition to displaying the digital instruments, controls and sensors.

Welding rectifiers VDU-1202P produced by PJSC «PPWE of the E.O. Paton Electric Welding Institute» were included into the machine set as welding current sources.

Many years of development of similar apparatuses by designers of SC «EDTB of the E.O. Paton Electric Welding Institute of the NAS of Ukraine» were taken into account during design work performance*, and modern components from leading world manufacturers were applied [3-5]. In view of that, we can state that Ash115M2 machine has incorporated all the best elements that are now offered by electroslag welding and welding equipment.

**A.K. Polishchuk, M.I. Dubovoj, V.D. Kovalev, P.A. Panukhnik and M.A. Strelnikov took part in the work.*

1. *www*.oktb-paton.org.ua
2. *www*.paton.ua
3. (1980) *Electroslag welding and surfacing*. Ed. by E.O. Paton. Moscow: Mashinostroenie.
4. Paton, B.E., Dudko, D.A., Yushchenko, K.A. et al. (1987) Electroslag welding. Results, problems and prospects of development. *Avtomatich. Svarka*, **5**, 32–42.
5. Yushchenko, K.A., Lychko, I.I., Sushchuk-Slyusarenko, I.I. (1999) Effective techniques of electroslag welding and prospects for their application in welding production. *Welding and Surfacing Rev*., Vol. 12, 108.

Received 26.09.2016

doi.org/10.15407/tpwj2016.10.10

INFLUENCE OF TECHNOLOGICAL FACTORS OF MICROPLASMA SPRAYING OF TiO_2 ON THE DEGREE OF SPRAYING MATERIAL UTILIZATION

Yu.S. BORISOV, S.G. VOJNAROVICH, A.N. KISLITSA and **S.N. KALYUZHNY**
E.O. Paton Electric Welding Institute, NASU
11 Kazimir Malevich Str., 03680, Kiev, Ukraine. E-mail: office@paton.kiev.ua

The work is a study of the degree of the influence of technological parameters of microplasma spraying on the coefficient of material utilization during formation of a resistive coating from titania. Investigations were conducted with application of a multifactorial experiment with fractional replicas 2^{4-1}. As a result of processing of experimental data, a regression equation was derived, which allows assessment of the degree of the influence of microplasma spraying parameters, such as current, spraying distance, plasma gas flow rate and powder consumption on the value of the material utilization coefficient. It is established that current value has the greatest influence on it. During investigations it was shown that selection of the parameters of microplasma spraying of resistive paths from TiO_2 powder will allow minimizing material losses. 4 Ref., 2 Tables.

Keywords: *microplasma spraying, TiO_2, material utilization coefficient, resistive heating element*

Thermal spraying (TS) technologies are becoming ever wider accepted during manufacture of flat low-temperature resistive heating elements (RHE) [1, 2]. Such RHE are multi-layer heat-resistant coatings, consisting of an insulation and current-conducting layer, which may be formed directly on the heated metal surface. RHE of this type offer the advantage of lower temperature in the conducting layer, allowing their electrical safety to be increased, as well as cost-effectiveness and longer service life [3].

However, manufacture of small-sized RHE by TS methods involves material losses, which consist of losses for spattering, spraying particles rebounding, as well as losses due to the geometrical factor. Losses related to the geometrical factor at traditional plasma-arc spraying are due to spray spot diameter of 20–25 mm that is several times larger than the resistive path width of 3–5 mm. Material losses for spattering and rebounding can be characterized by material utilization coefficient (MUC). This parameter not only shows the cost-effectiveness of the process, but is also used as optimization parameter.

Table 1. Ranges of MPS process parameter variation

Variation ranges	Factors			
	I, A	G_m, l/min	H, mm	P_{pow}, g/min
Upper level +	45	2	160	1.8
Lower level –	35	1	80	0.6
Main level 0	40	1.5	120	0.8
Variation ranges	5	0.5	40	0.4

Increase of the degree of spraying material utilization under the conditions of deposition of resistive paths, can be achieved by application of the technology of microplasma spraying (MPS) due to small diameter of the spray spot (3–5 mm). Moreover, such a technology has minimum thermal impact on the substrate that enables producing a coating on thin-walled parts without their deformation [4].

The objective of this work consisted in determination of spraying material losses for spattering and rebounding, as well as studying the degree of the influence on MUC of the main process parameters, such as current I, A, spraying distance H, mm, plasma gas flow rate G_{pl}, l/min and powder consumption P_{pow}, g/min.

Studies were performed with application of the method of mathematical planning (multifactorial experiment with fractional replicas 2^{4-1}). Ranges of variation of microplasma coating process parameters and results of an experiment to determine MUC at microplasma spraying of TiO_2 powder on a plate are given in Tables 1, 2.

MUC values were determined using flat samples from steel of St3 grade of 20 mm diameter and 1 mm thickness. Before the start of spraying, uncoated sample weight was determined in analytical scales VLR-200 with the accuracy of up to 10^{-5} g. Coating spray-deposition was conducted for 15 s in microplasma spraying unit MPN-004 at stationary position of the plasmatron with TiO_2 powder of «Metachim» company with powder particle size of 15–40 μm, in

© Yu.S. BORISOV, S.G. VOJNAROVICH, A.N. KISLITSA and S.N. KALYUZHNY, 2016

the modes according to experiment plan with application of mathematical planning method.

Coating weight m_{coat} was calculated as the difference in sample weight after and before spraying. Powder consumption m_{pow} was calculated before each experiment by weighing the quantity of powder fed by the metering device during 15 s.

Material utilization coefficient was found from the following formula

$$\text{MUC} = \frac{m_{coat}}{m_{pow}} \cdot 100\,\%.$$

Mathematical processing of obtained experimental data, given in Table 2, allowed calculation of the regression equation for MUC, having the following form:

$$\text{MUC} = 15.75 + 1.45I + \\ +35G_m - 0.39375H + 7.5P_{pow}.$$

Comparison of experimental results, obtained at application of the regression equation, with calculated data shows their good agreement that is indicative of adequacy of the used model (see Table 2). Obtained regression equation enables evaluation of the influence of each MPS parameter on MUC value. In case of current rise, MUC increases due to increase of plasma jet temperature, and higher heat input into powder particle heating. This technological parameter has the greatest influence on MUC at MPS.

With increase of gas flow rate MUC becomes smaller. This is attributable to the fact that at increase of gas flow rate not only plasma jet temperature becomes lower, but also its velocity becomes higher. Increase of plasma jet outflow velocity causes increase of the velocity of spraying material particles that, in its turn, shortens the time of their staying in the high-temperature zone of the plasma jet and leads to lowering of the degree of their heating.

MUC lowering is observed at increase of spraying distance that is related to partial cooling of spraying particles and their transition into the solid state when approaching the base.

MUC values given in Table 2, show that in microplasma spraying of TiO_2 resistive material, maximum degree of spraying material utilization is achieved in mode #2 and is equal to 89 %. In this MPS mode, plasma jet enthalpy reaches 6.6 kW·h/m^3 that allows particle heating up to melting temperature and at minimum value of spraying distance of 80 mm ensuring particle interaction with the substrate in the molten state.

Table 2. Values of MPS parameters and results of the experiment to determine MUC

Mode number	I, A	G_m, l/h	H, mm	P_{pow}, g/min	MUC	
					Experimental	Calculated
1	45	120	160	1.8	75	74
2	45	120	80	0.6	89	96
3	45	60	160	0.6	44	44
4	45	60	80	1.8	78	84
5	35	120	160	0.6	47	50
6	35	120	80	1.8	88	91
7	35	60	160	1.8	28	38
8	35	60	80	0.6	65	61
9	40	90	120	0.8	68	64

Conclusions

1. Evaluation of the influence of MPS parameters such as current, plasma gas flow rate, spraying distance and powder consumption on the material utilization coefficient during spraying of TiO_2 coating was performed. It is found that current has the greatest impact on material utilization coefficient, as plasma jet temperature rises with increase of this parameter value that promotes greater heat input into powder particle heating.

2. It is found that at microplasma spraying of TiO_2 resistive material, maximum degree of spraying material utilization is equal to 89 % at plasma jet enthalpy of 6.6 kW·h/m^3 that allows heating the particles up to melting temperature, and ensuring particle interaction with the substrate in the molten state at minimum value of spraying distance of 80 mm.

1. Anshakov, A.S., Kazanov, A.M., Urbakh, E.K. et al. (1998) Development of low-temperature heater by plasma cladding method. *Fizika i Khimiya Obrabotki Materialov*, **3**, 56–61.
2. Baklanov, D.I., Belyajkov, I.N., Virnik, A.M. et al. *Method of manufacture of resistance heating element*. Pat. 2066514 RF. Int. Cl. H 05 B 3/12. Moscow: In-te for High Temperatures. Fill. 14.09.1993. Publ. 10.09.1996.
3. Ershov, A.A., Urbakh, E.K., Faleev, V.A. et al. (1995) Plasma cladding of resistive layers of electric tape. In: *Proc. of Conf. on Physics of Low-Temperature Plasma*. Petrozavodsk: PGU, 1995, Pt 3, 409–411.
4. Borisov, Yu.S., Vojnarovich, S.G., Kislitsa, A.N. et al. (2013) Manufacture of resistance electrical heater by microplasma cladding process. *The Paton Welding J.*, **9**, 50–51.

Received 06.06.2016

PATON PUBLISHING HOUSE

www.patonpublishinghouse.com

SUBSCRIPTION

«The Paton Welding Journal» is Published Monthly Since 2000 in English, ISSN 0957-798X.

«Avtomaticheskaya Svarka» Journal (Automatic Welding) is Published Monthly Since 1948 in Russian, ISSN 005-111X.

«The Paton Welding Journal» is Cover-to-Cover Translation of Avtomaticheskaya Svarka» Journal into English.

If You are interested in making subscription directly via Editorial Board, fill, please, the coupon and send application by Fax or E-mail.

The cost of annual subscription via Editorial Board is $348 for «The Paton Welding Journal» and $180 for «Avtomaticheskaya Svarka» Journal.

«The Paton Welding Journal» can be also subscribed worldwide from catalogues subscription agency EBSO.

SUBSCRIPTION COUPON

Address for journal delivery _____

_____

Term of subscription since _____ **20** _____ **till** _____ **20** _____

Name, initials _____

Affiliation _____

Position _____

Tel., Fax, E-mail _____

We offer the subscription all issues of the Journal in pdf format, starting from 2009.

The archives for 2009–2014 are free of charge on *www.patonpublishinghouse.com* site.

ADVERTISEMENT

in «Avtomaticheskaya Svarka» and «The Paton Welding Journal»

External cover, fully-colored:
First page of cover (190×190 mm) — $700
Second page of cover (200×290 mm) — $550
Third page of cover (200×290 mm) — $500
Fourth page of cover (200×290 mm) — $600

Internal cover, fully-colored:
First/second/third/fourth page of cover (200×290 mm) — $400

Internal insert:
Fully-colored (200×290 mm) — $340
Fully-colored (double page A3) (400×290 mm) — $500

- Article in the form of advertising is 50 % of the cost of advertising area
- When the sum of advertising contracts exceeds $1001, a flexible system of discounts is envisaged

Size of journal after cutting is 200×290 mm

Editorial Board of Journal «Avtomaticheskaya Svarka» and «The Paton Welding Journal»
E.O. Paton Electric Welding Institute of the NAS of Ukraine
International Association «Welding»
11 Kazimir Malevich Str. (former Bozhenko Str.), 03680, Kiev, Ukraine
Tel.: (38044) 200 60 16, 200 82 77; Fax: (38044) 200 82 77, 200 81 45
E-mail: journal@paton.kiev.ua; www.patonpublishinghouse.com